THE LOW CYCLE FATIGUE BEHAVIOUR OF ALPHA-TITANIUM

by

ROBIN STEVENSON

B.Sc. University of Glasgow

(1967)

Submitted in partial fulfillment of the requirements

for the degree of
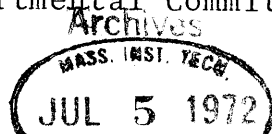
Doctor of Philosophy

at the

Massachusetts Institute of Technology

May 1972

Signature of Author. . . . .
                    Department of Metallurgy and Materials Science
                                               May 5, 1972

Certified by . . . .
                                             Thesis Supervisor

Accepted by. . . . .
            Chairman, Departmental Committee on Graduate Students

THE LOW CYCLE FATIGUE BEHAVIOUR OF ALPHA-TITANIUM

by

ROBIN STEVENSON

Submitted to the Department of Metallurgy and Materials
Science on May 5, 1972 in partial fulfillment of the
requirements for the degree of Doctor of Philosophy.

ABSTRACT

The cyclic stress-strain curves for commercial
purity α-titanium of grain sizes of 7μ and 80μ have been
determined over the range of plastic strain amplitude
±0.0005 to ±0.01. In addition samples of 14μ and 28μ
grain size were cycled at a plastic strain amplitude of
±0.01. All testing was conducted in push-pull mode
under conditions of constant plastic strain amplitude.
The response of the material to continued cycling was
monitored by plotting the stress-strain hysteresis
loops autographically.

Two modes of "hardening" behaviour have been observed.
At high plastic strain amplitudes the material hardens
monotonically at a decreasing rate until saturation is
attained. At low plastic strain amplitudes the material
initially hardens, but subsequently softens - the magnitude
of the softening increasing with decreasing plastic strain
amplitude. The influence of grain size upon this
behaviour was slight.

Examination of the dislocation substructure by trans-
mission electron microscopy disclosed that the dislocation
substructure also exhibited two modes. Like the mechanical
behaviour the form of substructure was strongly influenced
by the imposed plastic strain amplitude and only slightly
by grain size.

Material strained at high plastic strain amplitude
exhibited an elongated "cell structure", the cell walls
of which may be composed of either edge dipoles or screw
dislocations. Material strained at low plastic strain
amplitudes exhibited a structure which consisted of dipole
clusters. It was established that the majority of the
dislocations within either the clusters or the cell walls
were of $\vec{a}$ type although some dislocations whose Burgers
vector included a $\vec{c}$ component were observed. Attempts

to differentiate between the three different $\vec{a}$ type
Burgers vectors were made difficult by strong residual
contrast, and the assignation of Burgers vectors could
not be made with absolute certainty   It is, however,
suggested that all basal dislocations in either $_\rightarrow$a
dipole cluster or a cell wall possess the same $\vec{a}$ type
Burgers vector. Extensive twinning was observed in
only the 28μ and 80μ grain size samples fatigued at a
plastic strain amplitude of ±0.01.

A model based on a jog dragging mechanism is put
forward to account for the formation of edge disloca-
tion dipoles. It is shown that the model of dipole
formation suggested predicts the observed trend in the
morphology of the edge dipoles. It is also shown that
the observed mechanical behaviour may be rationalised
if the assumption is made that edge dislocations move
more rapidly than screw dislocations.

Thesis Supervisor: John F. Breedis
Title: Associate Professor of Metallurgy

TABLE OF CONTENTS

Table of Contents 4

List of Figures 7

List of Tables. 12

Acknowledgements. 13

1. Introduction. 14

2. Review of the Literature. 16

    2.1. Fatigue Hardening/Softening 16

        2.1.1 Mechanical Behaviour 16

        2.1.2 Dislocation Substructure 23

        2.1.3 Theories 25

    2.2. Tensile Behaviour of α-Titanium 27

3. Experimental Procedure. 30

    3.1. Sample Preparation. 30

    3.2. Mechanical Testing. 33

    3.3. Electron Microscopy 39

    3.4. Optical Microscopy. 42

        3.4.1 Grain Size Determinations. 42

        3.4.2 Observation of Twins 42

4. Results 44

    4.1. Mechanical Testing. 44

        4.1.1 Tensile Tests. 44

        4.1.2 Fatigue Tests. 46

LIST OF FIGURES

LIST OF TABLES

ACKNOWLEDGEMENTS

1. INTRODUCTION

In recent years, titanium and its alloys have been increasingly employed in aerospace applications, particularly in high performance aircraft, where design criteria include the behaviour of the material under cyclic loading.

It is generally recognized that fatigue failure occurs as the result of the sequential operation of three different, although strongly related processes - fatigue hardening/softening, crack initiation and crack propagation. A conventional S-N diagram, permits no distinction to be made between these various processes individually, and thus the effect of metallurgical variables, eg grain size on the individual processes can only be guessed at, unless testing is conducted under conditions in which only one of the processes is operating.

It is known that the fatigue life of α-titanium is significantly improved by refining the grain size. In view of the fact that the tensile behaviour of α-titanium is likewise strongly affected by grain size refinement it is desirable to establish whether or not the effect of refining the grain size is to alter the character of the initial fatigue hardening/softening or to inhibit crack initiation or crack propagation. Since it is generally agreed that crack initiation is affected by the dislocation

substructure developed during fatigue hardening/softening it is clearly desirable to observe the resultant dislocation substructures.

The present investigation was instituted to determine the effect of grain size on the fatigue hardening behaviour of α-titanium over a range of plastic strain amplitudes. All testing was conducted in the push-pull mode to eliminate the strain gradients inherent in tests conducted in alternating torsion or bending and under conditions of constant plastic strain amplitude since this quantity may be related to dislocation motion more readily than either total strain or stress. Transmission electron microscopy was employed to determine the nature of the dislocation substructure formed as testing proceeded.

It was hoped that the information on the dislocation substructures and the observed mechanical behaviour could be correlated to provide a clearer understanding of the microstructural aspects of cyclic deformation in α-titanium and of the influence of fatigue hardening/softening upon expected life.

2. REVIEW OF THE LITERATURE

Numerous investigations have been conducted in an attempt to determine the influence of cyclic loading and the resultant dislocation substructure on mechanical properties. The vast majority of these investigations have been conducted on face-centred cubic metals and alloys, and although a limited number of investigations have been conducted on body-centred cubic metals, virtually no work has been performed on materials with a hexagonal structure.

No attempt will be made in this section to review those phenomena associated with cyclic deformation which are specific to face-centred cubic materials and alloys, since this has already been done in several recent reviews.[1][2] Rather, only those features of the phenomenon which may be of more general applicability will be considered here.

2.1 Fatigue Hardening/Softening

2.1.1 Mechanical Behavior

It has commonly been observed that the cyclic deformation of an annealed sample results in an initially high rate of hardening (the term work hardening, since it is commonly associated with the hardening observed in unidirectional testing, will not be used here) which

gradually decreases until further cycling results in no
further change in mechanical properties (saturation)[3].
A very extensive investigation on the influence of
plastic strain amplitude and orientation on the hardening
behaviour of copper single crystals has shown that the
hardening behaviour is sharply influenced by these
factors[4], in a manner which is reminiscent of the effect
of strain and orientation on the work hardening observed
during unidirectional testing. Both high and low rates
of hardening could be induced by varying the plastic
strain amplitude for any given orientation, the plastic
strain amplitude at which the transition from low to high
hardening rates occurred being very sensitive to crystal
orientation. In crystals oriented for single slip, rapid
hardening could be induced only at high plastic strain
amplitudes while, in crystals oriented for duplex slip,
rapid hardening was observed even at very low plastic
strain amplitudes - the association of hardening
behaviour with the number of operative slip systems was
confirmed by observing slip traces. Crystals which had
hardened rapidly exhibited more than one set of slip
traces, while those which hardened slowly exhibited only
one set of slip traces. Similar results have been
reported for fatigued aluminum[5] and both results
substantiate the work of Gough[6] who reported that in

zinc, the same slip systems operate during cyclic deforma-
tion as operate during unidirectional deformation. A
comparison of the hardening rates of polycrystalline and
single crystal copper disclosed that except when the
single crystal is oriented for extensive duplex slip,
polycrystalline samples invariably harden much more rapidly
than single crystals.[4]

One distinct feature of cyclic deformation is that
in addition to hardening, it is possible for continued
cycling to soften an originally cold worked sample. Further,
in materials which exhibit a wavy slip mode, the saturation
stress developed under constant plastic strain amplitude
is independent of the history of the sample[3] - initially
annealed samples display the same saturation behaviour as
the initially cold worked samples. The ability of the
material to undo the effects of previous deformation is,
however, related to the conditions imposed during cyclic
deformation, and if extensive cyclic deformation is not
imposed on a previously cold worked sample, history
dependent effects may be observed no matter what the slip
mode (planar or wavy) of the material.[3][4]

The statement that the cyclic deformation of an
annealed sample results in hardening is applicable to face
centred cubic metals only, the behaviour observed in tests

conducted on body-centred cubic and hexagonal metals is somewhat more complicated.

Klesnil et al.[7], in tests conducted on polycrystalline low carbon steel, under constant stress amplitude, found that if the applied stress was greater than the macroscopic yield stress, that monotonic hardening occurred. If, however, the applied stress was less than the macroscopic yield stress, the material would first soften, then harden, and subsequently saturate. At very low stress amplitudes (stresses comparable to the fatigue limit) the material softens and saturates. In addition, tensile tests indicated that in those cases where softening and hardening occurred, a progressive decrease in the magnitude of the Lüder's strain occurred - a feature which has been observed by various other investigators in iron[8], molybdenum[9] and niobium.[10]

Klesnil and Lukas[11] explained this behaviour by considering that only local yielding had occurred on the first cycle, and that the softening occurred as yield was initiated in adjacent grains. When all the grains were deforming plastically, the sample then behaved "normally" and hardened. It should, however, be pointed out that if a cyclic stress-strain curve is constructed from the data of Klesnil et al.[6], that at low plastic strain amplitudes, the cyclic stress-strain curve lies below the unidirectional stress-strain curve and thus, overall, cyclic

softening has occurred. (To avoid confusion the terms
cyclic softening and cyclic hardening will be used to
relate the saturation behaviour of the material to the
unidirectional behaviour. The terms hardening and softening
will be used to describe the response of the material to
continued cycling.) The phenomenon of cyclic softening
in annealed polycrystalline body-centred cubic material at
low plastic strain amplitudes appears to be general since
it has also been observed to occur in niobium[10] and
molybdenum.[12] In neither case, however, does softening
occur immediately when cycling is initiated, but is instead
preceded by a period during which the sample hardens -
these tests were performed under constant strain conditions.
On the basis of their results on molybdenum, Beardmore and
Thornton[11] have proposed that this behaviour is due to
the time dependence of dislocation nucleation in body-
centred cubic metals.

Very little work has been performed on single crystals
of body-centred cubic metals. Hempel[13] determined that
during the fatigue of alpha-iron the same slip systems are
observed to operate during unidirectional testing and that
the S-N diagram is independent of crystal orientation - an
observation which has also been reported by Lipsitt and
Horne.[14] Lawrence and Jones,[15] in tests performed
under constant stress, observed the occurrence of the

hardening-softening behaviour previously observed in polycrystals, however in many cases the presence of a well defined saturation stage cannot be deduced from their data. Yoshikawa and Okamoto[15] performed a series of tests at constant total strain on both single and poly-crystalline samples of iron at temperatures of 25°C and -72°C. At 25°C it was found that both the single crystal and polycrystalline samples (except at very low strain amplitudes - $\Delta\varepsilon_\rho \sim \pm 10^{-4}$) cyclically hardened, while at -72°C both hardening and softening occurred depending upon the applied strain amplitude. In single crystal samples, monotonic softening was observed, while polycrystals initially softened and then hardened before attaining saturation. An additional feature noted during this investigation was that the hysteresis loop was asymmetrical when softening occurred, but that as saturation was attained, the asymmetry would disappear. In specimens which hardened monotonically, no significant asymmetry was ever observed. In view of this asymmetry, tests were conducted with initial cycles in tension and compression respectively - no effect of the direction of initial stress application was observed on the softening behaviour.

Information on the fatigue hardening of single crystls of hexagonal metals under reversed cyclic deformation is restricted to zinc[17][18][19], however, the response of

single crystals of beryllium subjected to cyclic
compression has been investigated by Lawley et al.[20]
The tests on zinc have been carried out in both push-
pull[17][18] and alternating torsion.[19] When tested in
push-pull, zinc showed the hardening and saturation
behaviour typical of face-centred cubic metals. When
tested in torsion, however, no well developed saturation
behaviour occurred and hardening continued until some
critical number of cycles was attained. Continued
cycling caused the material to soften.[19] Although
softening did not occur until late in the life (typically
10^5 cycles) it is likely that the observed softening is
genuine and not due to crack formation, since unidirectional
testing of fatigued samples resulted in elongations of
approximately 80% before failure.

Almost all of the work on fatigue hardening has been
performed at room temperature, and little is known of how
these phenomena are affected by temperature. It is known
that, in copper fatigued at large plastic strains, both
the saturation stress and the hardening rate increase as
the test temperature is decreased, while at low plastic
strain amplitudes the opposite effect is observed.[2] The
generality of this behaviour is unknown.

The effect of changing temperature or strain rate
in zinc is more marked, since it may result in a change in

deformation mechanism.[17][18] The effect of strain rate

on fatigue hardening in face-centred cubic metals has

never been explicitly determined. However, the ease

with which the data obtained by differing investigators

may be correlated suggests that strain rate does not

greatly influence the behaviour of these materials.

2.1.2 Dislocation Substructure

In all the materials which have been examined under

both long and short life conditions, it has been established

that two types of substructure occur depending upon the

expected life of the sample.

In the high stress-short life regime, a cell structure

is developed in iron[14][21], copper[3], α-brass[22],

aluminum[23], molybdenum[24] and austenitic stainless

steel.[25] The fact that a cell structure can be induced

in a stainless steel which was calculated to have a

stacking fault energy of only 8 ergs/cm^2, [25] is

indicative of the ability of cyclic deformation to promote

the formation of low energy dislocation arrays even under

relatively unfavorable conditions, since it is widely

acknowledged that extensive cross-slip is necessary for

the formation of a cell structure.

In tests conducted in the low stress-long life

regime, a cell structure is not formed, even in materials

characterized by a wavy slip mode. The structure consists of arrays of dislocations in the form of dipole clusters (copper[26], aluminum[27]), complex pile-ups (α-brass[28]) and a "band structure" consisting of clusters of dipoles and loops (α-iron[29]).

In addition to the influence of plastic strain amplitude or stress amplitude, the dislocation substructure is also sensitive to testing procedure. Tests on copper at constant stress amplitude with zero mean stress resulted in a typical long life dislocation substructure, while when the test was repeated with a non-zero mean stress a cell structure was observed to develop.[30]

The structures which have been outlined above are typical of the bulk material. Examination of the dislocation substructures occurring close to the surface had disclosed that the dislocation substructure observed in the vicinity of the surface may differ from that observed in the bulk material, particularly in persistent slip bands.[31]-[35] This is, however, purely a surface phenomenon and is not merely a characteristic of persistent slip bands, since at distances of up to 200μ from the surface the dislocation substructure is once again characteristic of that observed in the bulk material.[31][32]

Very few observations have been made of the dislocation

substructure generated by reversed cyclic loading in
hexagonal metals, and no systematic study comparable
to those conducted on face centred cubic metals of the
substructure resulting from deformation under a range
of imposed stresses or strains has been conducted.
None of the available micrographs shows a cell
structure,[34][17][19] which as noted earlier, is a
unifying characteristic in cubic materials, but the paucity
of available information permits no conclusions to be
drawn from this fact.

2.1.3 Theories

    Despite the extensive experimental work which has
been conducted on the various aspects of fatigue hardening,
it is surprising how little is understood of the fundamental
processes underlying the phenomenon. Feltner and Laird[3]
have suggested that, at least in copper, the same basic
mechanisms occur during cyclic deformation as during
unidirectional deformation. This parallelism between the
two modes of deformation is attractive, and may be used to
rationalize some of the observed results, however difficulty
is encountered in explaining the phenomenon of saturation
and cyclic softening since neither of these phenomena
are typical of unidirectional deformation. This is not to
suggest that there is no parallelism, merely that some care

must be exercised in employing it. As already noted, this concept permits a reasonable understanding of the observed phenomena provided it is not carried over to those features which are specific to fatigue.

Recently, Holt[37][38] has analyzed the formation of cells from a homogeneous distribution of positive and negative screw dislocations of like Burgers vector, using an approach analogous to that employed for spinodal decomposition. The results of this analysis indicate that dislocations of like sign will segregate into cell walls whose spacing will be proportional to the inverse square root of the dislocation density. Further, it is predicted that the flow stress of a material with a cellular dislocation substructure will be proportional to the inverse cell size - a relationship which has been observed in fatigued metals.[39] It is tempting to attempt to explain several features of the fatigue processes occurring at high plastic strain amplitudes on the basis of this model, notably cyclic softening. It should, however, be borne in mind that on those occasions when cell walls have been examined closely,[3][40] their structure has always consisted of dislocations of more than one Burgers vector, and it has not been established whether or not the inclusion of dislocations with different Burgers vectors would significantly alter the conclusions of the analysis.

In view of the apparent parallelism between cyclic
and unidirectional deformation, it is considered worthwhile
to briefly summarize the tensile properties of α-titanium.

2.2.   Tensile Behaviour of α-Titanium

Slip in α-titanium has been observed on all three
of the slip planes commonly observed in hexagonal metals
(basal, prism and pyramidal),[41][42][43] with the prism
and basal planes favoured at low interstitial concen-
trations[41][43] and the prism and pyramidal planes
favoured at higher interstitial concentration.[42][43]
It has been suggested by Churchman[43] that the preference
for pyramidal slip with increasing interstitial content
may be explaned by considering the effective concentration
of impurity atoms "seen" by a dislocation moving on any
of the three planes. Geometrical considerations indicate
that the effective interstitial content "seen" by a dislo-
cation moving on the pyramidal plane will be only one half
that "seen" by dislocations moving on either the prism or
the basal planes. In these investigations the Burgers
vector was determined to be $1/3 < 11\bar{2}0 >$ [41][42]

It is well known that any generalized deformation
requires the operation of five independent slip systems, a
requirement which cannot be met by the motion of dislocations

of $<11\bar{2}0>$ type Burgers vector only, since no matter how
many slip systems are operating, the number of <u>independent</u>
slip systems can never be greater than four. Some recent
investigations of slip in α-titanium using electron
microscopy have disclosed that dislocations with ($\vec{c} + \vec{a}$)
Burger's vectors (1/3 $<11\bar{2}3>$)[45][46] are also present.
The operation of the system $\{10\bar{1}1\}<11\bar{2}3>$ provides the
fifth system necessary to satisfy the Von Mises criterion.
However, no data is available on how freely these ($\vec{c} + \vec{a}$)
type dislocations can move.

In addition to the above deformation modes, extensive
twinning has also been observed to occur during deformation.
Twin planes have been reported as $\{10\bar{1}2\}$ [42][43],
$\{11\bar{2}1\}$[42][43], $(11\bar{2}2)$[42][43] and $(11\bar{2}4)$[47]. The frequency
of twinning is decreased by raising the temperature or
increasing the interstitial content.

In addition to strongly influencing the slip mode,
interstitial content (particularly oxygen content) also
has a marked effect on the dislocation substructure. In
material with a large interstitial content, bands of long
straight screw dislocations are observed. Continued
straining results in a more uniform dislocation distribution
and subsequently to the formation of complex tangles[44] -
a cell structure was not observed to form. In titanium of
higher purity, the initial dislocation structure is observed

to be much more uniform, and continued straining to approximately ten percent strain resulted in the formation of a cell structure.[44][48] In addition to the above structures, considerable quantities of debris, consisting of edge dipoles and prismatic loops were observed to form. Where a band structure was observed, the debris was associated with the bands. In the absence of a banded structure, the distribution of debris was observed to be much more uniform.[44] The tendency of high interstitial content to inhibit cell formation appears to be considerable, since recent work on the dislocation substructures resulting from the deformation of high interstitial content α-titanium to large strains has also indicated that cells are not formed, even after (logarithmic) strains of two.[49]

Sommer and Tung[50] conducted an investigation of the effect of temperature on the deformation of α-titanium of varying purities. The dislocation substructures which they observed indicate that the effect of increasing the test temperature is analogous to reducing the interstitial content, i.e. as the temperature is increased, a more uniform distribution of dislocations is observed. As the temperature is lowered, the structure reverts to discrete deformation bands.

3. EXPERIMENTAL PROCEDURE

3.1 Sample Preparation

The material employed in all the experimental work
was commercial-purity titanium (Titanium Metals Corporation
Grade Ti-50A) which was obtained in the form of centreless
ground rod having 0.312 inch diameter. The analysis is
given in Table 1. The rod was cold swaged to 0.265 inch
diameter prior to machining test specimens having the
geometry shown in Figure 1. After machining, the gauge
lengths of the samples were electropolished in a solution
consisting of 10 parts methanol, 6 parts n-butanol and
1 part perchloric acid for 30 minutes to remove machining
marks. During polishing, the solution was maintained at
a temperature of -45°C to inhibit the formation of titanium
hydride - the polishing potential used was 17 1/2 volts.

After electropolishing, the samples were encapsulated
in Vycor tubing under an argon atmosphere. Since the
mechanical properties of α-titanium are very sensitive to
interstitial content, and in particular to dissolved
oxygen, great care was taken to avoid oxygen take-up
during heat treatment. The procedure adopted was to first
evacuate the capsule to a vacuum of better than 2×10^{-5} Torr,
followed by twice purging with argon before a final backfill
with argon to a pressure of approximately one-half

TABLE 1

CHEMICAL ANALYSIS

Element	Weight Percent
Carbon	0.018
Iron	0.059
Oxygen	0.108
Nitrogen	0.0025
Hydrogen	0.0010
Titanium	Balance (~ 99.8)
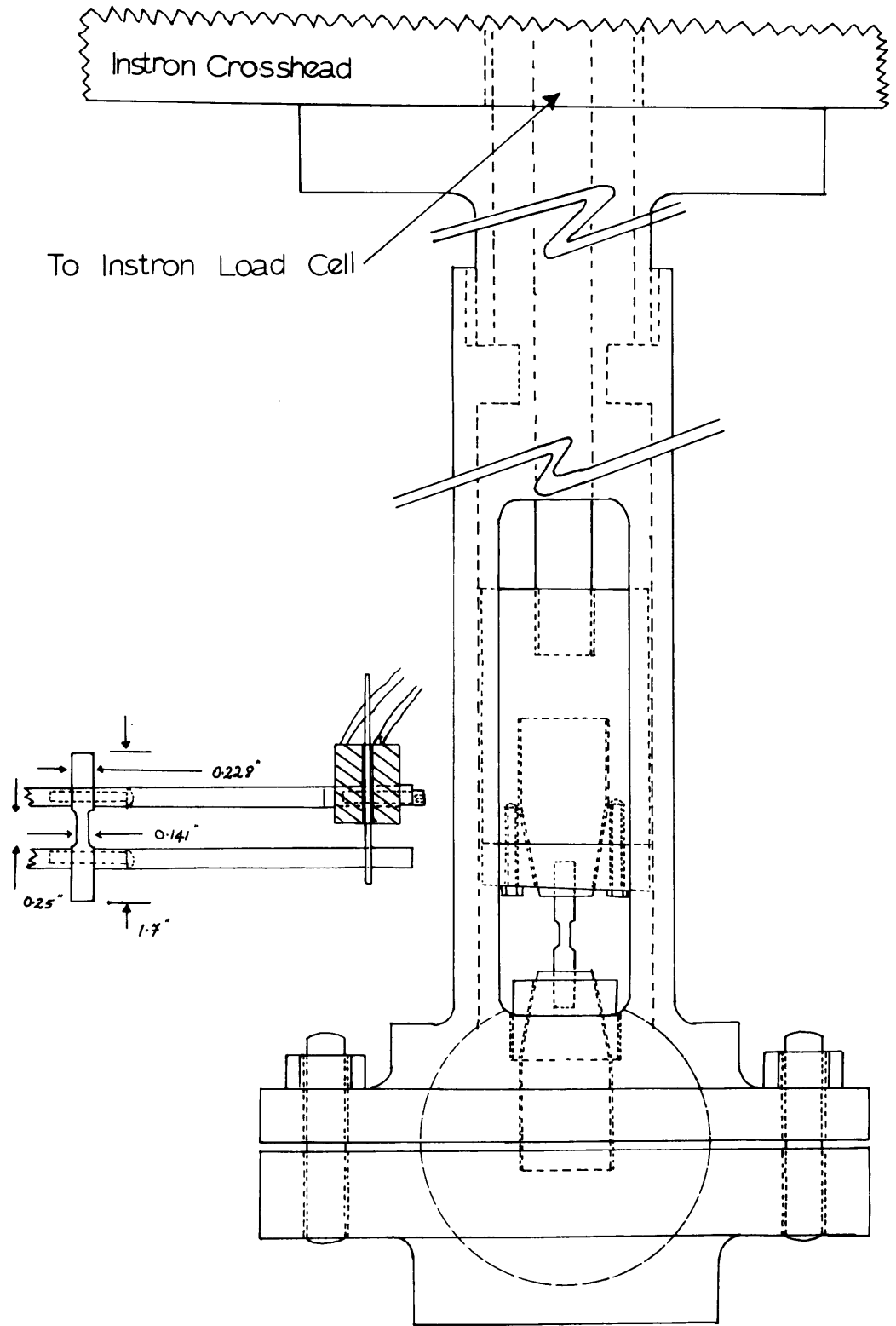
Figure 1. Specimen and Grip Assembly

atmosphere. As a further precaution, all samples were wrapped in titanium foil before being encapsulated; this served to getter any residual oxygen and also to preclude the possibility of any reaction between the sample and the Vycor capsule.

After encapsulation, samples were heat treated to obtain the desired grain size. It was found that a satisfactory range of grain sizes could be developed by heat treating at either 750°C or 650°C. The heat treatments and resultant grain sizes were: a) 15 minutes at 650°C for a grain size of 7μ, b) 15 minutes at 750°C for a grain size of 14μ, c) 100 hours at 650°C for a grain size of 28μ, d) 25 hours at 750°C for a grain size of 80μ. Heat treatment was carried out in batches of three or four samples, and it was found that the mechanical behaviour and grain size were reproducible within any one batch, but that minor variations occurred between batches, particularly at the smallest (7μ) grain size.

3.2 Mechanical Testing

All testing was performed on an Instron (Model TTD) tensile testing machine operated at a nominal strain rate of 3.6×10^{-3} sec^{-1}. Conventional grips were employed for those tests conducted in tension, while for fatigue testing a special grip assembly permitting true axial loading was used.

All fatigue tests were conducted under conditions of constant plastic strain amplitude, since this is a more fundamental parameter than either stress or total strain. Since plastic strain cannot be measured directly, it is necessary to determine the plastic strain from the total displacement and the applied load, both of which are directly measurable.

In the elastic region,

$$\frac{\sigma}{E} = \varepsilon_E \tag{1a}$$

or

$$P/A_0 \, \frac{1}{E} = \frac{\Delta \ell_E}{\ell_0} \tag{1b}$$

$$\Delta \ell_E = kP \tag{1c}$$

where k is a constant. Thus, there exists a linear relation between the applied load and the elastic displacement which it induces. It is therefore clear that if both the displacement and the load may be monitored electrically, that it is possible to generate a signal corresponding to the elastic displacement, subtract it from the signal corresponding to the total displacement and thus generate a signal corresponding to the plastic displacement, and hence the plastic strain.

A block diagram of the apparatus constructed to perform this function is shown in Figure 2 (a schematic and further details may be found in Appendix 1). As shown
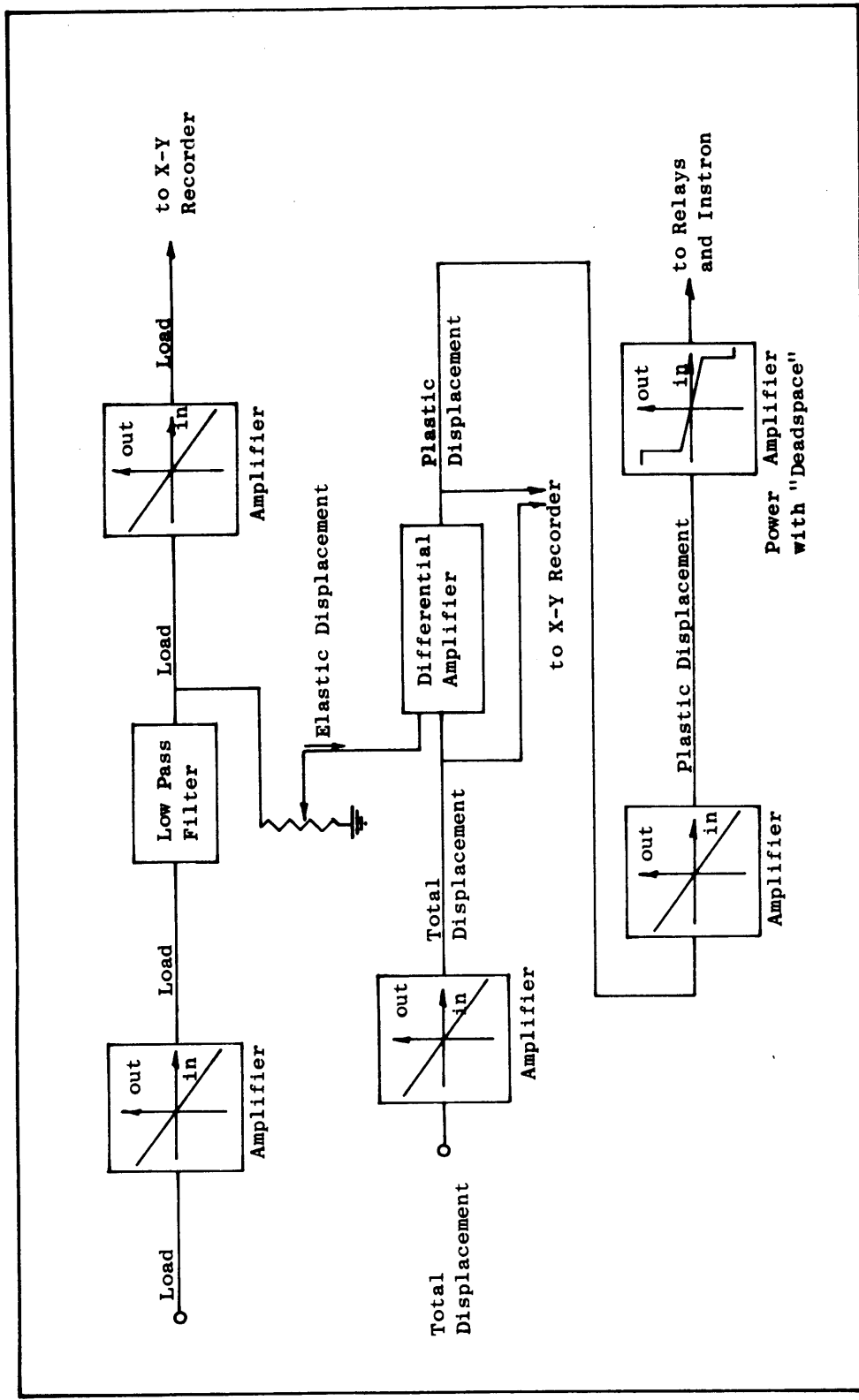
Figure 2. Block Diagram of Controller

in Figure 2, both the load and displacement signals are amplified, and a portion of the amplifier and filtered load signal and the amplified displacement signal are fed into a differential amplifier. To ensure that the output of the differential amplifier corresponds to the plastic displacement, it is necessary to load the specimen in the elastic region and adjust the variable resistor until no output is obtained from the differential amplifier. When this has been done the signal from this amplifier, which now corresponds to plastic displacement, is amplified again and then fed into a power amplifier, which is designed to act as a switch, since it produces no output until the input exceeds some preset value. When the input exceeds this preset value, the amplifier immediately saturates, delivering full power, and switches a relay which causes the Instron to reverse the direction of loading.

No matter how carefully all adjustments were made, it proved impossible to limit deviations from the preset plastic strain amplitude to less than ±0.0001 (corresponding to a displacement of ±2.5 x 10^{-5} inch) and this accuracy was obtainable only with considerable difficulty. Accordingly, except at the lowest plastic strain amplitude used (±0.0005) a test was considered acceptable provided the deviation from the nominal plastic strain amplitude was no greater than ±0.0002 - for tests conducted at a

nominal plastic strain amplitude of ±0.0005, the maximum
allowable deviation was ±0.0001.

A block diagram of the experimental arrangement is
shown in Figure 3. Load and displacement signals were
obtained from the Instron load cell and an LVDT
transducer attached to the shoulders of the sample
respectively, these were fed into the controller described
previously and the amplified signals corresponding to
load and displacement (plastic or total) generated by the
controller fed into an X-Y recorder. The response of the
sample to cyclic deformation was monitored by plotting
hysteresis loops at regular intervals during the course
of the test.

As noted earlier, a special grip assembly was employed
for fatigue testing - this is depicted, as is the specimen
employed, in Figure 1. The grip assembly used was largely
self-aligning, and the degree of adjustment provided by
the "ball and socket" arrangement employed in the lower
grip proved adequate to ensure true axial loading. To
minimize the possibility of inadvertently loading the
specimen above the yield stress during insertion into the
grips, serrated grips were employed. Tests showed that
grip slippage occurred only at loads 30 percent greater
than the maximum load employed during this work.

Testing was usually continued until saturation was
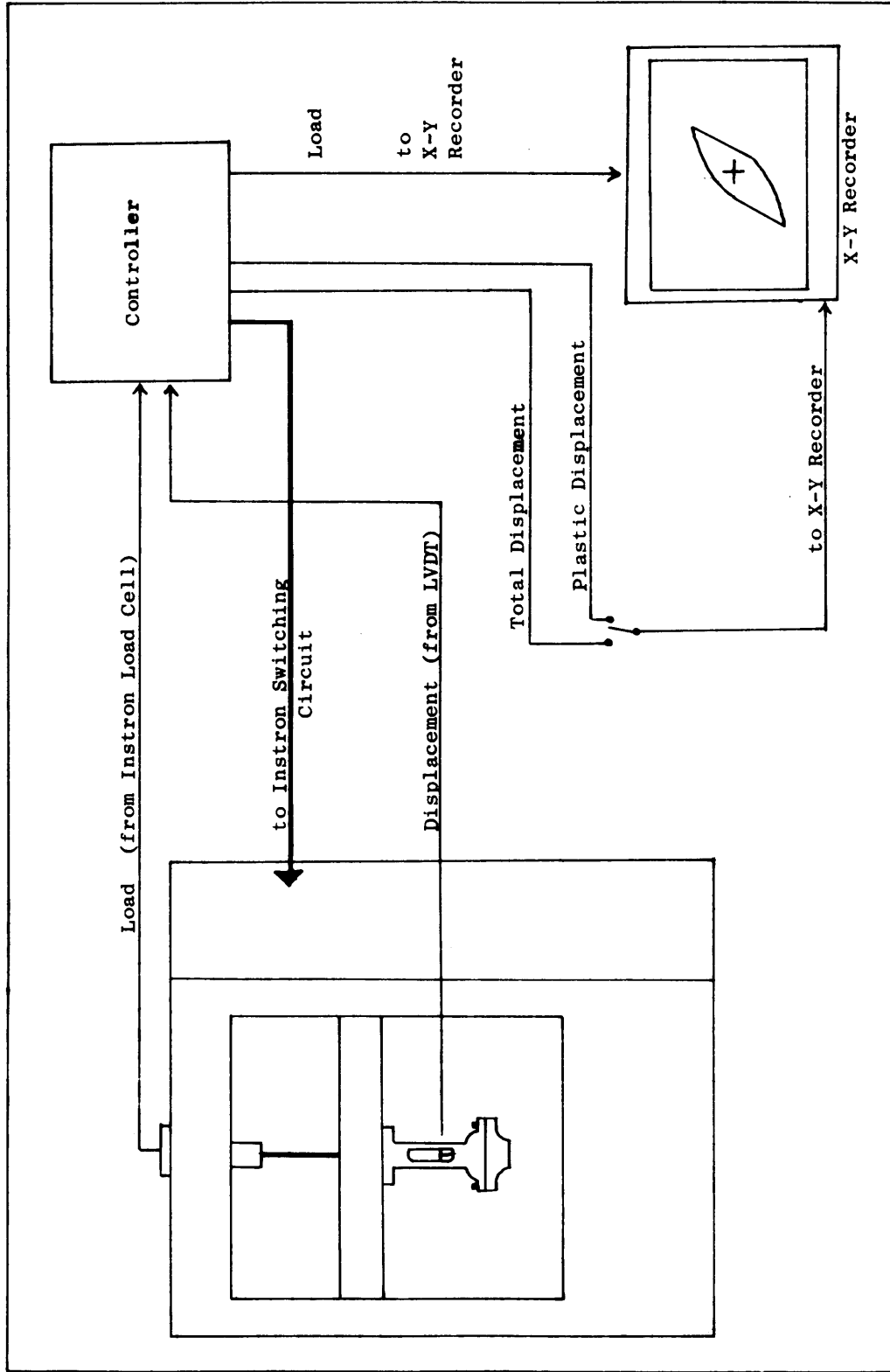
Figure 3. Block Diagram of Experimental Arrangement

attained, but in some cases tests were terminated prior
to saturation to provide foils for electron microscopy.
This permitted the development of the dislocation
substructure to be monitored as testing proceeded.

3.3 Electron Microscopy

After testing, foil blanks were cut from the
specimens by spark machining; the minimum thickness of
the blanks was 0.007 inch which was found to be adequate
to ensure that the foil was free of any damage introduced
by spark machining. Foil blanks were cut both normal and
parallel to the tensile axis. Such sectioning was necessary
since it was found that because of the very pronounced
texture existing in the samples, that foils cut normal
to the tensile axis tended to contain grains whose foil
plane was close to $\{11\bar{2}0\}$ while those cut parallel to the
tensile axis tended to contain grains whose foil plane was
close to $\{0001\}$. It is desirable to be able to obtain
these foil orientations since they permit the Burger's
vectors of any dislocations to be simply established.
Using the (0002) and $(10\bar{1}1)$ reflections, both of which are
readily accessible in $\{11\bar{2}0\}$ foils, permits a distinction
to be made between dislocations whose Burger's vector
includes a $\vec{c}$ component and those which do not, while foils
of type $\{0001\}$ permit ready access to reflections of the
type $(10\bar{1}n)$ which may be used to differentiate between

dislocations of the three $\vec{a}$ type Burger's vectors.[51]

The foil blanks were electropolished at -45°C and 17 1/2 volts using the solution described previously (15 parts methanol, 6 parts n-butanol, 1 part perchloric acid) - vigorous stirring was employed at all times.

The technique used in making foils was to firmly clamp the foil blank in a pair of tweezers, and blank off the edges of the foil blank using Microstop[†] lacquer. The blank was then positioned parallel to the bottom of the dish containing the polishing solution such that it obscured a narrow beam of light projected through the bottom of the dish. During polishing, the foil was observed with a stereo microscope at a magnification of 60x. Perforation was indicated when a small point of light was observed, and polishing was terminated immediately. The foil was then washed in methanol, the Microstop[†] removed using acetone, and the foil rinsed in clean acetone.

There were two difficulties with this method, the first is the considerable length of time required for the polish (about 70 minutes) and the second, is the tendency of the foils produced to be bent. In an attempt to overcome these difficulties, some foils were produced by electro-chemical indenting prior to the final electropolish

---

[†]Trademark, Michigan Chrome and Chemical Company.

by means of an acid jet. The solution used consisted of
30 parts methanol, 8 part perchloric acid and 1 part
hydrochloric acid[*] - this was used at a temperature of
10°C and a potential of 130 volts. After indenting,
foils were produced in the manner previously described,
except that no lacquer was used, and thus foils were
washed in methanol only. Foils produced in this way took
only approximately 15 minutes to polish and were less
bent, however the thin area obtained tended to be more
limited in extent. The reduction in the amount of thin
area is probably a consequence of indenting - the solution
used results in a surface which is somewhat rougher than
is desirable, however no better solution could be developed.

All foils were examined in a JEM-7 electron microscope
operating at 100kV. This microscope was equipped with a
goniometer stage capable of 30 degrees of tilt and a dark
field attachment. Where possible, micrographs were taken
in bright field under two-beam conditions - micrographs
were also taken using conventional dark field and weak
beam dark field. Wherever possible, micrographs taken

---

[*]CAUTION - This solution is DANGEROUS. If heated above
25°C it may spontaneously ignite or explode. Great
care should be exercised while mixing or using this
solution.

in multibeam bright field were avoided.

3.4 Optical Microscopy

3.4.1 Grain Size Determinations - It has already been

noted that grain size determinations in α-titanium are
complicated by the difficulty of obtaining a uniform
etch.[44] A number of etchants and etching procedures
were tried in the course of this investigation, and the
most satisfactory was a chemical etch consisting of 1
part hydrofluoric acid, 1 part nitric acid and 2 parts
glycerol. Specimens were mechanically polished to
0.3 micron alumina, given a short electropolish, etched
and examined under polarized light. The use of polarized
light minimizes the probability of failing to observe grain
boundaries, although as the grain size is reduced, even
the use of polarized light may fail to reveal all the grain
boundaries. All grain size measurements were made from
micrographs in the conventional manner using a minimum of
60 grains for each determination.

3.4.2 Observation of Twins - The procedure adopted for

viewing twins in deformed samples was the same as that
employed for grain size determinations, with the exception
that subsequent to mechanical polishing, samples were
electropolished for 20 minutes to remove any twinning

induced by mechanical polishing. To ensure that a 20
minute electropolish was adequate a sample was repolished
for 60 minutes subsequent to being examined, and re-
examined after the second electropolish - no difference
in the twin density or the distribution of twins was
discerned between micrographs taken prior to and subsequent
to the final electropolish.

4. RESULTS

4.1 Mechanical Testing

4.1.1 Tensile Tests - To obtain an adequate range of grain sizes, it proved necessary to anneal samples at temperatures of 650°C and 750°C. It is known that α-titanium develops a pronounced annealing texture. In an attempt to determine whether the annealing texture was affected by the temperature of annealing, a series of tensile tests was conducted on samples of varying grain sizes obtained by annealing at either 750°C or 650°C. A plot of Lower Yield Stress (or, 0.2% offset stress in the case of large grained samples) versus the inverse square root of grain size based on data obtained from these tests is shown in Figure 4. Some scatter in the data is apparent, but no gross change in mechanical behaviour with annealing temperature, except for that occasioned by grain size, can be detected. Both sets of data may be described by the same relation

$$\sigma_y = \sigma_o + k_y d^{-1/2} \tag{2}$$

where σ_o is 20.3 Kg/mm^2 (28,800 psi) and k_y is 1.09 $Kg/mm^{3/2}$. These values are in reasonable agreement with those obtained by Jones and Conrad.[44]
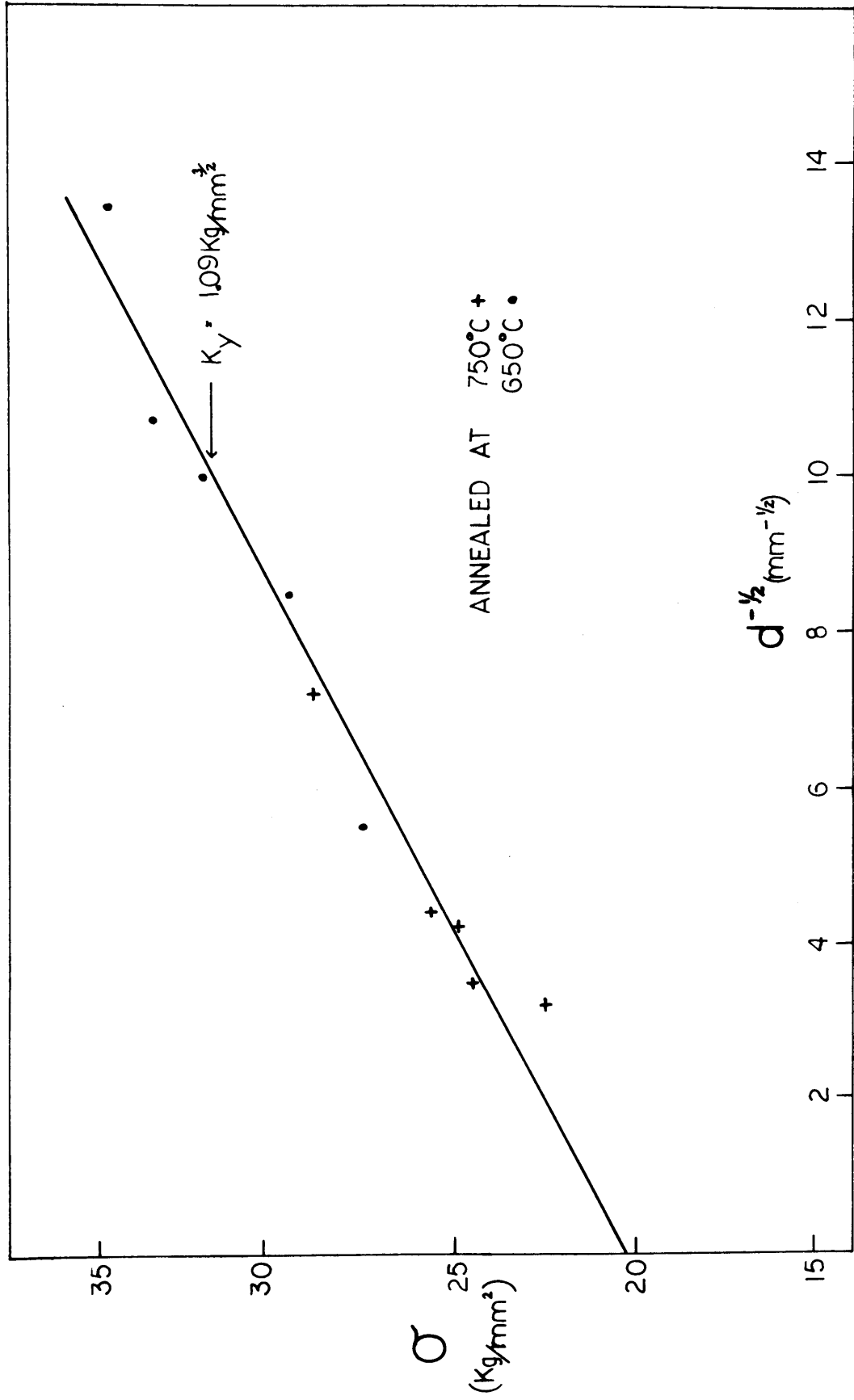
Figure 4. Plot of lower yield stress or 0.2% offset stress versus inverse square root of grain size for α-titanium annealed at 650°C and 750°C.

It is clear that the maximum deviation from the above
relation occurs in the samples having the smallest (5µ) and
largest (90µ) grain sizes. Part of the deviation observed
in the 5µ grain size sample may be attributable to the
difficulty of accurately determining grain sizes optically
at such fine grain sizes.[44] The explanation for
behaviour of the 90µ grain size sample is not so obvious.
However, optical microscopy disclosed that the density of
twins increased with increasing grain size. Too much
should not be made of this fact, since no special pains
were taken to strain each sample by the same amount. It
is however, possible that the behaviour of the 90µ grain
size sample is attributable to the fact that deformation
twinning is becoming more important as a deformation mode.

4.1.2 Fatigue Tests - Many parameters may be used to
monitor the mechanical properties of a material under cyclic
deformation. The parameter used in this investigation is
the average peak stress ($\bar{\sigma}$) defined as one-half of the sum
of the modulus of the peak tensile and peak compressive
stresses developed on any one cycle, that is,

$$\bar{\sigma} = 1/2 \ (|\sigma_P^T| + |\sigma_P^C|) \qquad (3)$$

where

σ_P^T = Peak Tensile Stress

σ_p^C = Peak Compressive Stress

This index of mechanical properties was adopted rather than the peak tensile or compressive stress alone, since it was noted that, particularly at low plastic strain amplitudes, the hysteresis loop was frequently asymmetrical, i.e., the maximum stress in one direction was significantly greater than the maximum stress in the other direction.

It is well known that the area within a hysteresis loop is a measure of the work done in deforming the sample through one cycle. The relationship between the work done in one cycle and stress and plastic strain is given by

$$\Delta W = A(|\sigma_p^T| + |\sigma_p^C|) \cdot \Delta \varepsilon_p \qquad (4)$$

where

ΔW = Work done/cycle

$\Delta \varepsilon_p$ = Plastic strain

A = Geometrical factor reflecting the loop shape.

Provided the loop shape does not change appreciably (i.e. A is constant), then in tests conducted at constant plastic strain amplitude

$$\Delta W \propto (|\sigma_p^T| + |\sigma_p^C|) \qquad (5)$$

Clearly, if the hysteresis loop is symmetrical, either
the peak tensile or the peak compressive stresses may be
used as an index of mechanical behaviour. However, if, as
in the present investigation, the hysteresis loop is
asymmetrical, account must be taken of both the peak
tensile and compressive stresses. The assumption of an
unchanging loop shape is reasonably good. The loop shape
does change during the course of the test, but except in
isolated instances, changes in loop shape were accompanied
by changes in peak stresses. Both the change in loop shape
and the changes in the peak stresses acted to either increase
or decrease the area of the loop. At no time was any
"competition" between these effects observed. Clearly,
provided account is taken of both the peak compressive and
the peak tensile stresses, any numerical factor may be
introduced. The factor of one-half ($\bar{\sigma} = 1/2(|\sigma_P^T|+|\sigma_P^C|)$)
was introduced to facilitate comparison of the data obtained
in this investigation with that obtained by other investigators
who employ peak stress (either tensile or compressive) as
their index of mechanical behaviour.

Before presenting the data from the fatigue tests
it is desirable to first consider the accuracy and
reproducibility of the data. It was determined that, as
mentioned earlier, it was impossible to control the imposed

plastic strain amplitude to better than ±0.0001, no
matter how much care was employed in conducting the test.
However, once established, the imposed plastic strain
amplitude did not change measurably throughout the course
of the test. The primary contribution of the inability to
accurately predict the imposed plastic strain amplitude
was therefore to reduce the reproducibility of the data.
It did not significantly effect the accuracy of measurements
made during the course of a test on one particular sample.

The uncertainty in measurements conducted on the same
sample during the course of the test is estimated (from
consideration of load cell inaccuracy, friction, errors in
the X-Y recorder, etc.) to be less than 2 1/2 per cent.
In fact, the accuracy of the data is probably higher than
this, since the load measuring system was always recalibrated
at the conclusion of the test - the maximum calibration error
detected was ±1%. Thus, in discussing the behaviour of
individual samples, an error of ±0.7 Kg/mm^2 (± ~1000 psi)
will be assumed.

In comparing the behaviour of samples tested at
differing plastic strain amplitudes, however, or in
defining the saturation stress characteristic of a given
plastic strain amplitude, account must be taken of the
deviation of the imposed plastic strain amplitude between

samples. As will be shown later, the saturation stress ($\bar{\sigma}_{sat}$) may be related to the imposed plastic strain amplitude by

$$\bar{\sigma}_{sat} = \bar{\sigma}' + B(\Delta\epsilon_p)^{1/2} \qquad (6)$$

where $\bar{\sigma}'$ and B are constants. Assuming this relationship to hold throughout the course of the test, the percentage error in stress is one-half the percentage error in the plastic strain amplitude. Since the error in the plastic strain amplitude may be considerable (±20% at a plastic strain amplitude of ±0.0005) it may be asked why the measured rather than the preset plastic strain amplitudes were not employed in reporting the data. This procedure is only possible when deviations from the preset plastic strain amplitudes are in the same direction on both tensile and compressive half cycles, e.g. the measured plastic strain amplitude is ±0.0006 rather than ±0.0005. In practice, however, it was usual for the plastic strain amplitudes in the tensile and compressive half cycles to differ, e.g. plastic strain amplitudes of +0.0006 and -0.0004. In light of this, the method adopted, that of reporting the behaviour as being typical of the nominal plastic strain amplitude and indicating the error is preferred.

The error bars appended on all data obtained from fatigue tests reflect both the errors in the measurements on individual samples, and the deviation between the imposed

and nominal plastic strain amplitudes.

Figure 5 indicates the effect of grain size upon the behaviour of samples tested at a plastic strain amplitude of ±0.01. The most noticeable features of these curves are that the initial rate of hardening appears to be unaffected by grain size, although the behaviour at later stages is affected by grain size, and the fact that neither the 28μ grain size samples nor the 80μ grain size samples exhibit a well defined saturation region. The apparent saturation region exhibited by 7μ grain size samples and 14μ grain size samples is slightly misleading, since, although the peak stress did not change in the saturation regime, the loop shape did change. The change in loop shape was such as to reduce the area of the loop, and thus the work done per cycle decreased as cycling continued. The magnitude of the effect was, however, minor.

Figure 6 shows the effect of plastic strain amplitude on 80μ grain size samples. It is clear that two distinct modes of behaviour exist, one being characteristic of high plastic strain amplitude fatigue and the other being characteristic of low plastic strain amplitude fatigue. At high plastic strain amplitudes (±0.006 and ±0.005) monotonic hardening followed by saturation is observed - the unusual behaviour of the samples fatigued at a plastic strain amplitude of ±0.01 will be considered in the Discussion.
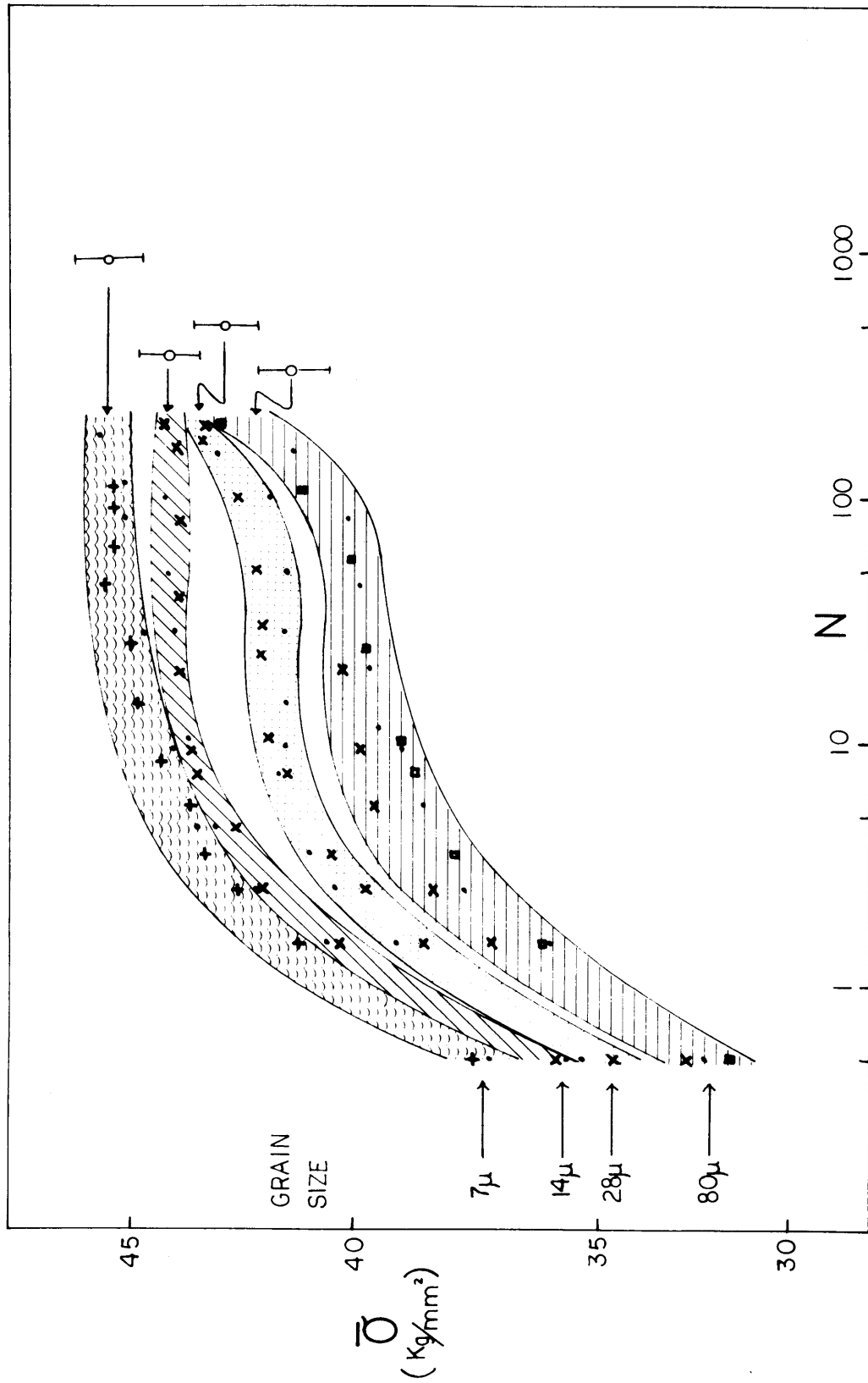
Figure 5. Average peak stress versus number of cycles for samples of 7μ, 14μ, 28μ and 80μ grain size fatigued at a plastic strain amplitude of ±0.01. All samples of one grain size are enclosed in cross-hatched bands.
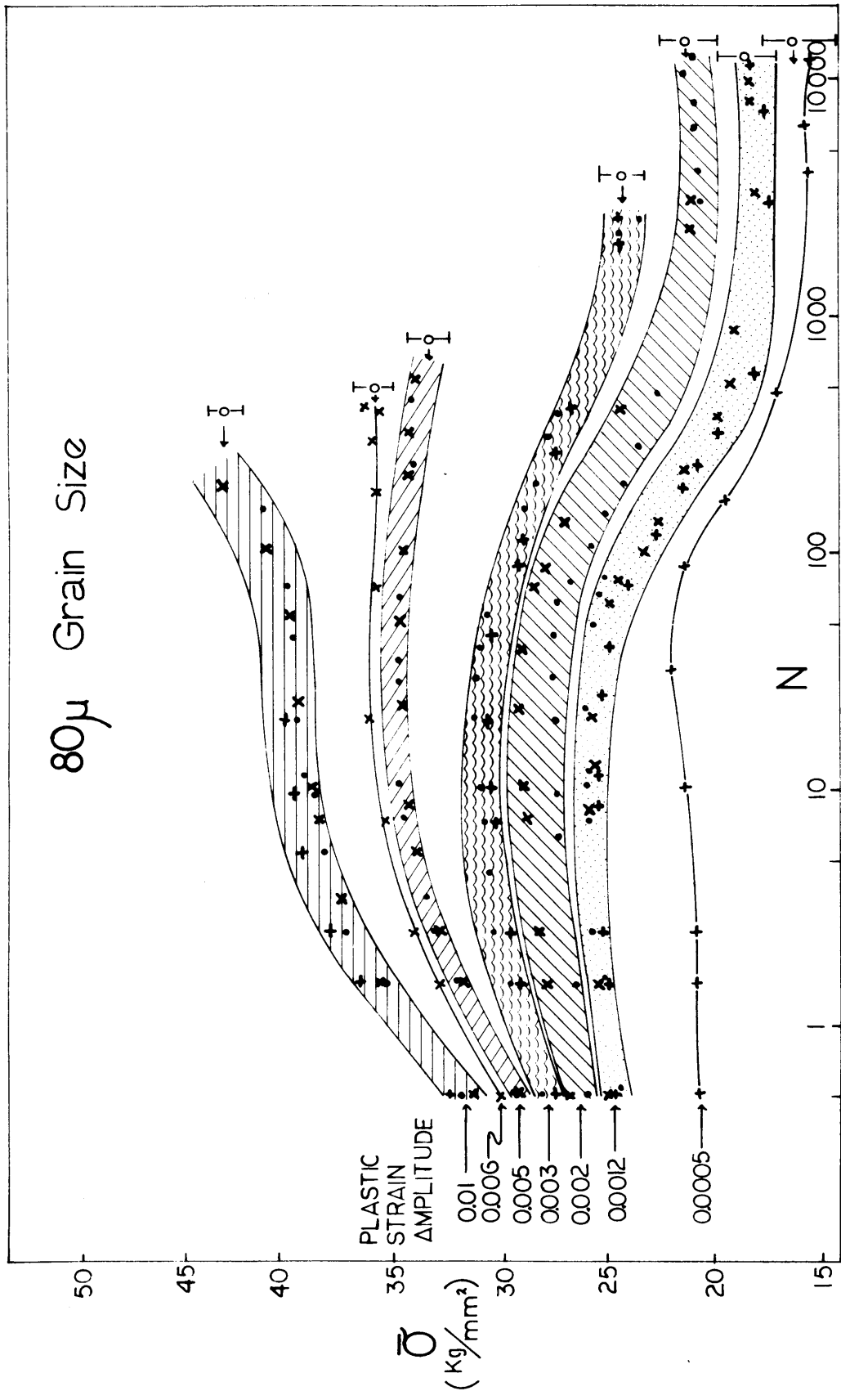
Figure 6. Average peak stress versus number of cycles for 80μ grain size samples fatigued at plastic strain amplitudes of ±0.0005, ±0.0012, ±0.002, ±0.0003, ±0.005, ±0.006 and ±0.01. Multiple tests at one plastic strain amplitude are enclosed in cross-hatched bands. Single tests are indicated by a curve through the data.

At low plastic strain amplitudes, however (±0.0005 to ±0.003) the samples initially harden but subsequently soften to a stress which is less than the initial flow stress (i.e. that developed on the first cycle).

The influence of plastic strain amplitude on the behaviour of the 7μ grain size samples is shown in Figure 7. The trend previously noted for two types of behaviour to exist depending upon plastic strain amplitude is obvious. Unlike the 80μ grain size material, however, the transition between the two modes of behaviour is more gradual, and the data for the two tests conducted at a plastic strain amplitude of ±0.005 is sufficiently disparate to suggest that the transition in behaviour occurs at approximately this plastic strain amplitude. One feature of the low plastic strain amplitude tests on the 7μ grain size samples which was not observed in tests on 80μ grain size samples is the "softening" which occurs between the first and second cycles. This softening is attributed to the lack of stiffness of the testing assembly - a complete analysis is given in the Dicussion.

It was remarked earlier that, particularly at low plastic strain amplitudes, the hysteresis loops tended to be asymmetrical. It was noted that the peak tensile stress was always greater than the peak compressive stress. Since all tests were conducted by initially loading the sample
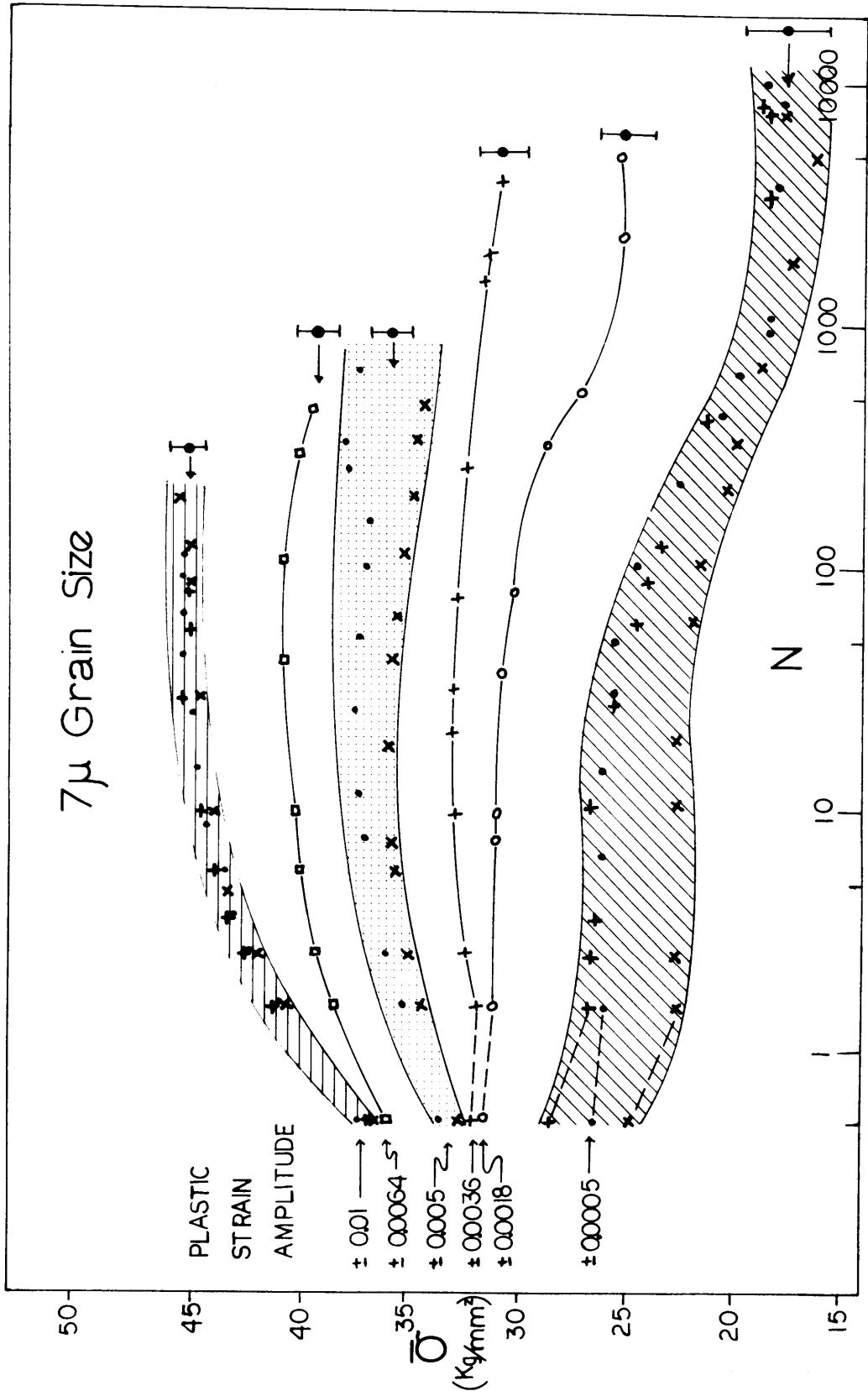
Figure 7. Average peak stress versus number of cycles for 7μ grain size samples fatigued at plastic strain amplitudes of ±0.0005, ±0.0018, ±0.036, ±0.005, ±0.0064 and ±0.01. Multiple tests at one plastic strain amplitude are enclosed in cross-hatched bands. Single tests are indicated by a curve through the data.

in tension it was considered that the asymmetry might be related to the direction of initial load application. Accordingly, in testing the 7μ grain size samples at a plastic strain amplitude of ±0.0005, one test was conducted in which the load was initially applied in tension.   For comparison, another sample from the same batch was tested at the same plastic strain amplitude (±0.0005), but in this case the load was initially applied in compression. Representative hysteresis loops obtained from these tests are shown in Figure 8. It will be noted that the direction of maximum peak stress is the direction of initial load application. The average peak stress obtained as a function of number of cycles for these two tests has already been shown in Figure 7. However to indicate the reproducibility of the data it has been replotted on an expanded scale and is shown in Figure 9. Considering the differences in the imposed plastic strain amplitudes (see Figure 8) the agreement between the two sets of data is good.

A convenient way of describing the behaviour of a material under cyclic loading is the cyclic stress-strain curve. This is generated by plotting the imposed plastic strain amplitude versus the saturation stress. In attempting to plot such a curve from the data contained in Figures 6 and 7, it was determined that there existed a discontinuity

Figure 8. Effect of direction of initial load application
on the form of the hysteresis loop. Plastic strain amplitude
±0.0005. 7μ grain size.

a) Load initially applied in compression.

b) Load initially applied in tension.

c) Form of the hysteresis loops developed at saturation
    for initial tensile and compressive loading.
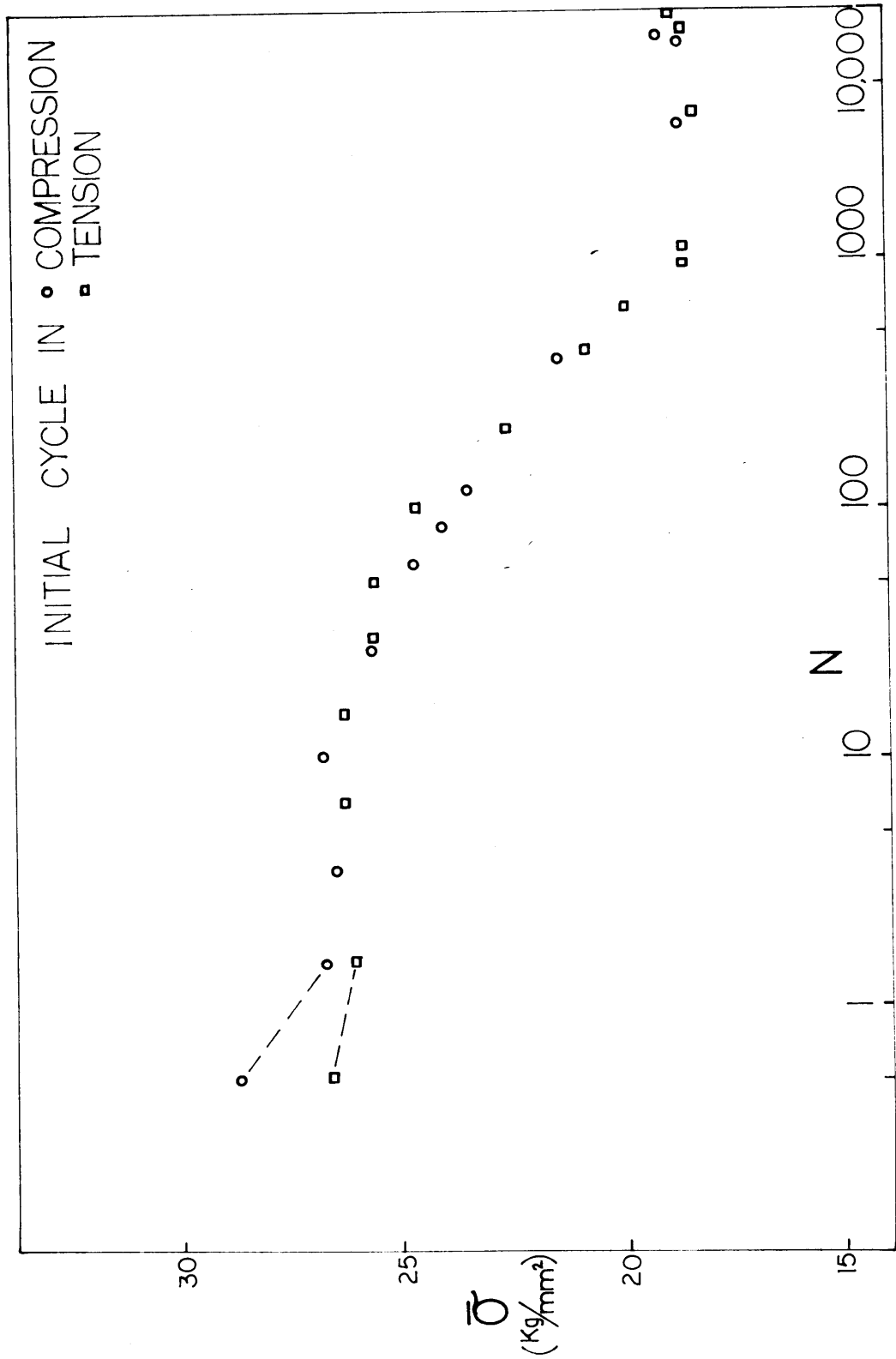
Figure 9. Effect of initial direction of load application on average peak stress. Average peak stress versus number of cycles for tests shown in Figure 8. Plastic strain amplitude ±0.0005. 7μ grain size.

in the curve. This occurred between those plastic strain
amplitudes where hardening only occurred and the plastic
strain amplitudes where hardening/softening behaviour was
observed. It was, however, determined that both sets of
data could be described by the relationship

$$\bar{\sigma}_{sat} = \bar{\sigma}' + B(\Delta\varepsilon_p)^{1/2} \tag{7}$$

where the constants $\bar{\sigma}'$ and B depended upon hardening mode.
Further, it became obvious that in those samples which
hardened and softened, the maximum stress was related to
plastic strain amplitude by a similar relation to that
already described. In addition, the constants $\bar{\sigma}'$ and B,
were the same as those typical of the saturation stress
in high plastic strain amplitude fatigue.

Figures 10 and 11 show the variation of maximum stress
and saturation stress with the square root of the imposed
plastic strain amplitude for the 80µ grain size and 7µ
grain size samples respectively. In Figure 10, the 80µ
grain size sample tested at a plastic strain amplitude of
±0.01 has not been included since no well defined saturation
region manifested itself. In plotting the data, the slight
softening observed in the 7µ grain size sample tested at
±0.0064 plastic strain amplitude and the 80µ grain size
samples tested at ±0.005 plastic strain amplitude has been
ignored. The small error bars indicated on the 7µ grain
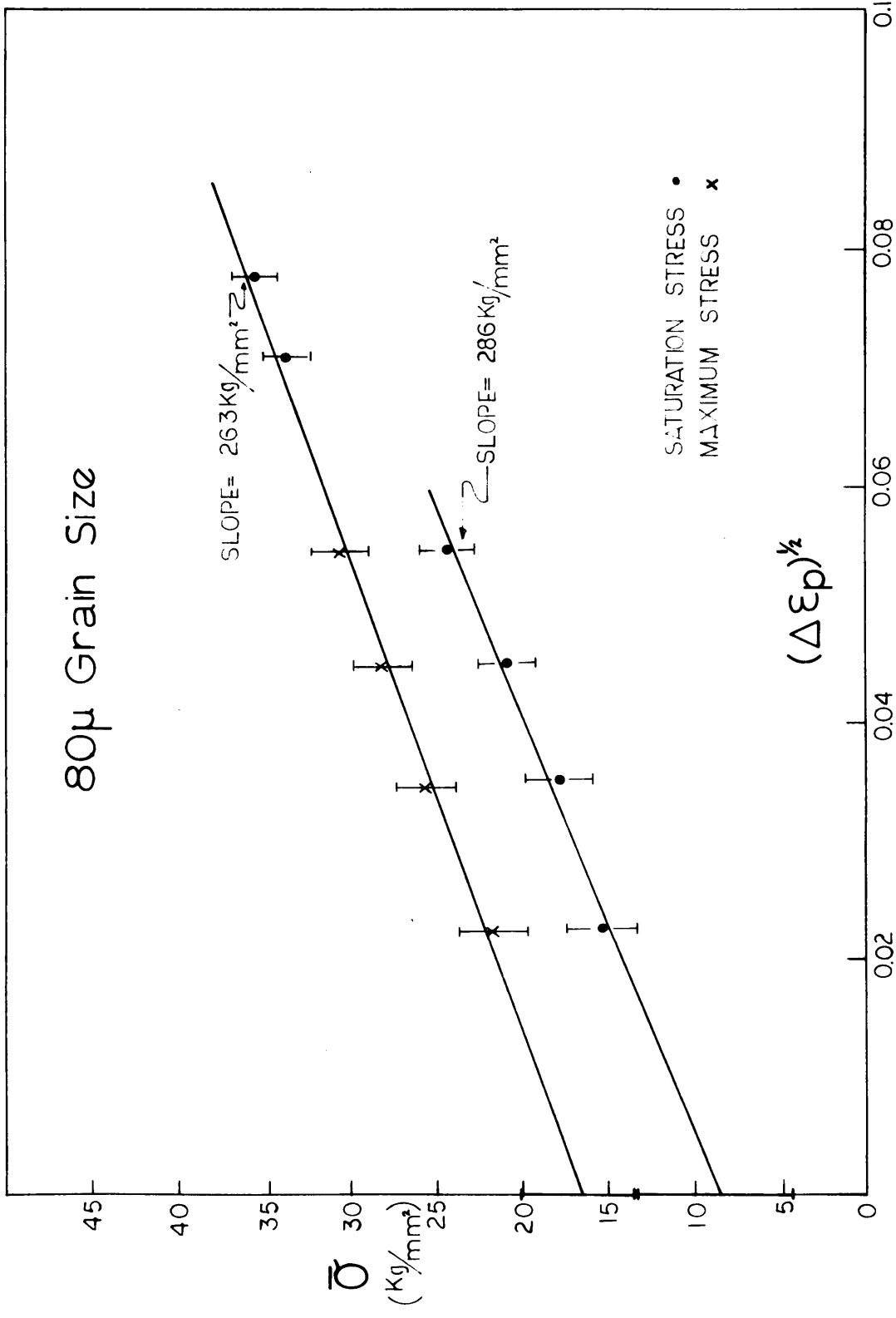
Figure 10. Average peak stress at saturation and maximum average peak stress versus square root of plastic stream amplitude. 80μ grain size.

61.
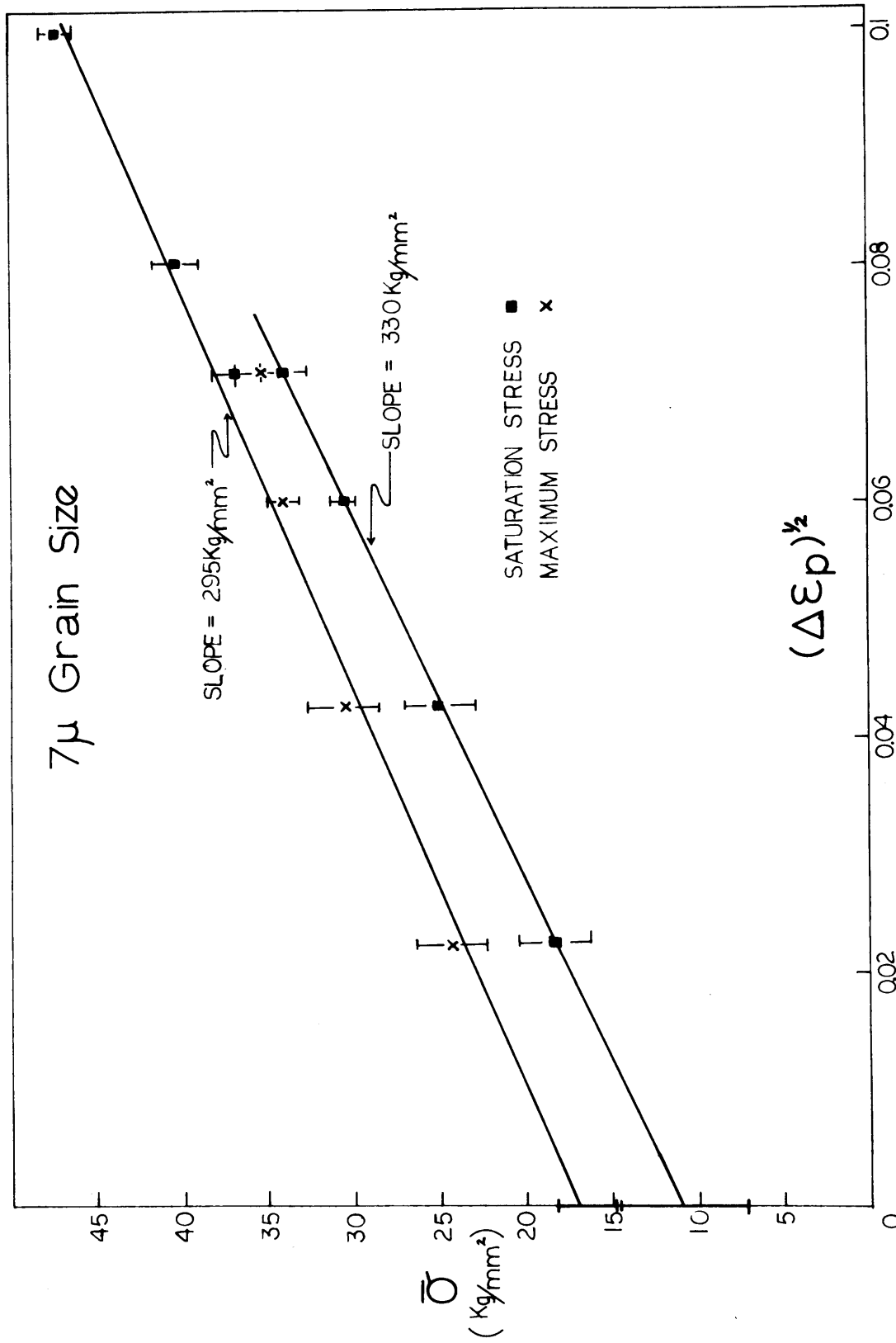
Figure 11. Average peak stress at saturation and maximum average peak stress versus square root of plastic strain amplitude. 7μ grain size.

size sample tested at ±0.0036 plastic strain amplitude, reflect the fact that on this test the measured plastic strain amplitude was precisely ±0.0036.

The same trend is clearly visible in both sets of data. There are two intercepts when the data is extrapolated back to zero plastic strain amplitude, the one characteristic of high plastic strain amplitude fatigue and the other characteristic of low plastic strain amplitude fatigue. These intercepts are separate and distinct, since the error bars associated with these intercepts, generated by drawing those curves which are just enclosed by the error bars on the data do not overlap. To be sure, the separation between the error bars is slight (~ 0.25 Kg/mm^2 or ~ 400 psi) but since maximum errors have been considered throughout, this difference is significant.

In addition to generating different intercepts, the curves, as drawn, indicate that in both the 7μ grain size and 80μ grain size cases, samples tested at high plastic strain amplitudes are more sensitive to plastic strain amplitude than those tested at low plastic strain amplitudes. However, the error in the data is such that numerous straight lines, each having a different slope, may be drawn, and thus no particular significance is attributed to this feature.

4.2 Electron Microscopy

The strong dependence of mechanical behaviour upon imposed plastic strain amplitude was discussed in the previous section. It was found that the dislocation substructure exhibited a similar dependence upon plastic strain amplitude. Two different dislocation substructures were observed, one typical of low plastic strain amplitude fatigue, the other typical of high plastic strain amplitude fatigue. For convenience, these structures will be discussed separately.

4.2.1 Low Plastic Strain Amplitude Fatigue

4.2.1.1 Structure at Saturation - As will be obvious in viewing the micrographs, no significant lattice rotations were observed to arise as a result of the dislocation substructure developed. Consequently, well defined Kikuchi bands were always observed which, as noted by Okamoto, Levine and Thomas[51], permit orientations to be determined somewhat more easily than spot patterns alone. It is also possible, and indeed somewhat trivial, when Kikuchi bands are present to tilt the crystal in such a way that a two beam case is readily obtained. In this part of the investigation, two beam bright field has been used almost exclusively since it is predicted that the contrast obtained in bright

and dark field is identical <u>provided</u> no more than one diffracted beam is strongly excited.[52] Care was taken to ensure that this condition always pertained.

Figure 12 indicates the form of the structure when viewed in a <11$\bar{2}$0> type direction. The operating reflection in Figure 12a is {10$\bar{1}$1} which images dislocations with two of the three <11$\bar{2}$0> type Burgers vectors and any dislocations whose Burgers vector includes a $\vec{c}$ component. In Figure 12b, (0002) has been used as the operative reflection. This reflection will image only dislocations whose Burgers vector includes a $\vec{c}$ component - all dislocations with $\vec{a}$ type Burgers vectors are rendered invisible, since both $(\vec{g}\cdot\vec{b})$ and $\vec{g}\cdot(\vec{b} \times \vec{u})$ are zero.[53] Arrays of dipoles may be seen clearly in Figure 12a at the edges of the dislocation clusters, but the density within the clusters themselves is too high to permit individual dislocations to be resolved. In the relatively dislocation free areas adjacent to the dense dislocation clusters, some isolated dislocations whose line vector is approximately normal to the line vector of those dislocations comprising the dipoles may be observed.

An unambiguous identification of edge and screw dislocations is impossible with a foil whose foil plane is {11$\bar{2}$0}. However, provided slip occurs only on the prism planes, it is possible to infer the nature of the dislocation

(a)

TRACE OF BASAL PLANE

2μ
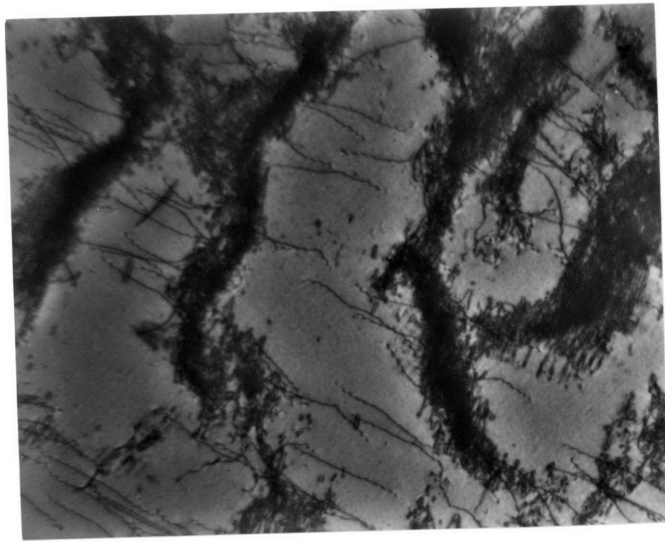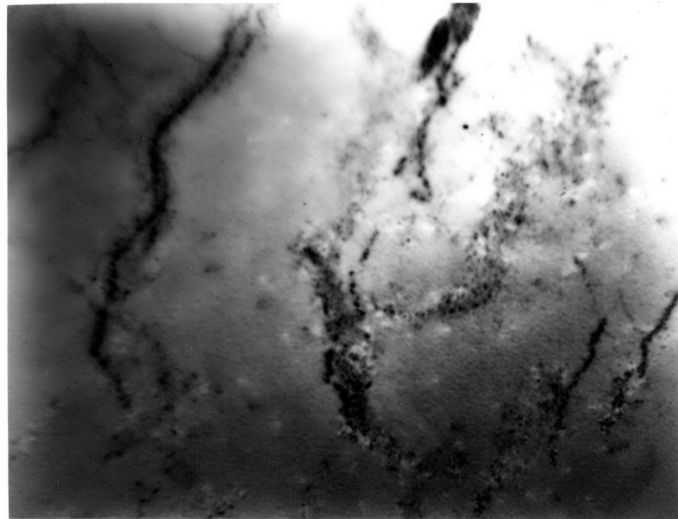
(b)

Figure 12. Structure developed at saturation in an
80μ grain size sample fatigued at a plastic strain
amplitude of ±0.002. Beam direction <11$\bar{2}$0>.
Operative reflection a) {10$\bar{1}$1}
                      b) (0002)

segments from geometrical considerations, provided the trace of the basal plane is known. Those dislocation segments which are normal to the basal trace must be largely edge in character, and those which are parallel to the basal trace must be largely screw in character. Using this analysis, it is clear that the dipoles are composed of edge dislocations and that those isolated dislocations in the regions of low dislocation density are screw dislocations. Clearly, the weight which can be attached to such a means of differentiating between edge and screw segments depends upon whether or not significant slip occurs on planes other than prism planes. In this regard it should be pointed out that any slip traces observed could be attributed satisfactorily to prism slip, and thus, in accord with Churchman,[43] it is believed that the dominant slip planes in material of this purity are the prism planes. Figure 12b indicates that a considerably density of dislocations with Burgers vectors which include a $\vec{c}$ component exist. These dislocations, however, are observed only in regions where a high density of dislocations possessing $\vec{a}$ type Burgers vectors exist.

Figures 13 and 14 are micrographs taken under the same conditions (<11$\bar{2}$0> beam direction, {10$\bar{1}$1} reflection) as Figure 12a. They have been included to indicate the variability of the structure observed. Figure 13 shows a

TRACE OF   BASAL PLANE

2μ
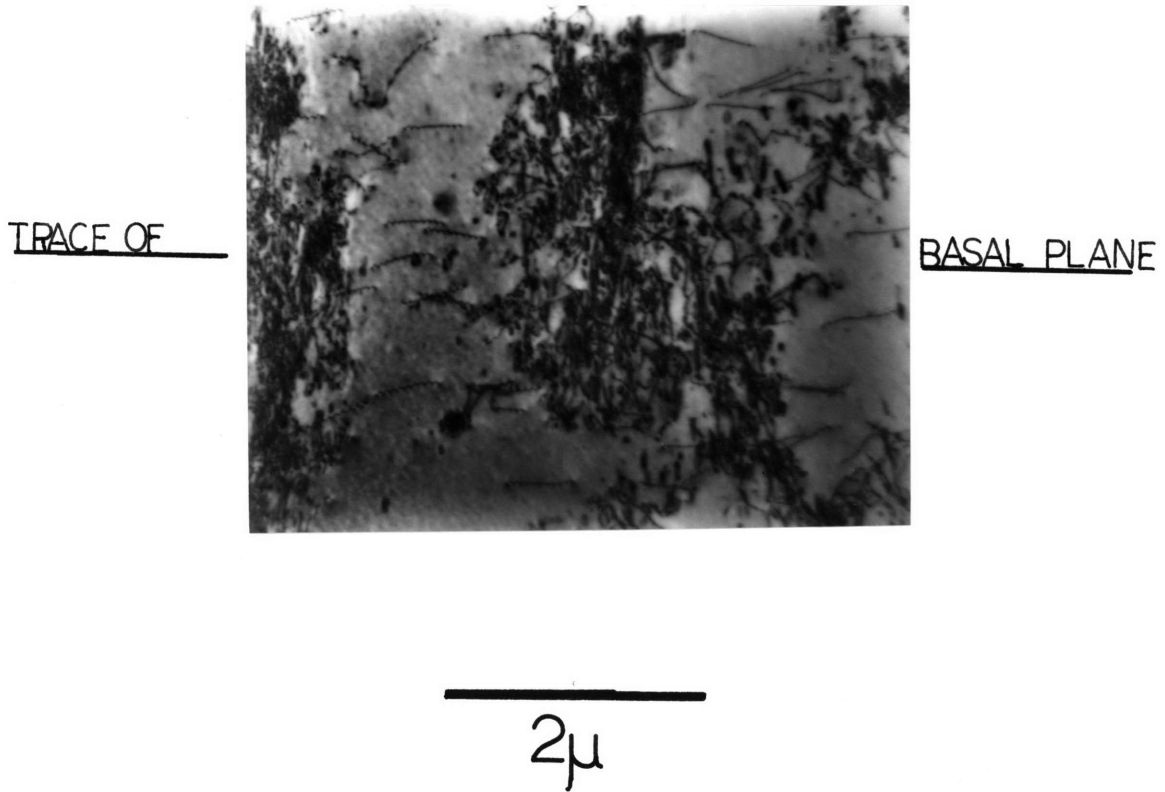
Figure 13. Structure developed at saturation in an 80μ
grain size sample fatigued at a plastic strain amplitude
of ±0.002. Beam direction <11$\bar{2}$0>. Reflection {10$\bar{1}$1}.
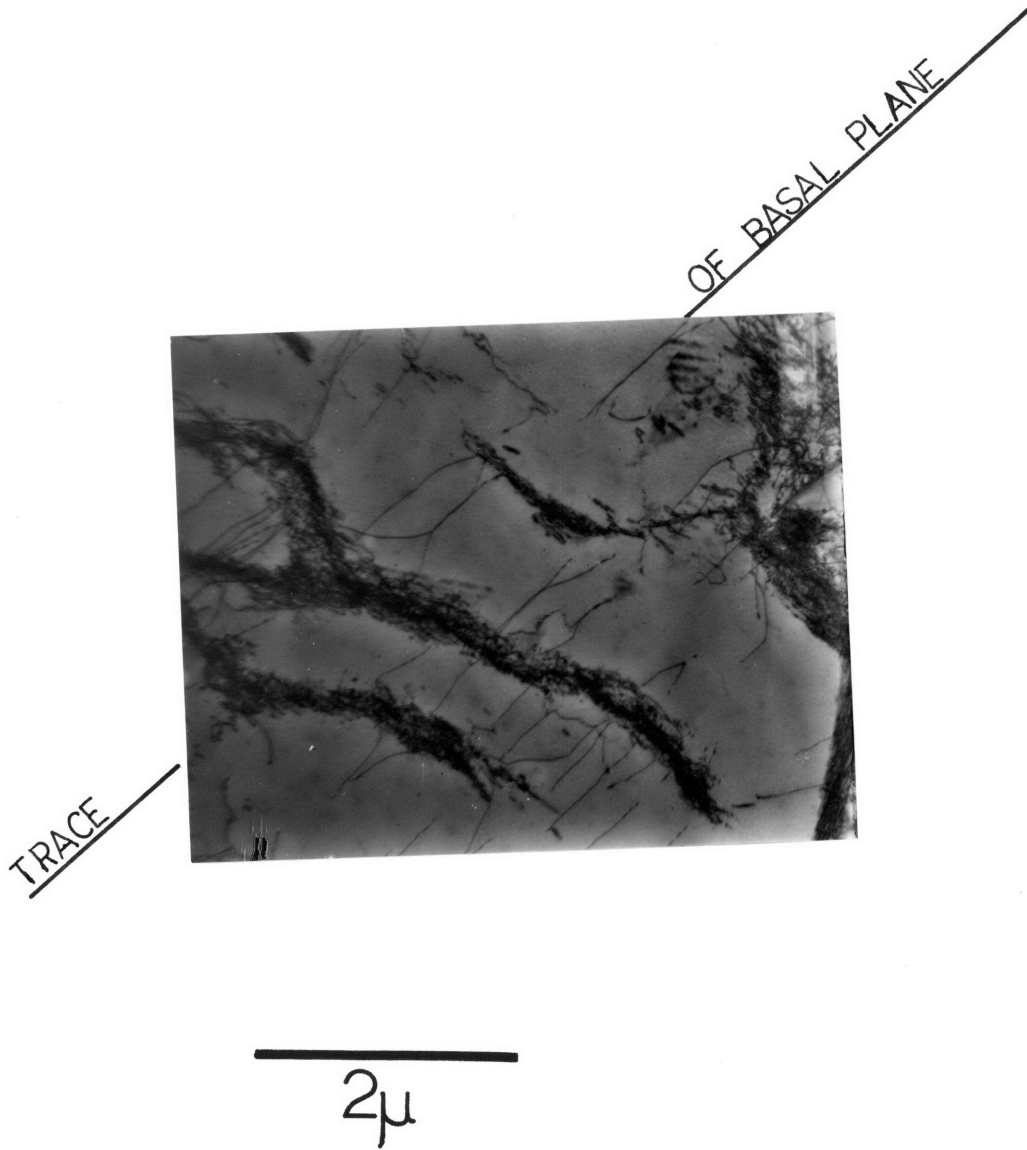
Figure 14. Structure developed at saturation in an 80μ grain size sample fatigued at a plastic strain amplitude of ±0.002. Beam direction <11$\bar{2}$0>. Reflection {10$\bar{1}$1}.

structure in which dipoles may readily be discerned, and showed a much more uniform dislocation distribution than Figure 12a - except for these reservations the structures are very similar. Figure 14 on the other hand, shows scant evidence of dipoles, but does manifest the feature of regions of high dislocation density separated by regions of low dislocation density. The feature of screw disloca-tions in those regions of low dislocation density is also apparent.

Foils with an (0001) foil plane were also examined, primarily in an attempt to distinguish between dislocations with differing $\vec{a}$ type Burgers vectors. Unfortunately, distinguishing between edge dislocations of differing $\vec{a}$ type Burgers vectors is difficult, since pure edge dislo-cations lie parallel to [0001], the foil normal. They thus have a very short projected length, even after the foil is tilted approximately 10° - the 10° tilt was necessary to obtain a satisfactory two beam condition. In addition to this, the intensity of $\{20\bar{2}0\}$ type reflections is greater than that of $\{10\bar{1}0\}$ type reflections and thus $\{20\bar{2}0\}$ type reflections were used. The extinction distance for $\{20\bar{2}0\}$ type reflections is, however, approximately 3000°A and thus, applying the normal criterion that the dislocation image width is one third of the extinction distance, the image width, and thus the resolution obtainable is 1000A. This may be improved by increasing the deviation from the Bragg

angle, since it is known that

$$\xi_{g(eff)} = \xi_g/(1 + w^2)^{1/2} \qquad (8)$$

where w is a measure of the deviation from the Bragg
angle.[54]

Increasing the deviation parameter also decreases the
contrast in bright field however, and thus the maximum
obtainable resolution is approximately 300A°. Further,
although application of the criterion $(\vec{g} \cdot \vec{b}) = 0$ predicts
invisibility for one of the $\vec{a}$ type Burgers vectors when
viewed using a {20$\bar{2}$0} type reflection, edge dislocations
should also satisfy the criterion $\vec{g} \cdot (\vec{b} \times \vec{u}) < 0.64$ [53]
for invisibility. It is readily demonstrated that in fact,
under these conditions, $\vec{g} \cdot (\vec{b} \times \vec{u}) \sim 2.3$, and thus disloca-
tions of all three $\vec{a}$ type Burgers vectors will be visible
when viewed using {20$\bar{2}$0} type reflections.

For the above reasons, only limited use was made of the
reflections characteristic of the [000l] zone axis, instead
the reflections used were those characteristic of the
<11$\bar{2}$3> zone axis. These are, for the [$\bar{1}$2$\bar{1}$3] zone axis,
the (0$\bar{1}$11), the (1$\bar{1}$01) and the ($\bar{2}$020) reflections. The
advantages of using this pole are that it is 30° (approxi-
mately) from the [0001], and thus the projected length of
edge dislocations is more reasonable, and the extinction
distance for {10$\bar{1}$1} type reflections is approximately 800A°.

The disadvantages are that one of the reflections is still a
$\{20\bar{2}0\}$ type which possesses all the disadvantages mentioned
previously, and the other is that even with $\{10\bar{1}1\}$ type
reflections, residual contrast is still troublesome since
$\vec{g} \cdot (\vec{b} \times \vec{u}) \sim 1$ for $\{10\bar{1}1\}$ type reflections.

In an attempt to improve the resolution obtainable
by using the $\{20\bar{2}0\}$ type reflection, a number of attempts
were made to employ weak beam dark field[55] using a
$\{10\bar{1}0\}$ type reflection. These attempts did not prove very
successful, possibly because of the thick foils which had
to be used ($\sim$2000A°) [56] to obtain a representative
dislocation structure. Attempts were also made to obtain
a complete set ($(0\bar{1}11)$, $(\bar{1}101)$ and $(\bar{1}010)$ reflections)
of weak beam micrographs - this was never successfully
accomplished.

One feature which was observed was somewhat puzzling.
Some micrographs, particularly those taken in thinner areas,
showed fringe contrast. The precise mechanism by which
this type of contrast develops is unknown; however it was
established that the fringe contrast would disappear as the
deviation from the Bragg angle increased and dislocations
were then observed to be giving rise to the fringes - this
is shown in Figures 15a, b and c. This feature has been
observed previously and shown to arise due to the presence
of dislocation dipoles.[57] The presence of dislocation
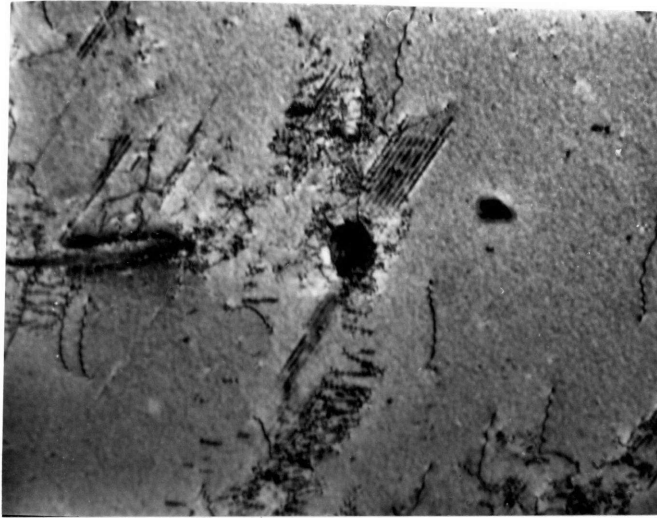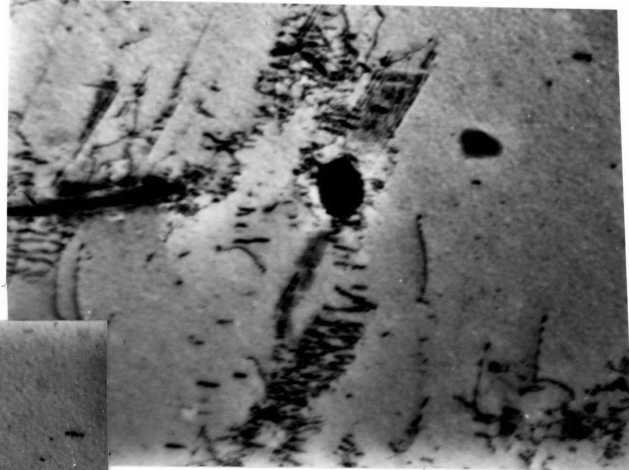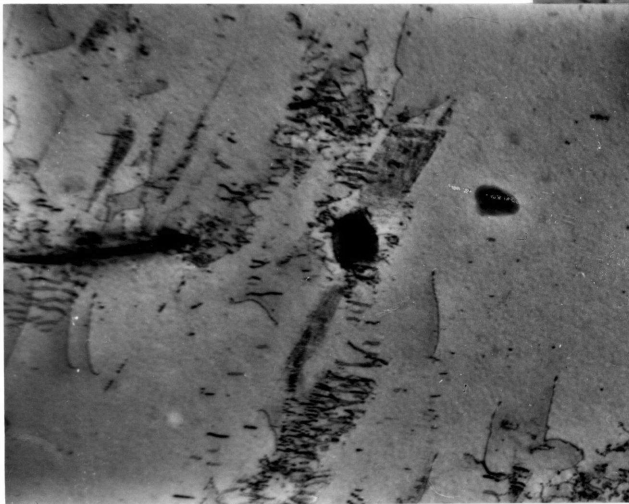
Figure 15. Effect of increasing deviation from the Bragg angle on contrast obtained from dislocation dipoles. 80μ grain sample fatigued to saturation at a plastic strain amplitude of ±0.002. Beam direction <11$\bar{2}$3>. Reflection {10$\bar{1}$1}.   a)   w = 0.48
                                    b)   w = 1.13
                                    c)   w = 1.89

dipoles may be observed in Figure 15c. Fringes were not
observed under all conditions and possibly the occurrence
of this type of contrast is affected by some geometrical
relationship between the $\vec{a}$ type Burgers vector and the
<11$\bar{2}$3> type zone axis used.

Figures 16a, b and c, and 17a, b, and c show the results
of attempting to carry out a Burgers vector analysis using
those reflections characteristic of the <11$\bar{2}$3> zone axis.
In both cases it will be noted that the dislocation
clusters show significant contrast in all three reflections.
Figure 18 shows a weak beam dark field micrograph of the
same region as in Figure 17 c, at higher magnification - the
improved resolution is obvious. As was noted, significant
contrast was observed under all three operating reflections
which suggests that perhaps the dislocation clusters are
composed of dislocations of more than one $\vec{a}$ type Burgers
vector.

If, however, the dislocation clusters are disregarded
and the extinction of the screw dislocations is considered,
it is obvious that in both cases there is a preponderence
of dislocations with one $\vec{a}$ type Burgers vector. This
feature was again common to all foils examined. In
particular, it was true of one foil in which the foil
normal was almost precisely (within 5°) [0001]. This
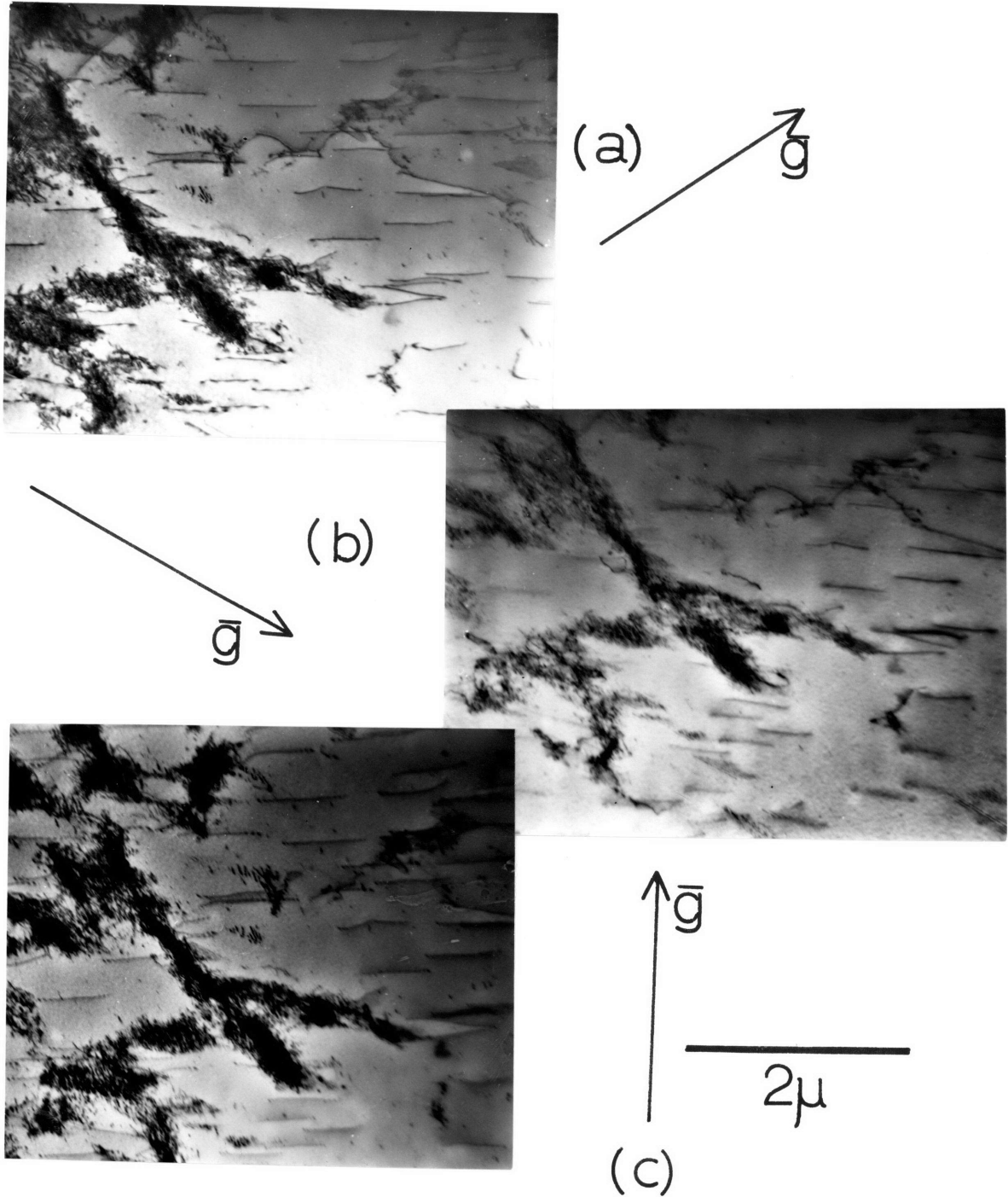
Figure 16. Burgers vector analysis of structure developed
at saturation in an 80μ grain size sample after fatigue
at a plastic strain amplitude of ±0.003. Beam direction is
[1̄21̄3]. Reflections a) (01̄11)
                       b) (11̄01)
                       c) (2̄020)
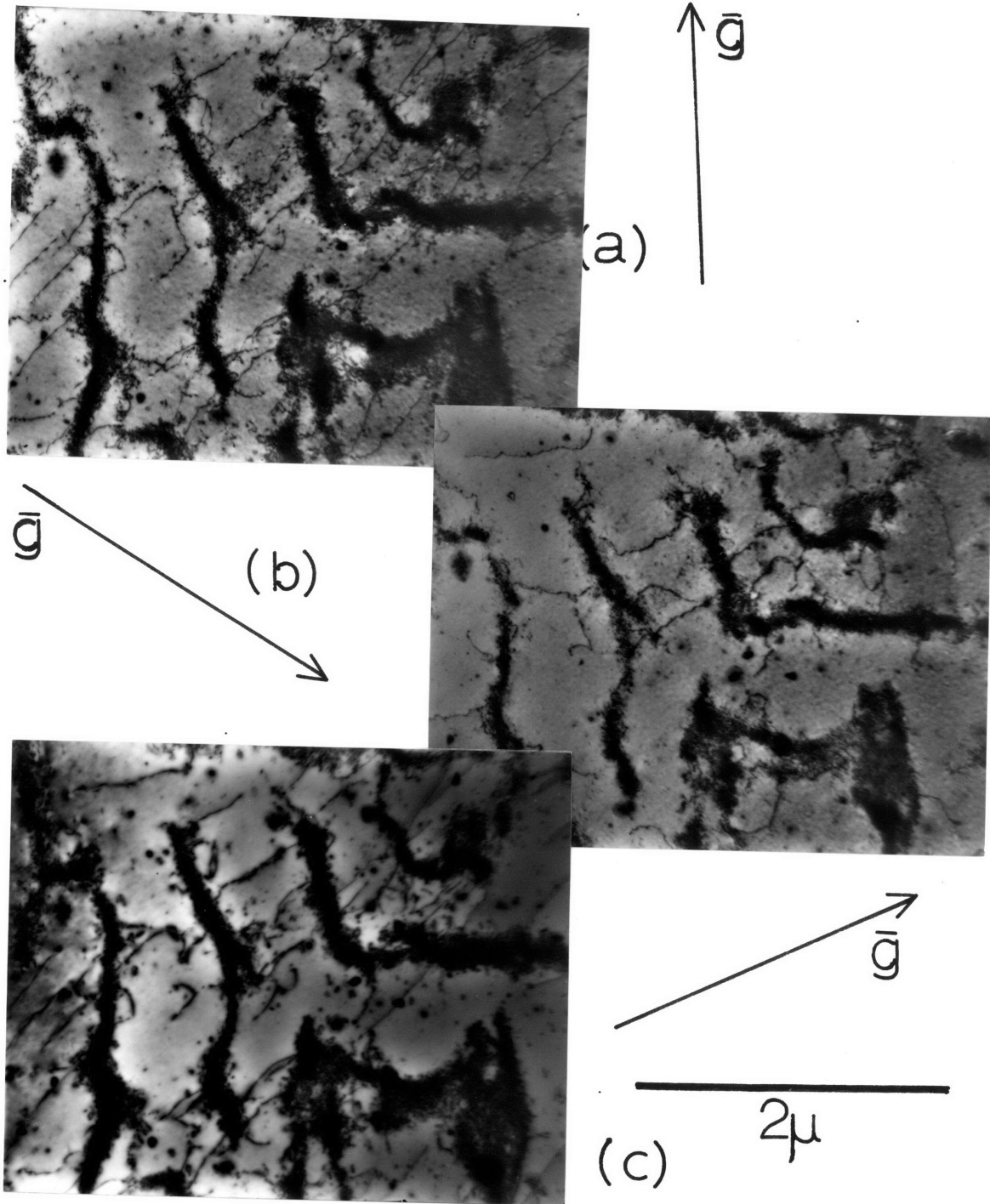
Figure 17. Burgers vector analysis of structure developed
at saturation in an 80μ grain size sample after fatigue at
a plastic strain amplitude of ±0.003. Beam direction is
[1̄2̄1̄3]. Reflections   a) (01̄11)
                        b) (11̄01)
                        c) (2̄020)
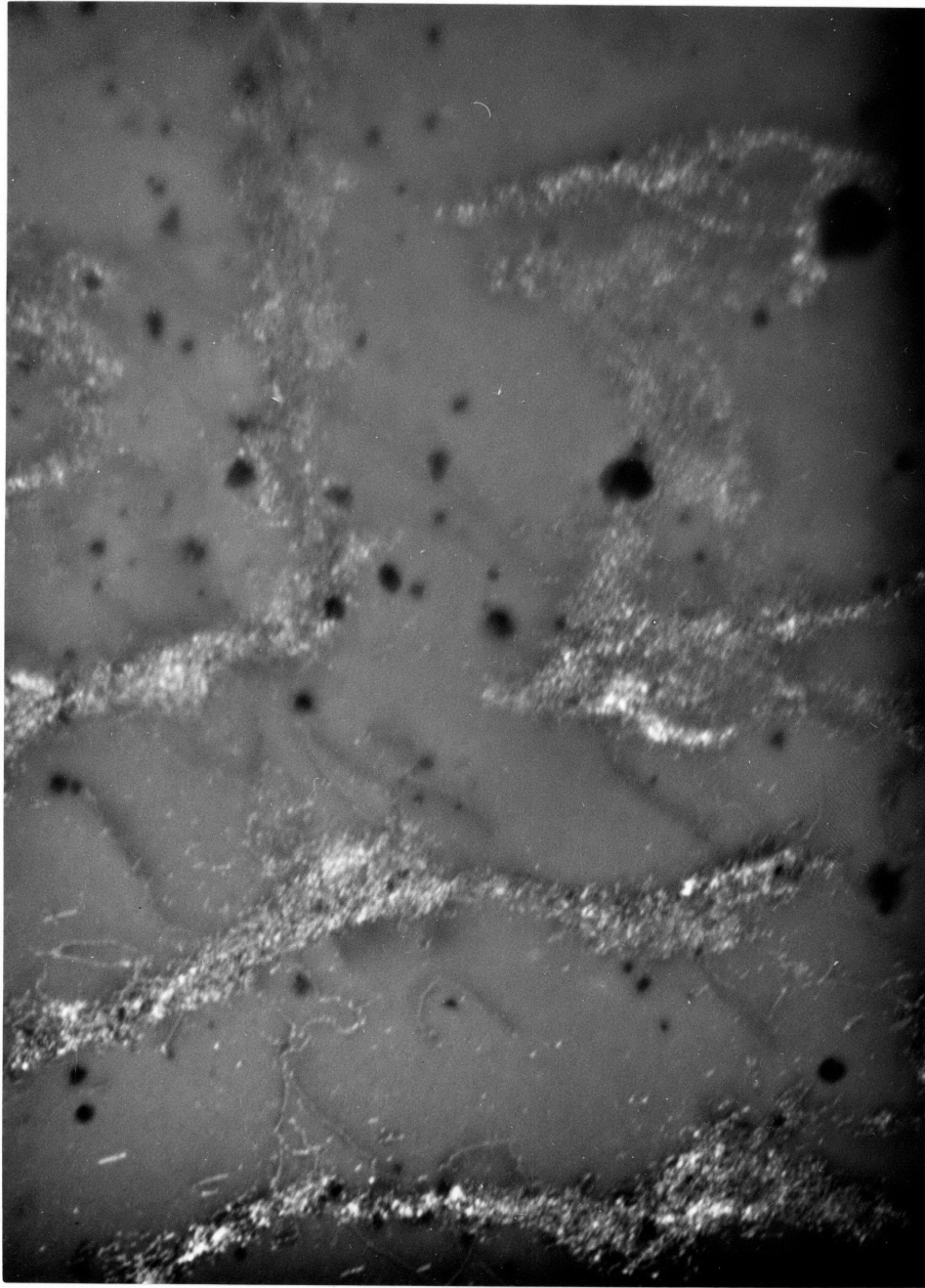
Figure 18. Weak beam micrograph of structure developed at saturation in an 80μ grain size sample after fatigue at a plastic strain amplitude of ±0.003. Beam direction is [$1\bar{2}\bar{1}3$]. Reflection ($\bar{1}010$). Same area as Figure 17.

suggests that the predominance of one type of Burgers
vector does not arise due to any unconscious selectivity
in cutting the foil blanks.

Since it is hard to imagine how it is possible for
there to be two types of edge dislocations present, but
only one type of screw dislocation, it is felt that the
dislocations in the clusters consist of only one of the
$\vec{a}$ type Burgers vectors. The inability to eliminate all the
contrast from the dislocation clusters is attributed to
residual contrast from the high density of edge dislocations
in the clusters. This conclusion is supported somewhat by
Figure 19 which has been taken from the work of Partridge[60]
and shows localized regions of single slip in a grain of
fatigued α-titanium, although overall, the grain exhibits
duplex slip. (For comparison it should be noted that a
sample fatigued at a plastic strain amplitude of ±0.003
failed after approximately 4000 cycles.)

There is, however, an alternative explanation which
may be proposed for the failure to eliminate all contrast
from the dislocation clusters, namely the presence of
dislocations with ($\vec{c}$ + $\vec{a}$) or $\vec{c}$ type Burgers vectors. The
$\vec{c}$ component of such Burgers vectors will be imaged by the
$\vec{c}$ component of the {$10\bar{1}1$} type reflections. Figures 20a,
b, and c, show a Burgers vector analysis conducted using
only {$20\bar{2}0$} type reflections which do not image the $\vec{c}$
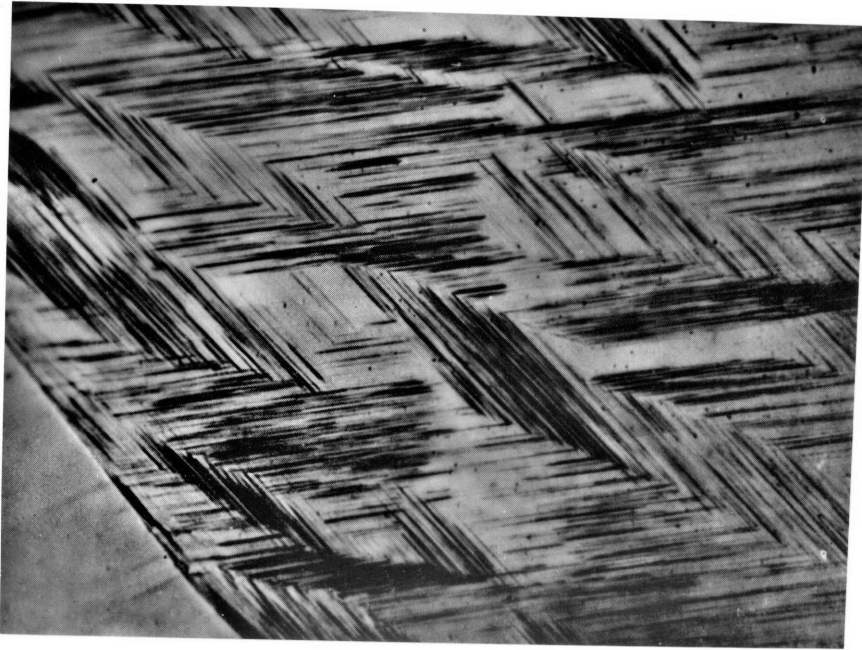
Figure 19. {10$\bar{1}$0} slip traces observed in specimen which
fractured after 10^4 stress cycles (x550). (From
Patridge, Ref. 60).
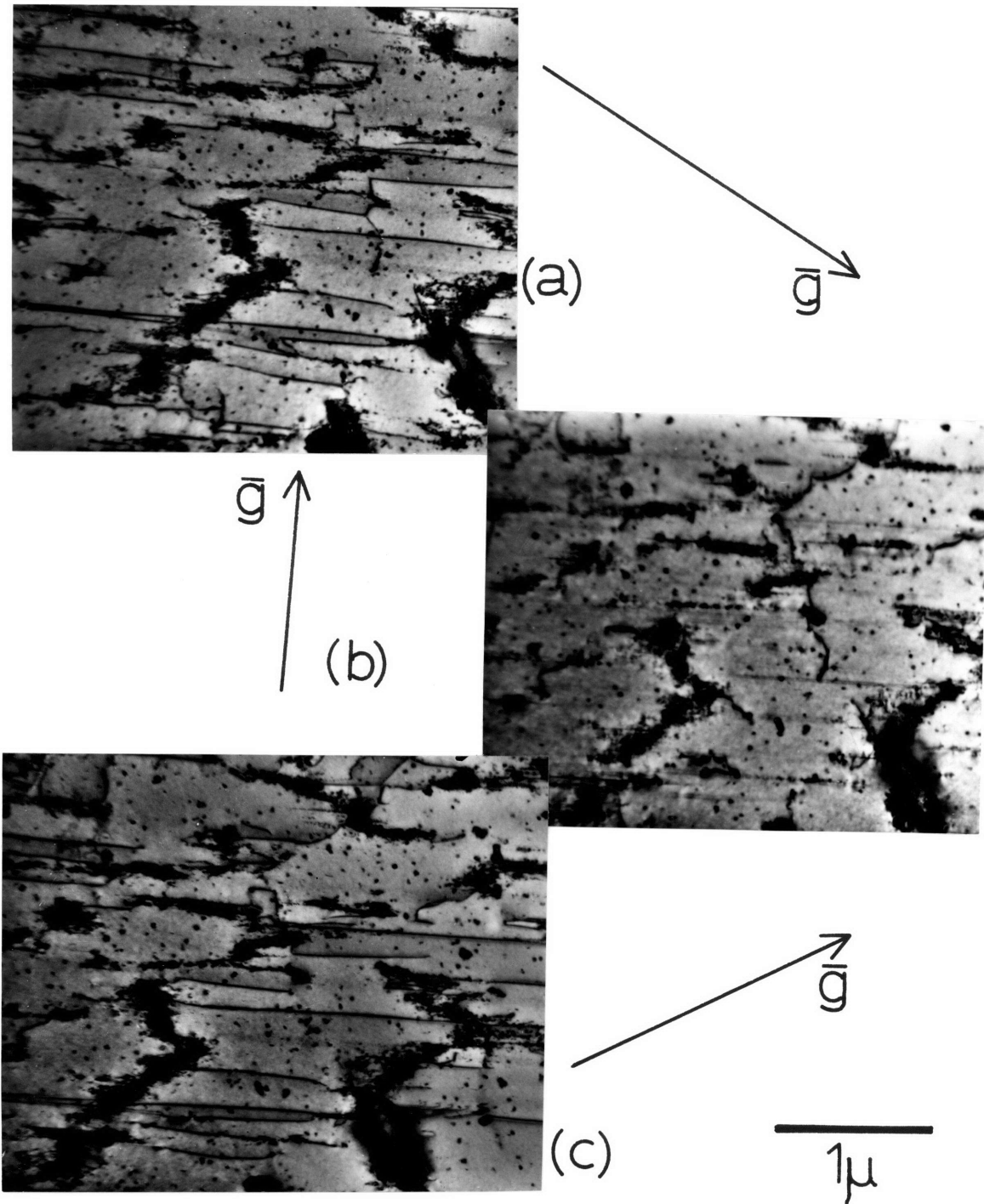
Figure 20. Burgers vector analysis of microstructure
developed at saturation in an 80μ grain size sample after
fatigue at a plastic strain amplitude of ±0.003. Beam
direction [0001]. Reflection a) $(20\bar{2}0)$
                               b) $(02\bar{2}0)$
                               c) $(2\bar{2}00)$

component of any ($\vec{c} + \vec{a}$) type Burgers vector. Again
significant contrast is observed in all three micrographs
from the dense dislocation clusters, although the screw
dislocations show extinction. Once again the inability
to totally eliminate all contrast from these clumps is
attributed to residual contrast.

It may be noted in Figure 20 that total extinction
of the screw dislocation does not occur, a "ghost" image
may be detected along the line of the dislocation. This
is attributed to the presence of edge segments normal to
the surface lying in the same slip plane as the screw
dislocation. The "ghost" image thus arises due to residual
contrast from the edge segments. A similar feature may be
observed in Figure 16, although in this case, because
the foil plane has been tilted through 30° from (0001),
the edge segments appear as short lines.

4.2.1.2. Structure Prior to Saturation - One sample was
strained in tension to a strain of 0.00016. Examination
of foils made from this sample showed a very low dislocation
density consisting of predominantly screw dislocations.

Another sample was fatigued at ±0.0012 plastic strain
amplitude until softening could just be discerned (after
80 cycles) - at this point the test was stopped. Figure
21a shows the dislocation substructure observed in a

TRACE OF BASAL PLANE

(a)
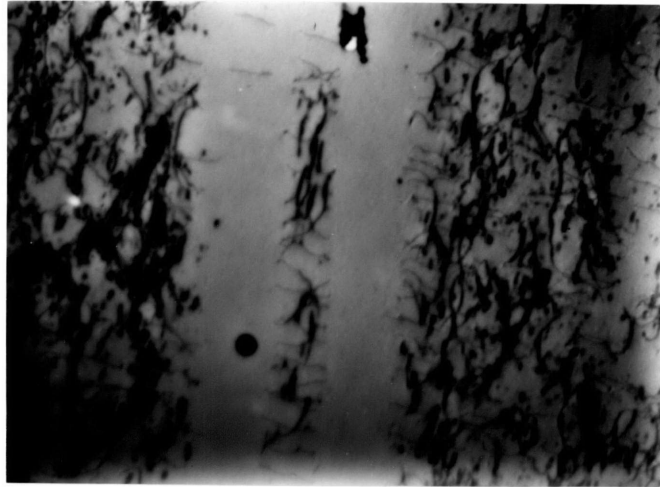
5μ

(b)
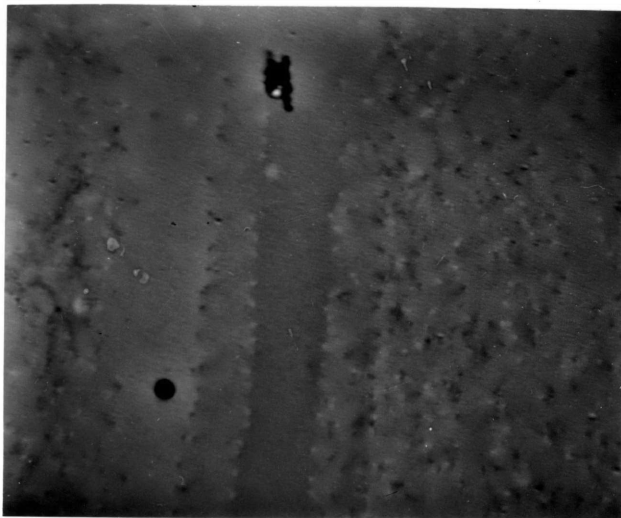
Figure 21. Structure developed after fatigue of an 80μ grain size sample fatigued at a plastic strain amplitude of ±0.0012 for 80 cycles. Beam direction <10$\bar{1}$0>. Reflection   a) {11$\bar{2}$0}
          b) [0002]

{10$\bar{1}$0} foil ({11$\bar{2}$0} type reflection). The structure is reminiscent of the structure observed by Snow[58] in ruthenium after stage I prism slip, and consists of edge dipoles and multipoles. The mechanism by which the edge multipoles and dipoles form is clearly related in some way to the motion of screw dislocations, since it may be observed that in region A, where screw dislocations cannot be observed, there are no dipoles, while in region B both screw dislocations and dipoles may be observed. Figure 21b illustrates the distribution of dislocations whose Burgers vector includes a $\vec{c}$ component. As in the case of the structure developed at saturation, it is clear that those dislocations with a $\vec{c}$ component, occur only in those regions where $\vec{a}$ type dislocations are observed. One further point which should be made is that contrast may be seen at the points of emergence of screw dislocations. This contrast is probably associated with surface relaxation effects.[69]

Figure 22 is a mosaic, and indicates the form of the substructure when viewed in an <01$\bar{1}$1> type direction using a {11$\bar{2}$0} type reflection (a {11$\bar{2}$0} type reflection images all three $\vec{a}$ type Burgers vectors). Figure 23 is a Burgers vector analysis of part of the mosaic. From the conditions under which the long straight dislocations disappear, it is obvious that they are screw. Clearly,
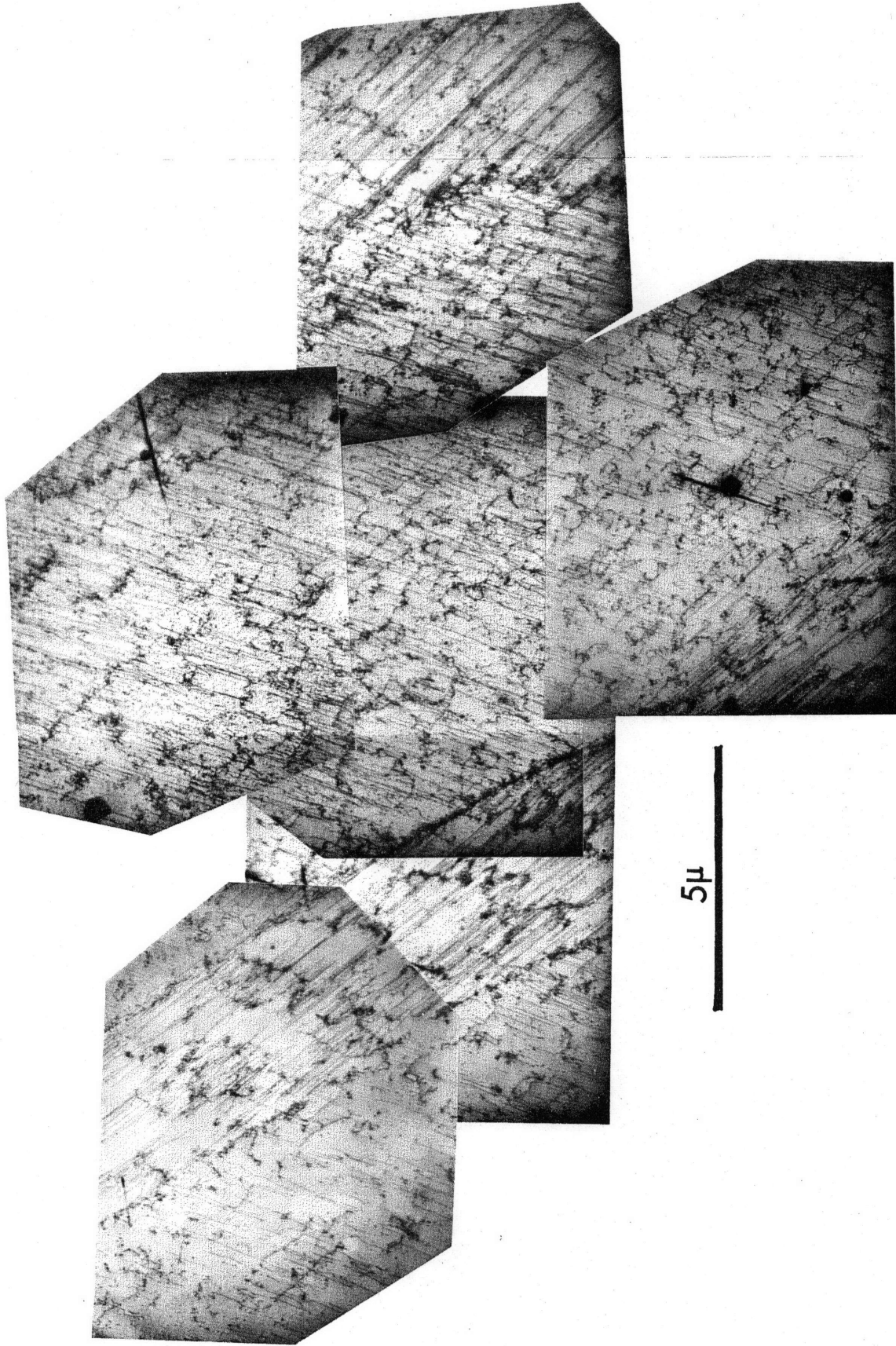
Figure 22 . Mosaic indicating the structure developed in 80μ grain size material cycled for 80 cycles at a plastic strain amplitude of ±0.0012. Operating reflection (2$\bar{1}\bar{1}$0). Beam direction [01$\bar{1}$1].

5μ

83
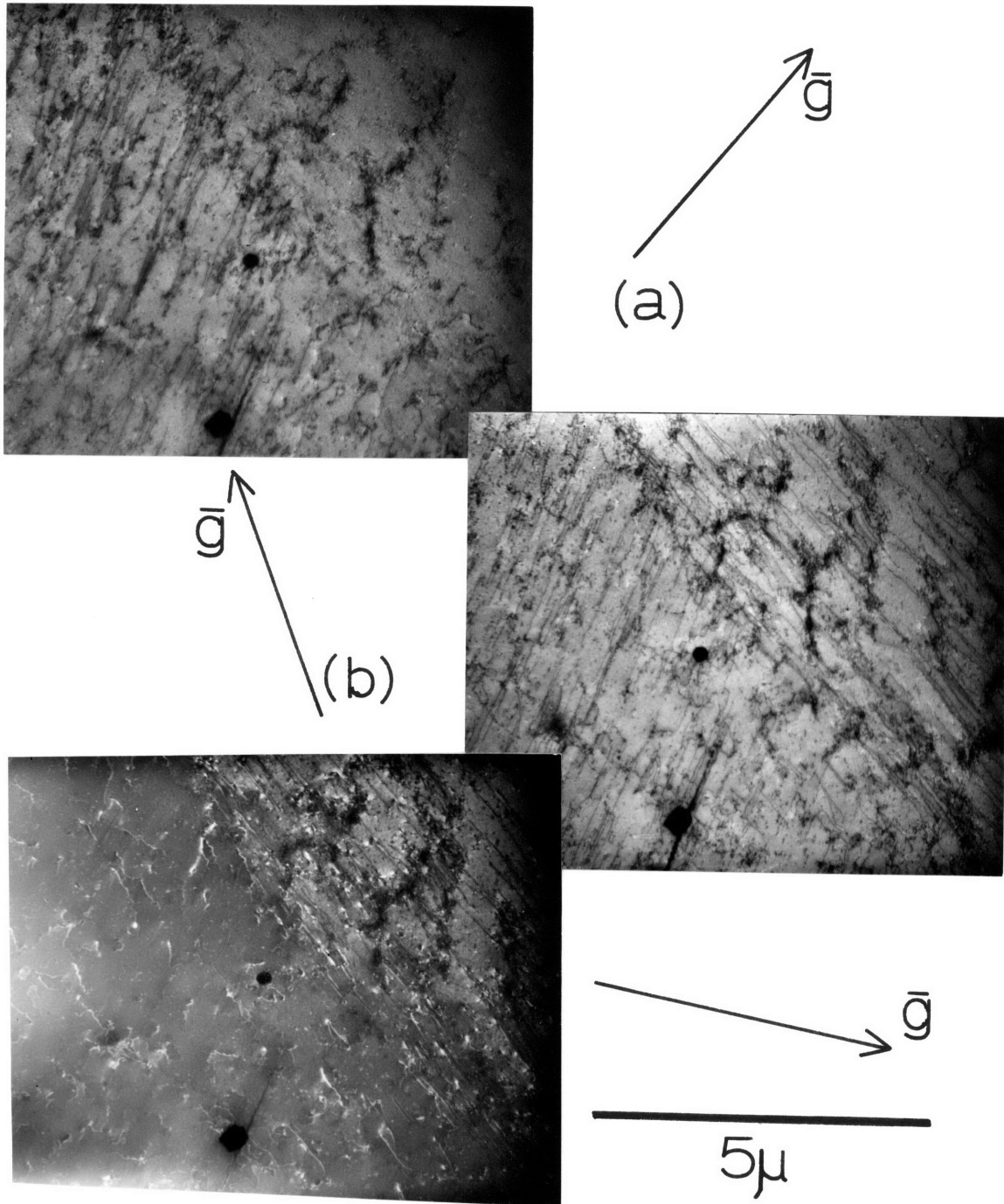
Figure 23. Burgers vector analysis of structure developed in 80μ grain size material cycled for 80 cycles at a plastic strain amplitude of ±0.0012. Area is part of that contained in Figure 22. Beam direction [$\bar{1}2\bar{1}3$]. Reflection a) (0$\bar{1}$11)
b) (1$\bar{1}$01)
c) ($\bar{2}$020)

however, there are two sets of screw dislocations, one on
each side of the boundary and each having a different
Burgers vector. It should be noted that the contrast from
the regions indicated by A cannot be eliminated. Just as
the nature of dislocation segments may be inferred from
geometrical considerations in foils of $\{11\bar{2}0\}$ orientation
provided prism slip is assumed, so can the nature of
dislocation segments be inferred in [0001] foils. The
criterion used is simply the projected length, since screw
dislocations will be long, and edge segments short.

On this basis, those short dislocation segments which
give rise to contrast under all conditions would thus be
edge segments, and the inability to eliminate contrast
completely would then be due to residual contrast. There is,
however, an alternative explanation, namely that these
dislocations are of $(\vec{c} + \vec{a})$ type and that the inability
to extinguish all contrast arises from the fact that the
dislocations are imaged by the $\vec{c}$ component in the $\{10\bar{1}1\}$
type reflection. If indeed the contrast does arise because
these are $(\vec{c} + \vec{a})$ type dislocations, however, it is
difficult to imagine why they would be restricted to only
one area of the sample. Further, a careful comparison of
Figures 23a and b indicates that there is an almost one
for one correspondence between the structures of the clusters.
This would imply that the cluster is composed exclusively

of $<\vec{c} + a>$ type dislocations which is at variance with
the results of Figures 21a and 21b, and 12a and 12b.
These imply that the density of dislocations whose
Burgers vector includes a $\vec{c}$ component is much less than
the density of dislocations whose Burgers vector does not
include a $\vec{c}$ component.

For these reasons, the short dislocation segments
at point A in Figure 23 are felt to be $\vec{a}$ type dislocations
in edge configuration.

4.2.2 High Plastic Strain Amplitude Fatigue

4.2.2.1 Structure at Saturation - After high plastic

strain amplitude fatigue a cellular dislocation structure
is formed. Unlike the structure developed at low plastic
strain amplitudes in which no significant lattice rotation
occurred, it was noted that considerable lattice rotation
could occur from cell to cell. For this reason, well
developed Kikuchi bands were rarely observed and hence many
of the micrographs were taken in dark field.

Two types of cell structures were observed, one, which
may be a transition structure, consisted of long rows of
dipoles arranged such that the row is parallel to the trace
of the basal plane. Screw dislocations may also be
observed in the cell walls. This structure is illustrated
in Figure 24a and b when viewed in a $<11\bar{2}0>$ type direction

(a)

TRACE OF BASAL PLANE

2μ
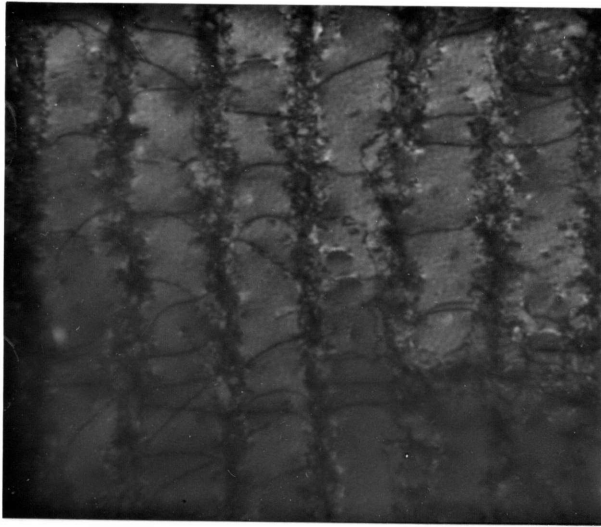
(b)
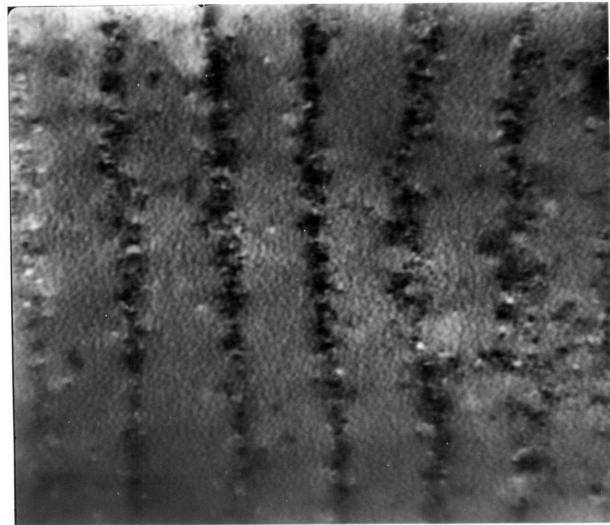
Figure 24. Dipole cell structure formed in 80μ grain size material cycled to saturation at a plastic strain amplitude of ±0.005. Beam direction <11$\bar{2}$0>.
Reflection   a) {10$\bar{1}$1} - Dark Field.
              b) [0002] - Dark field.

using a $\{10\bar{1}1\}$ type and (0002) reflection, respectively.
It may be noted that no significant lattice rotation is
observable.

The second cellular structure is similar to the
structure previously described, in that the cell walls
are arranged parallel to the trace of the basal plane.
However, few dipoles are observed, and some lattice
rotation between cells may be detected. This structure is
shown in Figures 25a and b when viewed in a $<11\bar{2}0>$
type direction using a $\{10\bar{1}1\}$ type reflection and an
(0002) reflection, respectively. Figure 26 shows the same
structure imaged by the same $\{10\bar{1}1\}$ reflection used for
Figure 25a after an approximately 30° tilt from the
$\{11\bar{2}0\}$ type pole. Using the geometrical argument
developed earlier, it is clear that the dislocations in
the cell wall must be screw dislocations.

Figures 24b and 25b indicate that, as was observed in
the structures typical of low plastic strain amplitude
fatigue, significant contrast is obtained when using an
(0002) reflection only from those regions in which $\vec{a}$
type dislocations are also observed.

Both types of cell structure were observed in samples
which hardened monotonically and it was possible for both
structures to exist in the same grain. It appeared, however,
that the probability of encountering the dipole cellular
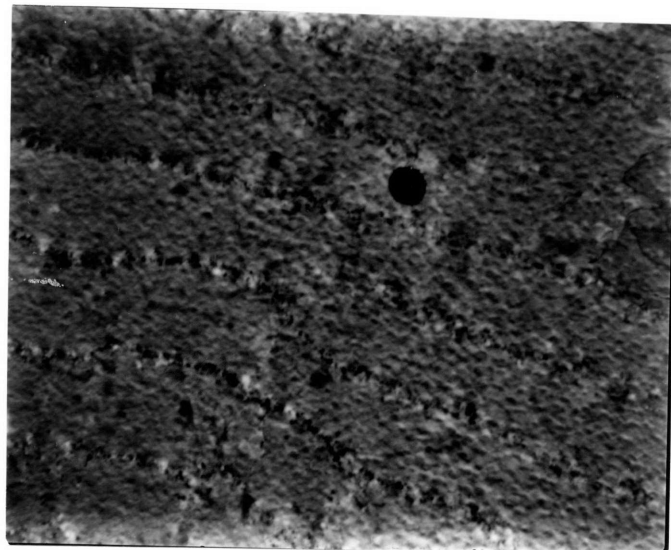
Figure 25. Cell structure formed in an 80μ grain size
sample cycled for 150 cycles at a plastic strain amplitude
of ±0.01. Beam direction <11$\bar{2}$0>.
Reflection a) {10$\bar{1}$1} - Dark field.
            b) [0002] - Dark Field
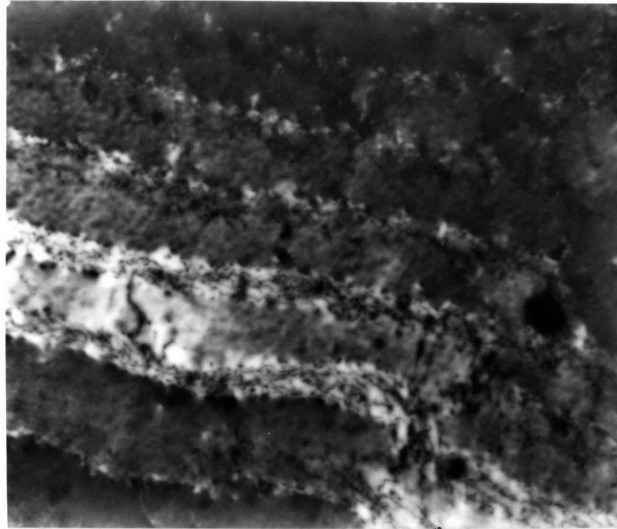
Figure 26. Cell structure formed in an 80μ grain size
sample cycled for 150 cycles at a plastic strain amplitude
of ±0.01. Same area as in Figure 25, but the foil has
been tilted through approximately 30° from the <11$\bar{2}$0>
pole. Reflection {10$\bar{1}$1} - Dark field.

structure was higher at the lower plastic strain
amplitudes.

Figures 27 and 28 are Burgers vector analyses of the
cellular substructure. As in the case of the low plastic
strain amplitude structure {0001} foils were used for
this purpose. In both Figure 27 and 28, the beam direction
is close to <11$\bar{2}$3>.

The cell walls in Figure 27 are composed of short
dislocation segments which never appear to go completely
out of contrast. On the basis of the geometrical considera-
tions outlined earlier, they are thus assumed to be
primarily edge in character. In addition, the majority
of the dislocations within the cells also exhibit contrast
under all conditions. On close examination it will be noted
that most of the dislocations within the cells consist,
like the cell walls, of very short dislocation segments.
Some of these segments lie in what is almost a straight line,
and may be a manifestation of the "ghost" images discussed
earlier.

Close study of the cell walls in Figure 28 discloses
that the dominant systematic structure of the cell walls is
what appears to be long straight parallel dislocations,
which possess a strong screw component. It is possible
that these are not in fact dislocations but are instead
fringes which, like stacking fault fringes, merely reflect
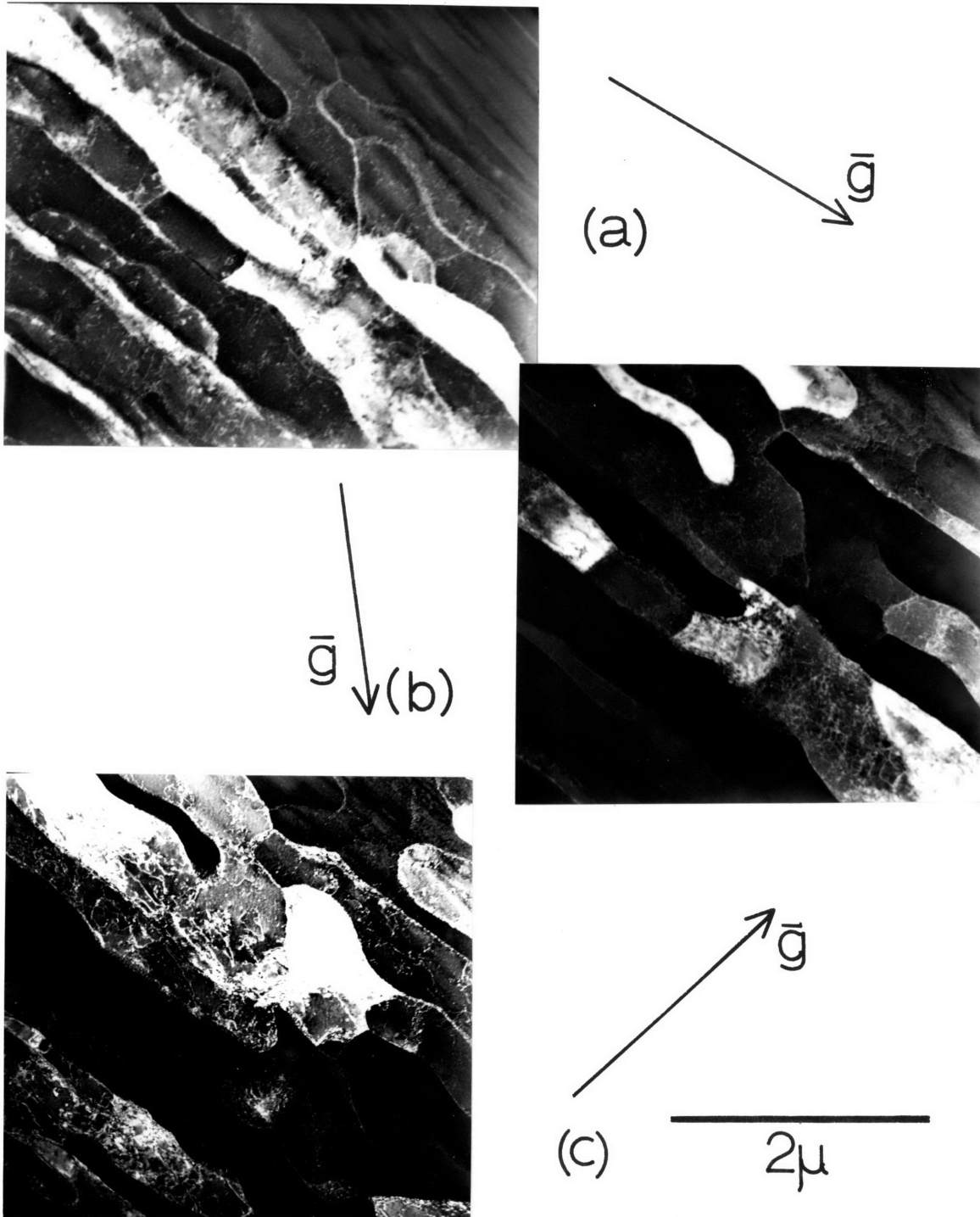
Figure 27. Burgers vector analysis of structure developed in an 80μ grain size sample fatigued at a plastic strain amplitude of ±0.01 for 150 cycles. Beam direction <11$\bar{2}$3>.
Reflection   a) (0$\bar{1}$11)   Dark field
             b) (1$\bar{1}$01)   Dark field
             c) ($\bar{2}$0$\bar{2}$0)   Dark field
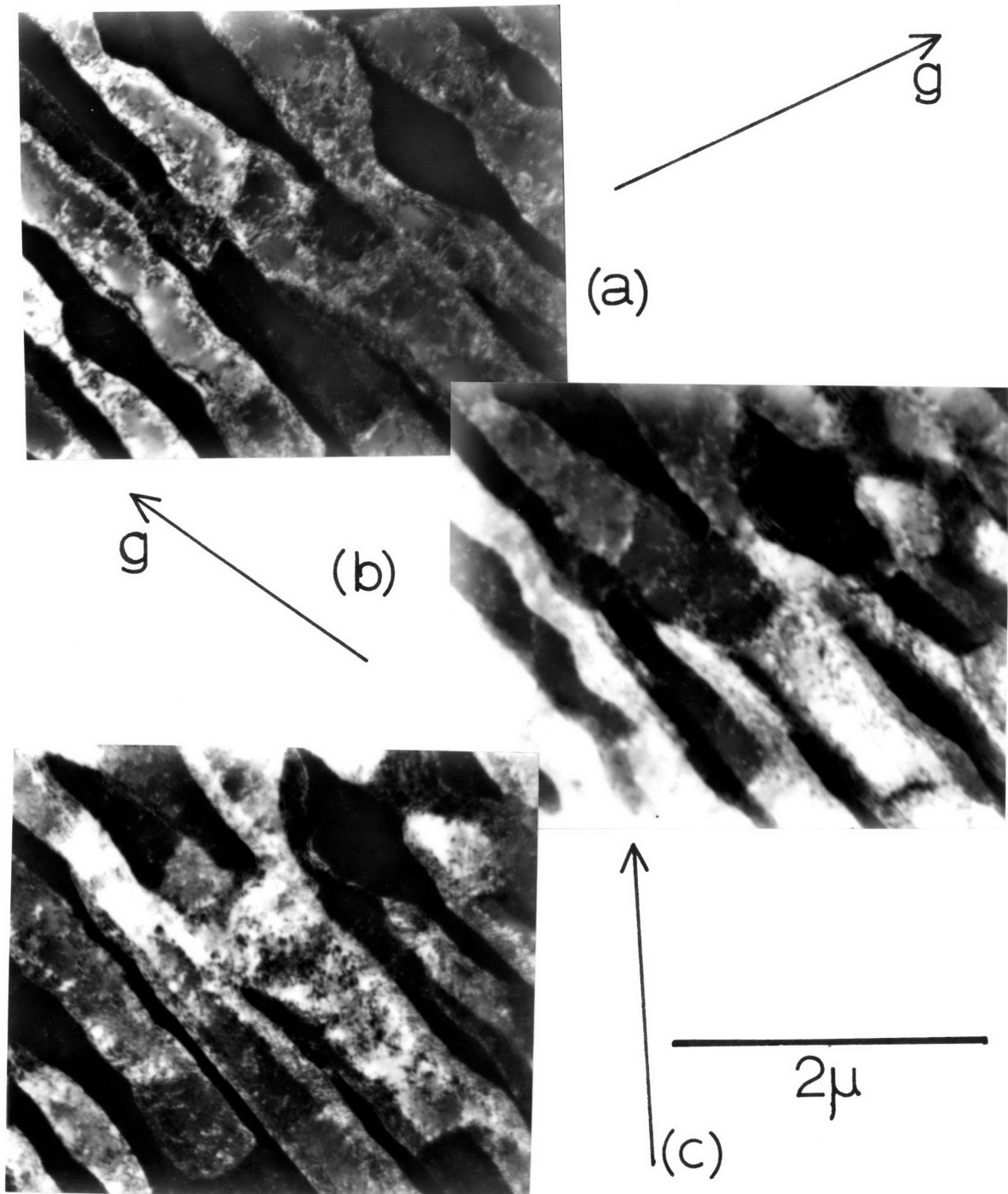
Figure 28. Burgers vector analysis of structure developed in an 80μ grain size sample fatigued at a plastic strain amplitude of ±0.01 for 150 cycles. Beam direction <11$\bar{2}$3>. Reflection a) (0$\bar{1}$11) Dark field
            b) (1$\bar{1}$01) Dark field
            c) (20$\bar{2}$0) Dark field

a lattice discontinuity. It is dubious whether this is
indeed the case, since the lines of constant contrast are
not precisely parallel at all points as might be expected
if indeed they were fringes. Further, the spacing of the
lines would imply an extinction distance of approximately
300A° if a reasonable foil thickness is assumed (2000A°).
This is considered somewhat unlikely. There is one further
possibility which cannot be dismissed so lightly, and that
is that the contrast is indeed fringe contrast which is
arising by a similar mechanism to that mentioned earlier in
connection with the structure typical of low cycle fatigue.
The disappearance of fringe contrast would then be
attributable to the fact that for that particular reflection,
the deviation from the Bragg angle was such that fringe
contrast did not arise. The results of Figure 27 tend to
argue against such an interpretation, however, since it is
hard to imagine why well developed fringe contrast similar
to that of Figure 28, would not occur at least once in
Figure 27.

For this reason the cell wall structure observed in
Figure 28 is considered to consist of parallel screw
dislocations. One consequence of the identification of
the fringe contrast with screw dislocations is that, since
all of the fringes vanish when using one reflection, then

all of the dislocations possess the same Burgers vector.
This conclusion is supported by Figure 29 which shows
the dislocation structure observed in a 7μ grain size
sample fatigued at a plastic strain amplitude of ±0.01
when viewed in a <11$\bar{2}$0> type direction using a {10$\bar{1}$1}
type reflection. A {10$\bar{1}$1} type reflection will image
dislocations with only two of the three $\vec{a}$ type Burgers
vector and any dislocation with a {$\vec{c}$} or {$\vec{c}$ + $\vec{a}$} type
Burgers vector. The structure observed in Figure 29
consists of rows of speckle type contrast, which, by
analogy with Figures 24b and 25b, are considered to outline
the cell walls. In addition, a relatively low density of
what are presumed to be $\vec{a}$ type dislocations may be observed
more or less randomly distributed throughout the grain.
This implies that the majority of the dislocations and,
in particular, the dislocations in the cell walls, are
dislocations which possess that $\vec{a}$ type Burgers vector
which is not imaged by the {10$\bar{1}$1} type reflection used.

4.2.2.2 <u>Structure Prior to Saturation</u> - Only a limited
number of foils were examined prior to saturation. Figure
30 indicates the nature of the structure observed after
20 cycles at a plastic strain amplitude of ±0.01 when
viewed in a <10$\bar{1}$0> type direction. This is a multibeam
case, the operating reflections are a {11$\bar{2}$4} type and an
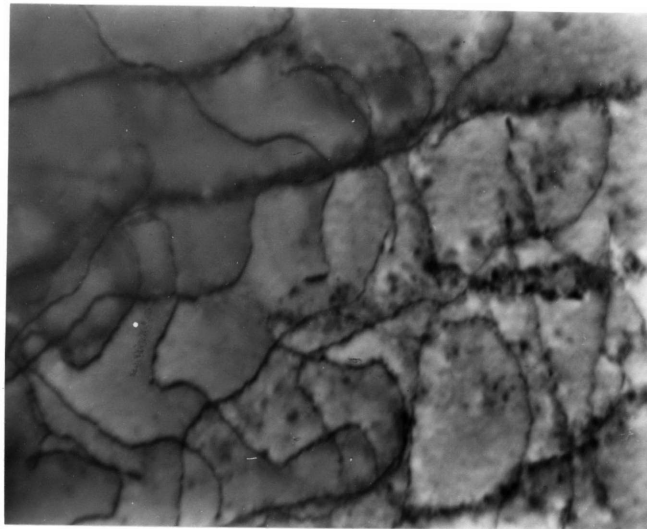
Figure 29. Structure developed in a 7μ grain size
sample at saturation after fatigue at a plastic strain
amplitude of ±0.01. Beam direction <11$\bar{2}$0>.
Reflection {10$\bar{1}$1}.
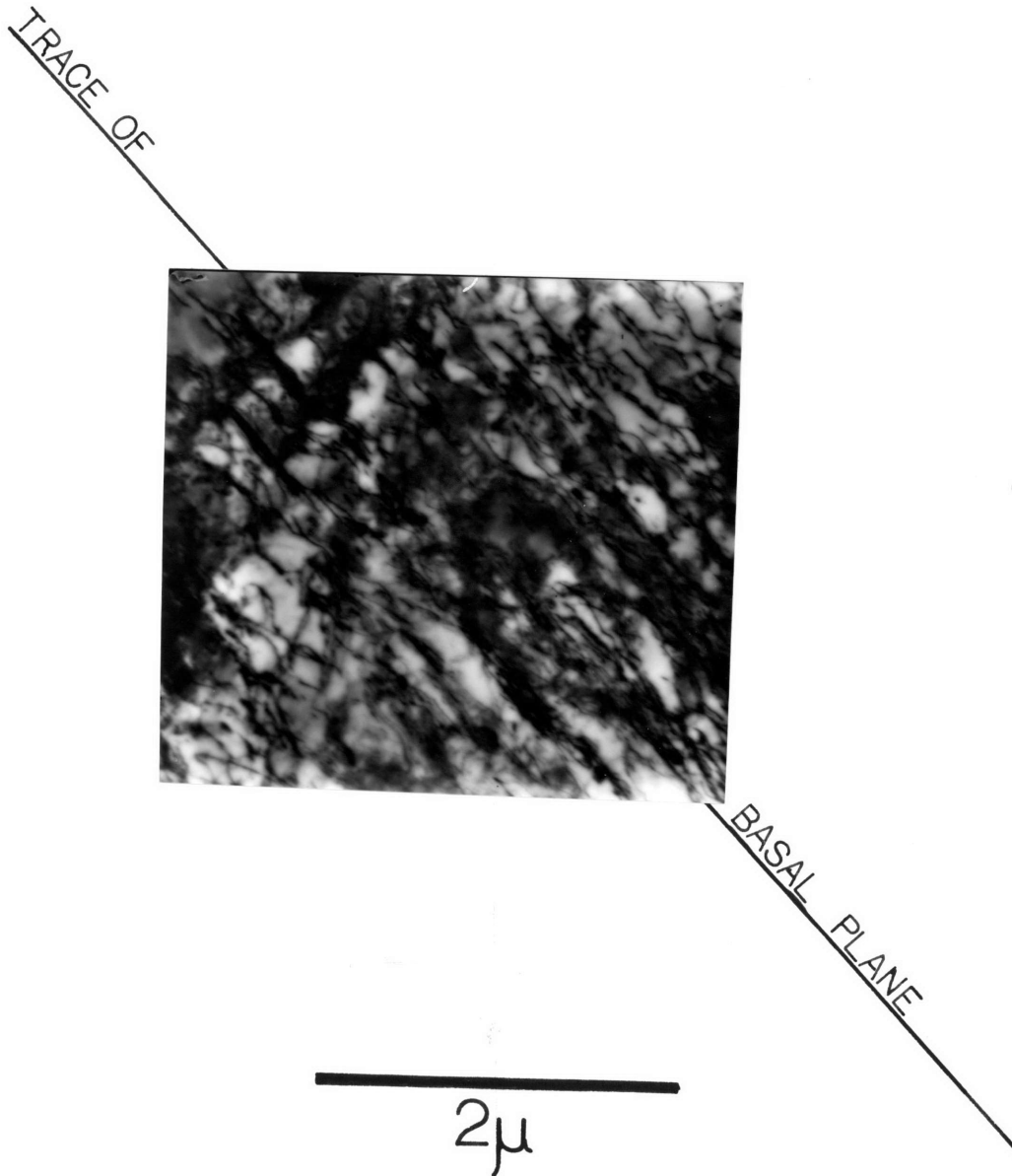
Figure 30. Structure developed in a 7μ grain size sample.
fatigued for 20 cycles at a plastic strain amplitude of
±0.01. Beam direction <10$\bar{1}$0>. Multibeam case, operating
reflections {11$\bar{2}$4} and (0002).

(0002). Using the same geometrical argument as was used before, the relatively long dislocation segments which have a tendency to appear in the form of bundles are screw in character.

It was remarked previously that in some of the foils from samples which had been cycled to saturation, both types of cellular structure (dipole and screw) were observed. Figure 31 is a mosaic showing the structure observed in a 7μ grain size sample which has been cycled at a plastic strain amplitude of ±0.01 for 40 cycles - the beam direction is <11$\bar{2}$0> type and the operating reflection is a {10$\bar{1}$1} type. In this grain, all the dislocation structures discussed previously can be discerned. It should be noted that the density of screw dislocations (i.e. long dislocation segments parallel to the trace of the basal plane) in the cell walls increases steadily with distance from the dipole structure. A few isolated cells are almost equiaxed in appearance although in general the cells display the elongated appearance noted previously. In no foil was an extensive zone of equiaxed cells observed. At most only two or three isolated equiaxed cells could be discerned, with a vast majority of the cells displaying the elongated appearance shown in the micrographs selected.

Trace of Basal Plane

2μ
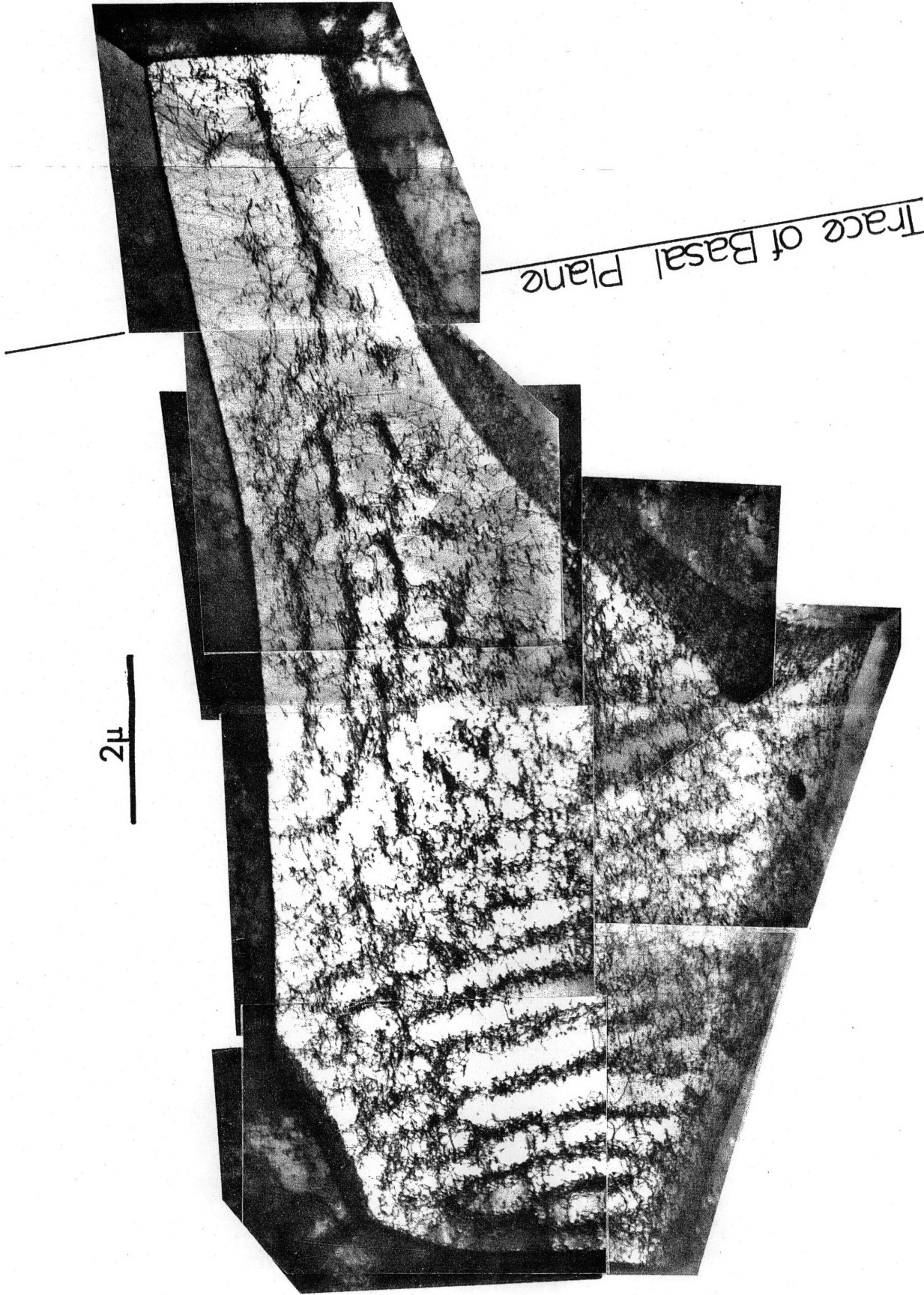
Figure 31. Mosaic indicating the structure developed in
7μ grain size material cycled for 45 cycles at a plastic
strain amplitude of ±0.01. Operating reflection (10$\bar{1}$1).
Beam direction [$\bar{1}$2$\bar{1}$0]. The trace of the Basal plane is
indicated.

5. DISCUSSION

5.1 Effect of Machine Stiffness

It is well known that the displacement undergone by a sample under test and the motion of the cross-head of a tensile testing machine are equivalent only when the stiffness of the machine is infinite. In general, the relationship between cross-head motion and sample displacement is given by

$$St = \Delta\ell_{sample} + P/K \qquad (9a)$$

$$= \ell_o(\varepsilon_P + \varepsilon_E) + P/K \qquad (9b)$$

where

t = Time

S = Rate of cross head motion

$\Delta\ell_{sample}$ = Displacement undergone by sample

P = Load

K = Machine stiffness

ε_E = Elastic strain

ε_P = Plastic strain

A similar relationship between rate of crosshead motion and the plastic strain rate imposed on the sample may be simply derived by differentiating the above equation with respect to time.

Assuming that the crosshead moves at a constant
speed, the result obtained is

$$S = \ell_0(\dot{\varepsilon}_P + \dot{\varepsilon}_E) + \frac{1}{K}\frac{dP}{dt} \qquad (10)$$

or on rearranging,

$$\dot{\varepsilon}_P = \frac{1}{\ell_0}\left(S - \left(\frac{1}{K}\frac{dP}{dt} + \ell_0\,\dot{\varepsilon}_E\right)\right) \qquad (11a)$$

$$= \frac{1}{\ell_0}\left(S - \frac{dP}{dt}\left(\frac{1}{K} + \frac{\ell_0}{A_0 E}\right)\right) \qquad (11b)$$

where A_0 = Initial cross sectional area of the sample.
This is valid for small strains.

The above equation indicates that there is no simple
correspondence between the rate of crosshead motion imposed
by the machine and the plastic strain rate imposed by the
machine during the duration of a test. This occurs
because, as is well known, the quantity $\frac{dP}{dt}$ changes
continuously as straining proceeds.

In testing material which exhibit no yield drop, this
change in plastic strain rate is generally small, since
the effect of straining is to change the _magnitude_ of the
terms containing $\frac{dP}{dt}$ but not their _sign_ relative to S.
In the case of materials exhibiting a yield point phenomenon
however not only does $\frac{dP}{dt}$ change in magnitude, but in the
immediate vicinity of the upper yield point it also changes
sign. Between the upper and lower yield point $\frac{dP}{dt}$ is negative.

At strains beyond the lower yield point, $\frac{dP}{dt}$ becomes positive. Thus it is clear that if strained in a "soft" testing machine, materials which exhibit an upper and lower yield point may undergo a considerable change in plastic strain rate in the immediate vicinity of the upper yield point. (In general, the term corresponding to the elastic strain rate is negligible when compared with the rate of crosshead motion. The only factor which can significantly (greater than 1 percent) change the plastic strain rate is the machine stiffness.) Further, it is clear that between the upper and lower yield points the plastic strain rate imposed on the sample will be greater than at any other time during the test. As a consequence of this, the mobile dislocation density will be greater than at any other time during the test since the two are related by the equation

$$\dot{\varepsilon}_P = bv\rho_m \tag{12}$$

and the dislocation velocity, since it is related to the applied stress will be a minimum at the lower yield point.

It is clear that the foregoing discussion need not be restricted to unidirectional testing, the same processes will occur on the first quarter cycle of a fatigue test conducted under conditions of constant plastic strain amplitude. It is, however, of some interest to examine

the effects of this initial burst in the mobile dislocation density on the subsequent behaviour of samples strained both unidirectionally and cyclically.

On continued unidirectional straining beyond the yield point, the plastic strain rate will decrease (due to the change in sign of $\frac{dP}{dt}$) and the mobile dislocation density is rapidly reduced by the interaction of the mobile dislocations with those obstacles existing within the material. In order to maintain the imposed plastic strain rate, it is necessary to increase the velocity of the mobile fraction of dislocations and thus the stress increases. In this instance, it is immaterial whether or not the excess mobile density is "trapped" (e.g. by forming complex tangles), or whether it is merely prevented from moving in one direction (e.g. a pileup at a grain boundary).

If, however, a similar analysis is performed for a fatigue test, it is obvious that the difference is of considerable importance. In the case of a fatigue test, those dislocations which are "trapped" are unable to move, even if the direction of applied stress is reversed, while dislocations which are immobile when the stress is applied in one direction, but which are not "trapped", may be free to move when the direction of the applied stress is reversed. Further, since the yield phenomenon occurs only

on the first quarter cycle, the strain amplitude experienced
by the sample on all subsequent cycles will be less than
that experienced at the yield point. Thus, if the large
number of mobile dislocations generated at the yield
point is not "trapped", but is instead free to shuttle
back and forth as cycling proceeds, it might be expected
that the imposed plastic strain amplitude could be maintained
at a lower stress on subsequent cycles than was required
for the first cycle. If those dislocations generated on
the first quarter cycle never became "trapped", this process
would continue indefinitely. This is, however, extremely
unlikely, and a more realistic view would be that some
dislocation "trapping" would occur as cyclic straining
continued. This would manifest itself as an increase in
the applied stress necessary to maintain the imposed
plastic strain rate with a diminishing mobile dislocation
density.

The above discussion leads to a simple explanation for
the pronounced decrease in stress between the first and
second cycles observed in 7μ grain size samples cycled at
low plastic strain amplitudes. The measured stiffness of
the Instron was 410,000 lbs/in and the calculated stiffness
of the grip assembly alone was 195,000 lbs/in. Thus,
using the relation

$$1/K_{total} = 1/K_{Instron} + 1/K_{grips} \qquad (13)$$

the overall stiffness of the test assembly was 140,000 lbs/in.
Measurements made from load-time curves indicated that for
the 7μ grain size material (which exhibited a pronounced
yield drop), the imposed plastic strain rate between the
upper and lower yield points was 4.4×10^{-3} sec^{-1}, while
beyond the lower yield point, the plastic strain rate
imposed was 2.8×10^{-3} sec^{-1}. Comparable figures for
the 80μ grain size material (which exhibits a yield plateau)
are 2.9×10^{-3} sec^{-1} at the yield plateau and
2.8×10^{-3} sec^{-1} elsewhere. The "softening" observed to
occur between the first and second cycles in the 7μ grain
size samples cycled at low plastic strain amplitudes is
thus considered to be due to the lack of stiffness of the
test assembly. Its disappearance at higher plastic
strain amplitudes merely reflects the fact that straining
to larger strains during the first quarter cycle is effective
in "trapping" the initially mobile dislocations. The fact
that no such effect was observed in material of 80μ grain
size is attributed to the fact that the large grain size
material does not exhibit an upper yield point-lower yield
point phenomenon but instead exhibits a yield plateau.
Consequently, the plastic strain rates imposed on the sample
during the initial and subsequent stages of straining are
comparable.

The lack of machine stiffness is also considered to be

the cause of the overshoot observable on the first quarter
cycles of tests shown in Figures 8a and b. Clearly there
must be some delay between the time the relays which
reverse the direction of straining are actuated, and the
time at which the direction of motion of the crosshead
does in fact reverse. The effect of this delay will be
to slightly increase the plastic strain amplitude over
its nominal value due to the incremental strain accumulated
during this delay. If the imposed plastic strain rate is
constant, then the excess strain amplitude (assuming a
constant delay time) will also be constant. If, however,
the plastic strain rate is higher during the first quarter
cycle, then the overshoot will likewise be greater on the
first quarter cycle.

As in the case of the "softening", the extent of the
overshoot decreased and finally disappeared as the imposed
plastic strain amplitude was increased. This result would
be expected, since as the plastic strain amplitude is
increased beyond the yield point, the plastic strain rate
experienced just prior to stress reversal will become
typical of that experienced during the later stages of the
test.

5.2 Effects of Deformation Twinning

It has been shown by Patridge[60] that cyclically
deforming α-titanium containing previously induced twins

results in fragmentation of the twin, i.e. a well defined
twin volume bounded by a macroscopically planar matrix-
twin interface no longer exists. Partridge attributed this
behaviour to localized detwinning.

It is clear that if twinning and detwinning can occur,
that this process provides a means of satisfying the imposed
plastic strain amplitude, and thus must be taken into account
in attempting to explain the observed fatigue behaviour.

The influence of twinning on the observed results
is considered to be minimal, with the possible exception
of those 80μ grain size and 28μ grain size samples which
were fatigued at a plastic strain amplitude of ±0.01.
Metallographic examination of selected samples indicated
that, with the exceptions noted above, the density of twins
was low. Additionally those twins which were present, tended
to have the morphology characteristic of twins formed by
unidirectional rather than cyclic deformation.

In the case of the 80μ and 28μ grain size samples,
fatigued at a plastic strain amplitude of ±0.01 however,
a high (~ 20 percent volume fraction) density of twins
was observed to have formed after 200 cycles. The twins
formed exhibited the fragmented appearance mentioned
earlier. In addition an 80μ grain size sample fatigued at
a plastic strain amplitude of ±0.01 was examined optically
after being subjected to only 20 cycles. In this case, only

a moderate (~ 10 percent volume fraction) density of twins
was observed and the twins formed resembled those formed
by unidirectional rather than cyclic deformation.

Reference to Figure 5 indicates that it is between
20 and 200 cycles that the 28μ and 80μ grain size samples
(neither of which exhibits a well defined saturation
stress) exhibit their increased hardening rate when tested
at a plastic strain amplitude of ±0.01. In view of this,
the inability of these samples to exhibit a saturation
region is tentatively ascribed to twinning.

Precisely how twinning acts to produce the observed
hardening is not known. It is conceivable that the
hardening arises as a result of twinning's decreasing the
effective grain size, however this explanation does not
explain the observed change in morphology of the twins as
cycling continues. On the other hand, if the hardening is
due to the fact that twinning-detwinning is becoming an
important deformation mode, it is hard to explain the
apparent stabilization of the stress at approximately 80
cycles. If twinning-detwinning becomes an important
deformation mode beyond 80 cycles, it is hard to imagine
that it was not an important deformation mode earlier, and
thus no stabilization of the stress would be expected to
occur.

For the above reasons, the association of the observed

absence of saturation with twinning is somewhat unsatis-
factory. It was, however, the only major difference which
could be discerned between those samples which exhibited
a well defined saturation regime and those samples which
did not exhibit a well defined saturation regime, and thus
is the explanation preferred to explain this phenomenon.

5.3 Effect of $<\vec{c} + \vec{a}>$ Slip.

It was pointed out that significant contrast was
obtained when using an (0002) reflection, only from those
regions where a high density of dislocations of $\vec{a}$ type
Burgers vectors was observed. Close examination of the
micrographs, however, reveals that with the notable
exception of Figure 12b, well developed contrast typical
of dislocations was rarely observed. Further, a comparison
of Figures 21a and 21b indicated that contrast of the type
most frequently observed may result from surface relaxation
effects. It therefore seems probable that the density of
$(\vec{c} + \vec{a})$ type dislocations is somewhat lower than the
contrast exhibited by micrographs taken using (0002) as
the operating reflection might indicate.

The fact that $(\vec{c} + \vec{a})$ type dislocations are present
only in dense clusters of $\vec{a}$ type dislocations and that
their density is so very much lower than that of $\vec{a}$ type
dislocations suggests that the $(\vec{c} + \vec{a})$ dislocations play

a relatively minor role during cyclic deformation and
that the bulk of the imposed plastic strain is accommodated
by the motion of $\vec{a}$ type dislocations.

In view of the requirement that a generalized
deformation requires the operation of five independent
slip systems, the low density of $(\vec{c} + \vec{a})$ type disloca-
tions is surprising. At small strains it is, however,
possible that the requirement of continuity may be
accommodated by elastic rather than plastic strain except
in the immediate vicinity of the grain boundary where the
elastic strain would be a maximum. All of the micrographs
shown were taken within the bulk of the grain.

5.4 Effects of Elastic Anisotropy

In all discussion on the contrast effects to be
expected from dislocations, it has been implicitly assumed
that the contrast expected will be that characteristic of
a dislocation in an isotropic medium. Before continuing
therefore, it is desirable to establish whether or not such
an assumption is valid.

A recent paper by Jones and Edington[61] considered the
effects of elastic anisotropy in hexagonal metals on the
contrast to be expected from dislocations. It was pointed
out that the images of pure screw or pure edge dislocations
of 1/3 <11$\bar{2}$0> type Burgers vector lying on the prism plane

will obey the criteria established for dislocations in
isotropic media. The anisotropy of the material in
question will influence the result for mixed dislocations
of 1/3 <11$\bar{2}$0> Burgers vector lying on the prism plane and
for all dislocations of 1/3 <11$\bar{2}$3> type Burgers vector
except under very specific conditions.

The elastic anisotropy of hexagonal materials may be
described by the parameters

$$A_{shear} = 2C_{44}/(C_{11} - C_{12}) \tag{14a}$$

$$A_{compression} = (C_{11} + C_{12} - 2C_{13})/(C_{33} - C_{13}) \tag{14b}$$

(Isotropy is indicated by A = 1.)
The values reported for α-titanium are

$$A_{compression} = 1.04$$

$$A_{shear} = 1.33 \text{ [61]}$$

In view of the fact that the majority of the
dislocations observed were in screw or edge configuration
and the relatively small elastic anisotropy of α-titanium
it is felt that the procedure adopted (i.e. assuming an
isotropic medium)is valid

The only feature which might be invoked to invalidate
the above conclusion is the presence of "ghost" images
remarked upon previously (Figures 16 and 20). The
identification of the long straight dislocation segments as

being screw in character is not completely clear cut,
it is possible that they are indeed mixed dislocations with
a strong screw component. It is therefore possible that
the "ghost" images arise due to residual contrast from the
edge component, the somewhat unusual configuration being
induced by elastic anisotropy. This possibility must be
carefully considered since one of the conclusions reached
by Jones and Edington[61] was that the effects of elastic
anisotropy would be most marked when $\vec{g} \cdot \vec{b} = 0$.

By considering the length of the "screw" dislocations
observed in Figure 20 and assuming a foil thickness which
is close to the maximum thickness for reasonable intensity
(2500A°) it is possible to compute the maximum edge
component which could be associated with the dislocation.
From this, the maximum value of $\vec{g} \cdot (\vec{b} \times \vec{u})$ may be computed
and is found to be less than 0.4. Reference to Figure 4
of Jones and Edington's paper indicates that under the
conditions of Figure 16 (this work) the contrast obtained
is barely discernable when $\vec{g} \cdot (\vec{b} \times \vec{u}) = 0.4$

For this reason, the previous interpretation of the
"ghost" images (that they arise due to residual contrast
from steeply inclined edge segments) is preferred, and the
assumption of elastic isotropy is interpreting contrast
effect is considered valid.

5.5 Effect of Grain Size

It is readily apparent by comparing Figures 10 and
11 that the effect of grain size is at best small. The
straight lines drawn indicate, that in common with
unidirectional testing, improved mechanical properties may
be obtained by grain size refinement. It is obvious, however,
that if due consideration is given to the errors in the
data, that a series of lines may be drawn to support any
point of view.

The small influence of grain size is perhaps best
illustrated by Figure 4 which indicates that samples of all
grain sizes, when tested at a plastic strain amplitude of
±0.01 initially harden at approximately the same rate.

The only way in which grain size is observed to
influence the mechanical behaviour is that the transition
from low to high plastic strain amplitude behaviour apparently
occurs at slightly higher plastic strain amplitudes for the
7μ grain size material than for the 80μ grain size material.

Just as grain size was observed to have little effect
on the mechanical behaviour, no significant effect of grain
size upon dislocation substructure could be observed.
Although the majority of the micrographs presented were
taken using foils from 80μ grain size samples, sufficient
foils of 7μ grain size material were examined to indicate
that no major effect of grain size upon dislocation

substructure exists.

The above conclusion, that grain size (at least in the range examined -7μ and 80μ) has no effect upon fatigue hardening substantiates the work of Klesnil[62] who could detect no effect of grain size upon the fatigue hardening behaviour of α-iron. Like α-titanium, the grain size of α-iron strongly influences its life when tested under constant stress amplitude.[63]

5.6 Nature of the Observed Dislocation Substructures.

5.6.1 Low Plastic Strain Amplitudes

It was pointed out that the structure observed at low plastic strain amplitudes consisted of dense arrays of $\vec{a}$ type dislocations in edge orientation, and that no unambiguous determination of specific $\vec{a}$ type Burgers vectors could not be made, due to residual contrast. It was however noted that the screw dislocations associated with this structure, both at saturation (Figures 16, 17 and 20) and prior to saturation (Figures 22 and 23) are predominantly (in any one region) of the same $\vec{a}$ type Burgers vector. In association with the results of Partridge[60] (Figure 19) this suggests that localized single slip occurs within any one region of the grain.

In view of the extensive evidence of dipole formation (Figures 12, 13, 15 and 21) it is considered that the

structure developed at saturation after low plastic strain
amplitude fatigue consists of dense clusters of edge
dislocation dipoles of the same $\vec{a}$ type Burgers vector.

5.6.2. High Plastic Strain Amplitudes

The structure developed after fatigue at high plastic
strain amplitude is a cellular dislocation substructure.
Two forms of the cellular dislocation substructure were
observed, one in which cell walls were composed of dislo-
cation dipoles, and another in which the cell walls were
composed of screw dislocations.

Again the effects of residual contrast precluded an
unambiguous determination of the nature of the $\vec{a}$ type
Burgers vectors when the structure consisted of edge
dipoles. However, in the case of the cellular structure
in which the cells walls are composed of screw dislocations,
the evidence of Figure 28 indicates that the Burgers
vector of the dislocations which comprise the cell walls
is the same. This conclusion is substantiated by Figure
29, which also implies that all the dislocations comprising
the cell walls have the same $\vec{a}$ type Burgers vector.

Since in Figure 29, the cell morphology is unknown,
it is not known which of the two types of cell wall are
formed in this grain and thus the nature of the dislocations
which comprise the cell wall when a dipole-type cell wall
cannot be determined unambiguously.

It was however noted that there was a tendency for
the dipole cell wall structure to be more prominent after
fatigue at intermediate plastic strain amplitudes. In
view of the identification of a single $\vec{a}$ type Burgers
vector made at both low and high plastic strain amplitudes,
however, it is thought that the dipole cell wall is also
composed of dislocations of the same $\vec{a}$ type Burgers vector.

5.7 Mechanisms of Substructure Formation.

5.7.1 Mechanism of Dipole Formation.

Dipoles have been observed in many materials subjected
to both unidirectional and alternating strain. As a
result of this, several[64]-[67] mechanisms have been
proposed to explain dipole formation. The theories may
conveniently be divided into two classes. These are the
trapping mechanism and the jog dragging mechanisms.

According to the trapping mechanism, edge dislocation
dipoles are formed when the edge segments of dislocations
of opposite sign gliding on parallel slip planes attract
each other strongly.[65] If the attractive force between
the edge segments is greater than the applied force, a
stable dipole will result.

The jog dragging mechanisms, are based on the fact
that if a screw dislocation acquires a jog of sufficient
height, continued motion of the screw dislocation results
in the formation of an edge dislocation dipole. The various

mechanisms proposed differ only in the process by which the initial jog is formed. Gilman[64] proposed that jogs are formed by double cross slip, a minor variant of which was put forward by Groves and Kelly[66], while Fourie and Wilsdorf[67] suggested that the mechanism of jog formation is the interaction of screw dislocations with point defects.

It was pointed out by Fourie and Murphy[68] that the presence of an edge dipole,by inducing local cross slip in approaching screw dislocations,will act as a nucleus for the formation of subsequent dipoles, thus giving rise to dipole clusters.

The operative mechanism of dipole formation during the fatigue of α-titanium is almost certainly one of the jog dragging mechanisms. The edge trapping mechanism can be ruled out for two reasons. The first is that Figure 21a indicates that dipoles are formed only where screw disloca- tions are observed. The second, which is a little more indirect, is that if the mutual trapping of edge disloca- tions were occurring, a high density of dipoles should be observed in the early stages of deformation. This is contradicted by the observations.

For these reasons, it is felt that a jog dragging mechanism is operative. It is known that cyclic deformation

is an effective means of generating point defects. The
fact that dipoles are not observed immediately, but
instead develop only after some number of cycles, during
which a reasonable number of point defects will be
generated, might be considered to support the point
defect mechanism of jog formation. It should be pointed
out, however, that, if cross-slip is thermally activated,
the delay in forming dipoles might merely reflect the
probability of the occurrence of local cross-slip.

5.7.2 Distribution of Dipoles

It was pointed out that dipoles may be observed as
dipole clusters, or as constituents of cell walls depending
upon the imposed plastic strain amplitude. Since it is
clear that the same microstructural phenomena must be
occurring no matter what the imposed plastic strain
amplitude, it is obvious that the change in dipole distri-
bution must be explained without invoking any major altera-
tion in deformation mode.

5.7.2.1 Formation of Dipole Clusters - The mechanism for

the formation of dipole clusters is illustrated in Figure
32. A screw dislocation containing a jog (which may be
one of a pair generated by double cross slip or an isolated
jog produced by a point defect interaction) is moving
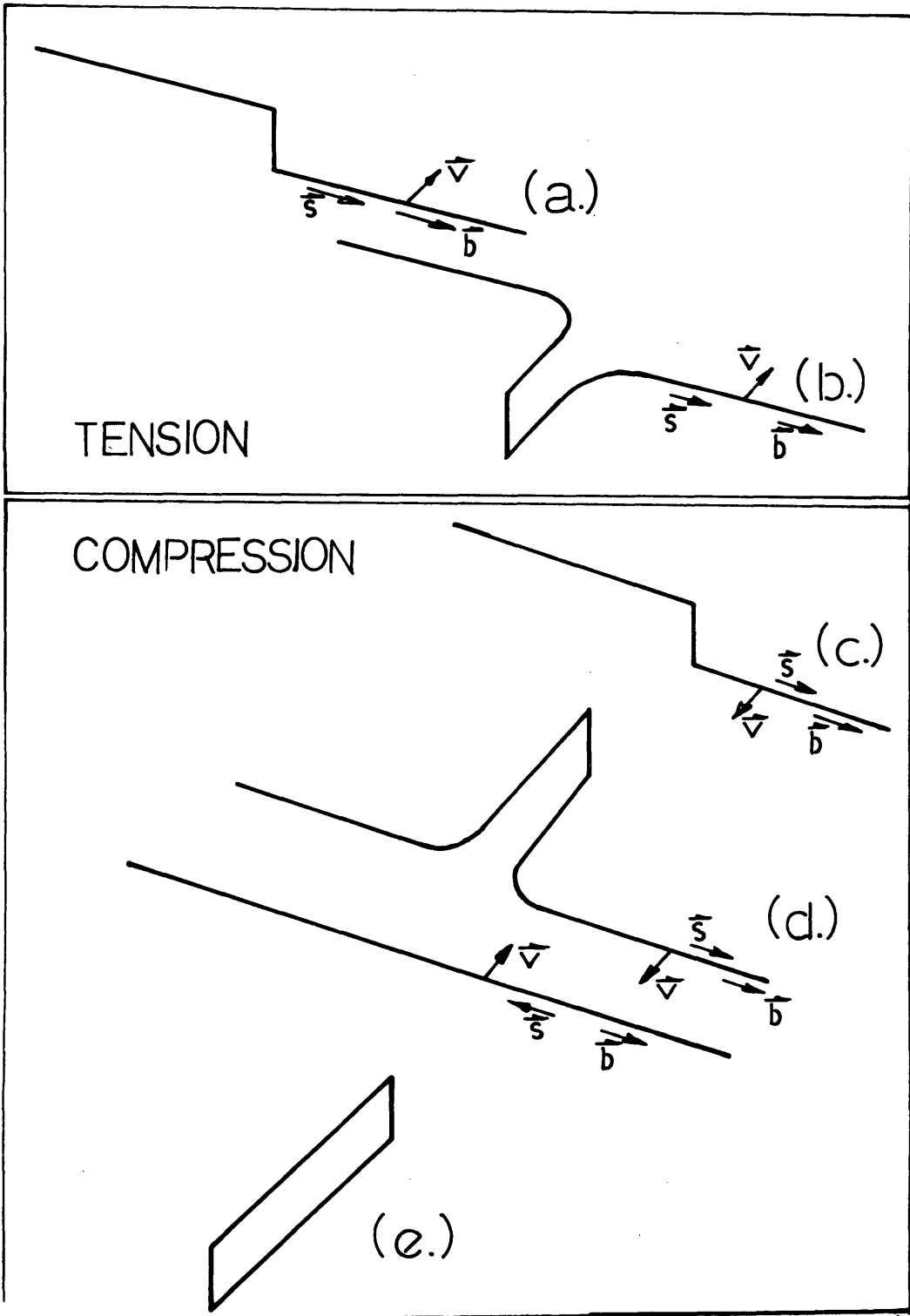
Figure 32. Sketch indicating a mechanism for the formation of dipoles in cluster morphology

along its slip plane (a). It is assumed that the jog
has been acquired at some distance from the dislocation
source. As the screw dislocation moved, the jog will
hinder its motion and an edge dipole will start to form
(b). At this point the direction of stressing is reversed,
and the previous edge dipole will be "unzipped" (c).
Further application of the stress in the reverse direction
results in the formation of another dipole and causes the
source to emit fresh dislocations of opposite sign
(relative to the original dislocation) (d). The screw
dislocations of opposite sign annihilate by cross slip,
thus pinching off the dipole (e). It is clear that once
one dipole is nucleated, continued operation of the source
can result in the double cross-slip of subsequent screw
dislocations and hence the formation of a dipole cluster
of indeterminate geometry.

5.7.2.2. Formation of Dipoles in Cell Walls - In the
previous section it was demonstrated that dipoles could
be formed during cyclic deformation by the operation of
only one source. It is also possible for dipoles to form
by the interaction of screw dislocations emitted by
different sources as illustrated in Figure 33.

In a manner precisely analogous to that indicated in
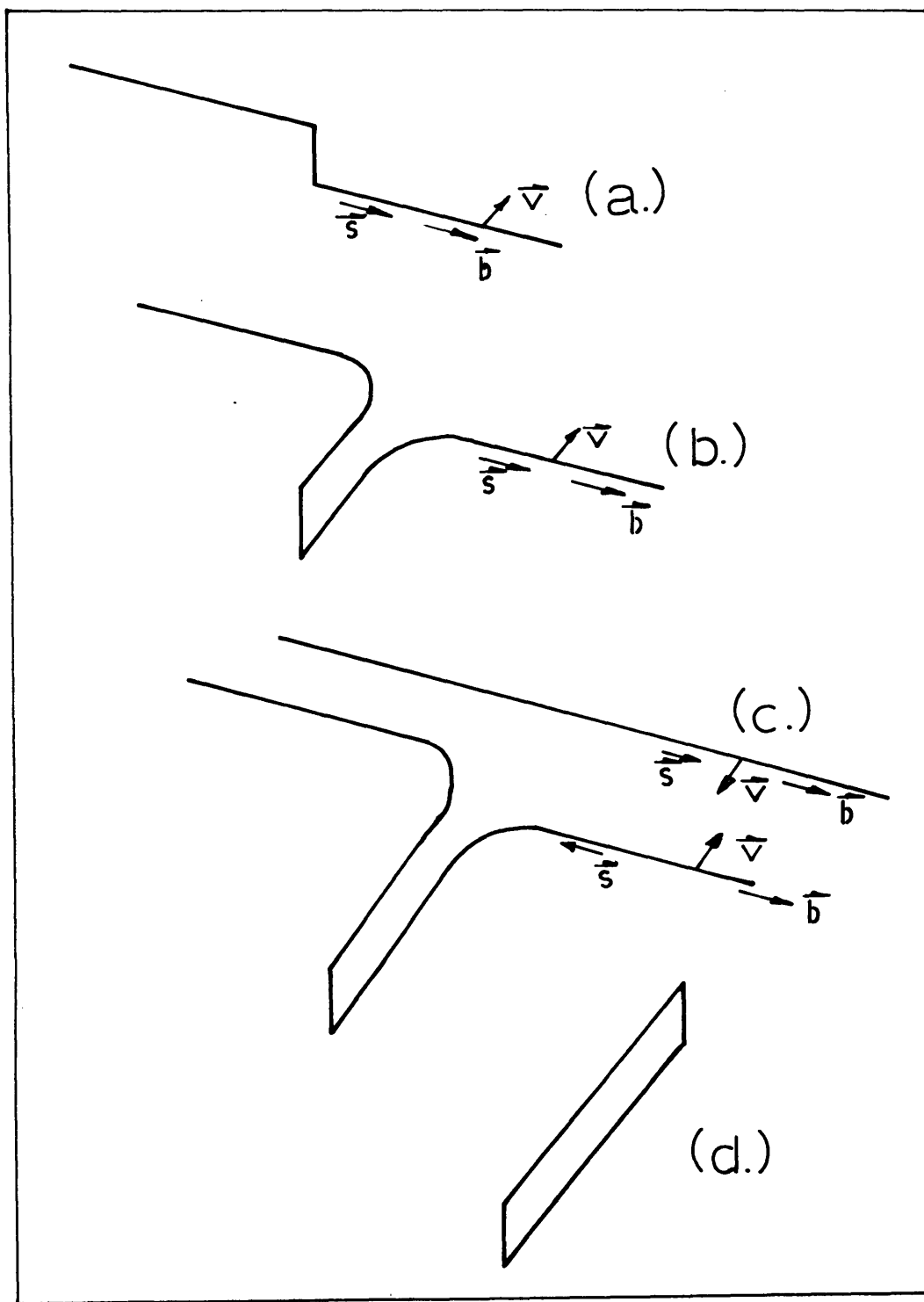
Figure 33. Sketch indicating a mechanism for the formation of dipoles arranged in cell morphology.

Figure 32, a jog is formed on a screw dislocation at some
distance from its source, (Figure 33(a)) which on
continued motion of the screw dislocation causes an edge
dipole to be dragged out (b). Now, however, it is
assumed that a screw dislocation of opposite sign emitted
by a second source approaches the original screw disloca-
tion (c). If the distance between the slip planes on
which the screw dislocations are moving is not great,
then they may cross-slip and annihilate (d) leaving a
dipole behind. In this instance, however, the formation
of dipoles occurs along a line parallel to the line of
interaction of screw dislocations, thereby giving rise to
a cellular morphology.

Once again the presence of a dipole acts to promote
the nucleation of more dipoles. In this case, the dipoles
will be formed along the line of interaction of screw
dislocations.

It is obviously possible for the screw dislocations
to be sufficiently far apart that cross-slip and
annihilation does not occur. In this case, however,
dipoles would still form, but the morphology would revert
to dipole clusters as described earlier.

5.7.2.3. Influence of Plastic Strain Amplitude on

Dipole Morphology - On the basis of the mechan-
isms put forward in the previous sections it is clear that
the probability of the formation of dipoles in cell walls
is proportional to the product of the density of screw
dislocations and the average distance through which each
screw dislocation moves. Thus at low plastic strain
amplitudes, a cluster morphology of dipoles would be
expected, while at increasing plastic strain amplitudes
the cellular morphology becomes more favourable.

This is in accord with the observations.

5.7.3 Formation of a Cell Structure

The means by which a cellular substructure consisting
of screw dislocations arises is not known. However,
within the framework of the discussion of the origin of
a dipole structure in cell walls some general observations
may be made.

It is obvious that the number of screw dislocations
emitted by adjacent sources need not be equivalent. It
is thus possible that in addition to the mutual
annihilation of screw dislocations already described, that
the cell wall may contain an excess of screw dislocations
of like sign. It is, therefore, trivial to extend the

cell wall composed of dipoles across which there is no lattice rotation (Figure 24a) to a cell wall composed of dipoles and excess screw dislocations which since the excess screw dislocations constitute (if some dislocation reorientation is permitted) a twist boundary which exhibits a lattice rotation across the cell walls.

It is less obvious why cell walls should exist in which virtually no dipoles can be detected, since as noted, the same microstructural process must occur no matter what the imposed plastic strain amplitude. If the double cross-slip model is correct, however, the dipoles formed will be alternately of vacancy and interstitial type. It is therefore possible for these to annihilate each other, if diffusion can occur.

It is conceivable that the excess screw dislocations will act as a short circuit path for diffusion, thus leading to the eventual annihilation of the dipoles and leaving only the screw dislocations behind. The screw dislocations then give rise to the lattice rotation clearly visible in Figure 25. It is not known whether or not this does occur, but it is the only explanation which does not require that jog formation be suppressed at high plastic strain amplitudes, but not at low plastic strain amplitudes. One factor which does mitigate against the above suggestion is that since a dipole once formed acts

to nucleate more dipoles the diffusional process must
act to eliminate the dipoles formed on one half cycle
before they can act as obstacles to the dislocations
generated on the next half cycle. At the strain rate used
in this investigation, this implies on assuming a dipole
sepatation of 300A° a diffusion coefficient of approxi-
mately 10^{-13} cm^2sec^{-1} which seems somewhat high.

5.8 The Influence of Structure on Mechanical Properties.

It has recently been demonstrated by Neumann[69]
that dislocation dipoles are not effective in obstructing
the motion of edge dislocations. There are several
possible reactions which may occur as a mobile edge
dislocation approaches an edge dipole under the influence
of an external stress. These reactions are,

1) The mobile dislocation moves past the dipole - no
   reaction.

2) The presence of the mobile dislocation causes the
   dipole to decompose into its constituent edge
   dislocations - decomposition.

3) The edge dislocation is trapped, thus forming a
   tripole - trapping.

4) One of the dislocations in the original dipole reacts
   with the edge dislocation to form a new dipole, while
   the other dislocation in the original dipole is free
   to move - rearrangement.

Neumann[69] has shown that of the four possibilities

trapping is much less likely than one of the other

three, decomposition, no reaction or rearrangement. An

edge dislocation dipole does however present a considerable

obstacle to the motion of a screw dislocation since it

must cross-slip in order to avoid it.

For this reason it is expected that in the presence

of the dipole structure formed at saturation during low

plastic strain amplitude fatigue, that the imposed

plastic strain amplitude may be accommodated at a lower

applied stress if edge rather than screw dislocation

segments move. In general, it is impossible to preferentially

generate dislocations of only one type (i.e. screw or edge)

since both edge and screw segments coexist in a dislocation

loop. The fact that a dipole may dissociate, however,

leads to the possibility of increasing the density of edge

dislocations without simultaneously increasing the density

of screw dislocations. If this does indeed occur, it

suggests that the deformation of the material at satura-

tion, after low plastic strain amplitude fatigue is

controlled by the motion of edge dislocations.

If the density of edge dislocations is inadequate

and if no means of generating edge dislocations preferen-

tially exists, then the deformation will be controlled

by the motion of both the edge and screw segments.

In the above discussion it has been assumed that the stress-velocity relation is the same for both edge and screw segments. If the velocities differ, the deformation will be controlled by the motion of the slowest moving segment.

There is some evidence that in α-titanium the edge segments move more rapidly than the screw segments. The evidence is indirect, and is based primarily on the observation that, after deformation, the structure consists of predominantly screw dislocation segments[47] which implies that the edge segments have moved away rapidly, leaving the slower moving screw segments behind. A recent study which attempted to measure dislocation velocities directly proved unsuccessful.[70]

Several of the observed results may be satisfactorily explained, if the assumption that edge segments move more rapidly than screw dislocations is made. In particular, the cyclic softening observed at low plastic strain amplitudes may readily be explained.

Before discussing the phenomenon of cyclic softening it is, however, necessary to justify again the index used to monitor mechanical behaviour (the average peak stress).

5.8.1. Average Peak Stress.

The use of the average peak stress $(\bar{\sigma} = 1/2(|\sigma_P^T| + |\sigma_P^C|)$ was justified earlier by noting that if an asymmetrical hysteresis loop is developed, the average peak stress is the only index which accurately reflects the work done per cycle. In order to use the average peak stress interchangeably with applied stress, as will be done subsequently, it is necessary to establish whether such an identification is defensible.

The most obvious source of asymmetry in the hysteresis loop is the existence of an internal stress. If the presence of an internal stress can be demonstrated, then the interchangeability of average peak stress with applied stress is "legal" since

$$\bar{\sigma} = 1/2(|\sigma_P^T| + |\sigma_P^C|) \tag{15a}$$

$$= 1/2(|\sigma_A + \sigma_{INT}| + |\sigma_A - \sigma_{INT}|) \tag{15b}$$

$$= \sigma_A \tag{15c}$$

where

σ_A = Applied stress in the absence of an
internal stress

σ_{INT} = Internal stress.

Two features of the asymmetry are noteworthy. The asymmetry diminishes with increasing plastic strain

amplitude and the stress was always greatest in the
direction of initial load application (see Figure 8).
This suggests that the effect may, like the softening
between the first and second cycles observed in 7μ
grain size materials and the overshoot phenomenon, be
associated with the lack of stiffness of the test
assembly.

The effect of the increased plastic strain rate
imposed during the first quarter cycle will be, as noted
earlier, to generate an increased density of mobile
dislocations. These excess dislocations will, since the
the sign of the dislocations emitted by a source reverses
upon stress reversal, assist the operation of a source
in one direction while impeding the operation of the
source in the other. This occurs since the internal stress
associated with the excess dislocations will be such as
to repel dislocations of one sign while attracting
dislocations of the opposite sign. It will thus prove
more difficult to cause deformation when the stress is
applied in the same direction as the initial stress
application.

This is graphically illustrated in Figure 8a where
although the imposed plastic strain in tension is greater
than the imposed plastic strain in compression, the stress
necessary to maintain the imposed plastic strain is

greatest in compression - the direction of initial stress application.

An alternate cause of the loop asymmetry might also be a differing plastic strain amplitude in tension and compression. The above results, however, indicate that such an effect is small in relation to the problem of machine stiffness and thus it will not be considered further.

For the rest of the Discussion, the average peak stress will be assumed to be equivalent to the peak applied stress.

5.8.2. Fatigue Softening

The occurrence of cyclic softening is readily explained if the assumption that edge dislocation segments move more rapidly than screw segments is valid.

In the initial cycles, the imposed plastic strain amplitude is accommodated by the motion of both screw and edge segments which are generated in the form of loops by some source. The stress developed is controlled by the motion of screw dislocations, since the density of edge dislocations is inadequate to accommodate the imposed plastic strain rate. As cycling continues, the motion of screw dislocations increases the density of edge segments by forming dipoles, the effect of which is to impede the further motion of screw dislocations and also

to act as preferential sources for the generation of edge
dislocations. Since the edge segments may move more
rapidly than the screw segments, the formation of dipoles
is accompanied by softening (increased density of edge
segments which function as sources of edge dislocations
and which also present little obstacle to the motion of
edge dislocations), and hardening (increased density of
edge segments which obstruct the motion of screw disloca-
tions). Depending upon which of the two features is
dominant, either macroscopic hardening or softening will
be observed. In the early stages of life, the creation
of obstacles to the motion of screw dislocations is the
dominant factor and hardening is observed. As cycling
is continued, the increased density of edge segments,
becomes more important and thus softening is observed.
Further cycling causes a balance to be struck between the
two processes and no further change in behaviour is observed
(saturation).

5.8.3. Fatigue Hardening

It is apparent that fatigue hardening may be explained
in an anologous manner. The only difference being that
at no time is the density of edge dislocations generated
adequate to satisfy both the imposed plastic strain ampli-
tude and the imposed plastic strain rate. Thus at all times
the deformation will be controlled by the motion of screw

dislocations. In this regard there is no difference
between the type of cell structure in which the cell walls
contain dipoles and the type of cell structure in which
the cell walls contain only screw dislocations.

In this case, however, the balance of factors which
gives rise to saturation behaviour is not obvious. As
was noted earlier, if dipoles are formed at low plastic
strain amplitudes, it is reasonable to assume that they
are also formed at high plastic strain amplitudes. The
fact that dipoles are not always observed might be taken
to imply that a balance is struck between the creation
of dipoles by slip and destruction of dipoles by diffusion
as suggested earlier. There is, however, no evidence to
either prove or disprove this statement, and thus it must
be concluded that the factors influencing the saturation
of samples which monotonically harden is unknown.

5.9. Effect of Plastic Strain Amplitude on Saturation Stress.

The association of high plastic strain amplitude
fatigue with the motion of screw dislocations and low
plastic strain amplitude fatigue with the motion of edge
dislocations permits a simple interpretation of the results
obtained on plotting saturation stress versus the square
root of plastic strain amplitude (Figures 10 and 11).

The upper curve will then reflect the stress
necessary to move a screw dislocation through the structure
developed after fatigue at high plastic strain amplitudes,
while the lower curve represents the stress necessary to
move an edge dislocation through the structure developed
after fatigue at low plastic strain amplitudes.

It is apparent, however, that the precise dislocation
configuration does not appear to be important. There is
little change in stress between 20 and 200 cycles although
Figures 30 and 24 show a distinctly different dislocation
distribution. Further, the fact that the maximum stress
developed during low plastic strain amplitude fatigue may
be described by the same relationship as that for the
saturation stress developed after high plastic strain
amplitude fatigue also indicates that differences in the
dislocation distribution do not affect the stress greatly
In all of these cases, the motion of screw dislocations is
thought to be the primary deformation mode.

Earlier it was stated that the curves represented
the stress necessary to move edge and screw dislocations
in the structures developed at saturation. If, however,
the lines drawn are extrapolated to zero plastic strain
amplitude it is possible that the intercepts represent
the friction stresses for edge and screw dislocations,

respectively. Such an interpretation assumes that the effect of the substructure enters only into the slope of the line, not the intercept. In the absence of any direct measurements of dislocation velocity, no definite conclusion may be drawn. However, the friction stress obtained from a Hall-Petch plot (of yield stress) represents the stress necessary to expand a dislocation loop in a virgin crystal. More properly, it represents the stress necessary to move the slowest moving segment of the dislocation loop in a virgin crystal.

It may be noted that the friction stresses for screw dislocations obtained from a Hall-Petch plot and from the intercepts obtained from the plots of $\bar{\sigma}_{sat}$ versus $(\Delta\epsilon_p)^{1/2}$ for the 7μ and 80μ grain sizes are, within the limits of experimental error, in agreement. This suggests that the effect of substructure is eliminated on extrapolating to zero plastic strain amplitude. It, therefore, does not seem unreasonable to assume that the effect of substructure is likewise eliminated in extrapolating the results characteristic of the motion of edge dislocations to zero plastic strain amplitude.

It is, therefore, tentatively suggested that the friction stresses for edge and screw dislocations in this material are approximately 12 Kg/mm^2 (14,000 psi) and

17 Kg/mm^2 (24,000 psi), respectively. This would imply that edge dislocations move at approximately eight times the velocity of screw dislocations, which is not unreasonable.

It is not obvious why the exponent in the relationship

$$\bar{\sigma}_{sat} = \bar{\sigma}' + k(\Delta\varepsilon_P)^n \qquad (16)$$

should be one-half.

It is known, however, that the relationship

$$\sigma = \sigma_o + \alpha Gb\rho_T^{1/2} \qquad (17)$$

is valid for many materials strained unidirectionally. If a similar relationship is valid during cyclic deformation, and there is no obvious reason why it should not be, then at low plastic strain amplitudes, the approximation

$$\rho_M \simeq \rho_T \qquad (18)$$

is probably valid. If this is so, then using the relation

$$\Delta\varepsilon_P = b\bar{x}\rho_M \qquad (19)$$

and making the further assumption that the mean free slip path at saturation is constant, then

$$\Delta \varepsilon_p \; \alpha \; \rho_M \qquad\qquad\qquad (19)$$

or

$$\bar{\sigma}_{sat} \; = \; \bar{\sigma}'_o \; + \; \alpha \; Gb \, (\Delta \varepsilon_p)^{1/2} \qquad\qquad (20)$$

This result is convenient, but in view of the assumptions necessary to derive it, no particular weight is placed on the result.

6.   CONCLUSIONS

1)   The fatigue hardening behaviour of α-titanium is affected only slightly by grain size.

2)   Two deformation modes were observed, the observed mode being strongly influenced by plastic strain amplitude. Associated with the two deformation modes, two dislocation structures were observed, one consisting of clusters of edge dipoles, the other a cellular structure. The cellular structure exhibited two variants, one in which the cell wall was formed from edge dislocation dipoles, the other in which the cell wall was composed of screw dislocations. The dislocations in both structures are composed almost entirely of dislocations of one of the three $\vec{a}$ type Burgers vectors.

3)   At low plastic strain amplitudes (< ±0.005), the major portion of the imposed plastic strain is accommodated by the motion of dislocations of $\vec{a}$ type Burgers vectors. No evidence was obtained for the existence of a comparable density of ($\vec{c}$ + $\vec{a}$) type dislocations at any of the plastic strain amplitudes employed. The occurrence of extensive twinning was observed only in the largest grain size material strained at the high plastic strain amplitude.

4)   A model based on a jog dragging mechanism is

proposed for the formation of edge dislocation dipoles. The model predicts the trend of the observed change in the morphology of the dislocation dipole structure with increased plastic strain amplitude. It is shown that if the assumption that edge dislocations move more rapidly than screw dislocations is made, that the trend of changes in mechanical behaviour with increasing plastic strain amplitude may be predicted. It is thus suggested that the assumption is valid. From data obtained by extrapolating a curve of saturation stress versus the square root of plastic strain amplitude, it is proposed that the friction stress for screw dislocations is approximately 17 Kg/mm^2 and that the friction stress for edge dislocations is approximately 10 Kg/mm^2.

7. SUGGESTIONS FOR FUTURE WORK

1) Since the explanation given for the various
dislocation substructures and the deformation modes
observed was keyed to the assumption that edge disloca-
tions move more rapidly than screw dislocations it is
clearly desirable to verify this experimentally. In
particular it is desirable that the values of the
friction stresses be obtained for edge and screw dislo-
cations and compared with the values cited in this work.
In view of the fact that a recent attempt to perform the
above experiment was unsuccessful, it is possible that
the experiment is inherently impossible to perform.

It is possible however, to perform a partial check
on the validity of the model by directly measuring
dislocation velocities in aluminum. Aluminum is known
to exhibit a range of dislocation substructures similar
to that observed in α-titanium - dipole clusters, dipoles
arrayed in the form of cell walls and cell walls composed
of screw dislocations. Since there was nothing in the
model presented which was specific to hexagonal metals,
it is clear that a similar mechanism might reasonably be
expected to occur on cyclically deforming aluminum.
Since there are no observations in the literature that
aluminum cyclically softens, this implies, on the basis of
the model presented, that the velocities of edge and screw

segments in aluminum are comparable. Clearly, if a direct measurement of dislocation velocities indicates otherwise, the model is invalidated.

2) It is known that during crack growth there exists a plastically deforming zone ahead of the crack slip. Since the rate of advance of the crack will be influenced by the dislocation structure which the crack encounters, it is clearly desirable to determine the stability of the structure formed after low plastic strain amplitude fatigue. Thus it is suggested that a series of tests be conducted on the effect of cycling to saturation at low plastic strain amplitude followed by cycling at higher plastic strain amplitudes on the resultant dislocation substructure.

3) A difficulty which recurred throughout this investigation was that it proved impossible to perform an unambiguous Burgers vector analysis due to residual contrast problems. It is therefore suggested that a similar series of tests to those performed in this investigation be conducted on single crystal samples, so that slip trace analysis may be used to augment the transmission electron microscopy observations.

4) It was pointed out that it was possible that the occurrence of cell walls in which no dipoles could be observed might be due to the fact that dipoles mutually annihilate by diffusion. If this is indeed correct, then increasing the plastic strain rate should reduce the time

required for diffusion and thus the onset of the formation of a dipole free cellular structure should be displaced to higher plastic strain amplitudes. Conversely, decreas- the plastic strain amplitude would enhance the formation of a dipole free cellular structure at low plastic strain amplitudes.

5) Several of the features observed during this investigation were attributed to the lack of stiffness of the test assembly used. To minimize these effects, it is suggested that a stiffer assembly be employed for any future tests.

APPENDIX I

DESIGN OF CONTROLLER

A schematic diagram of the controller described in
the section on Results is shown in Figure A1. The
controller makes extensive use of Operational Amplifiers.
(Op Amps)[71][72] An Op Amp is a high gain wideband
amplifier with very high input impedance and low output
impedance. When combined with a passive network in the
negative feedback path, the circuit exhibits behaviour
which is typical only of the network and is independent
of the characteristics of the amplifier. If resistors
comprise the negative feedback network, the circuit
functions as an amplifier, the gain of which is controlled
by the ratio of the feedback resistance and input
resistance.

A.1 Load Channel

The load channel accepts the D.C. signal generated
by the Instron load cell. The signal is first amplified
by a chopper stabilized amplifier A1 (gain x5 to x200)
before being filtered. The filter is designed to eliminate
any A.C. component with a frequency of greater than
20 Hertz.

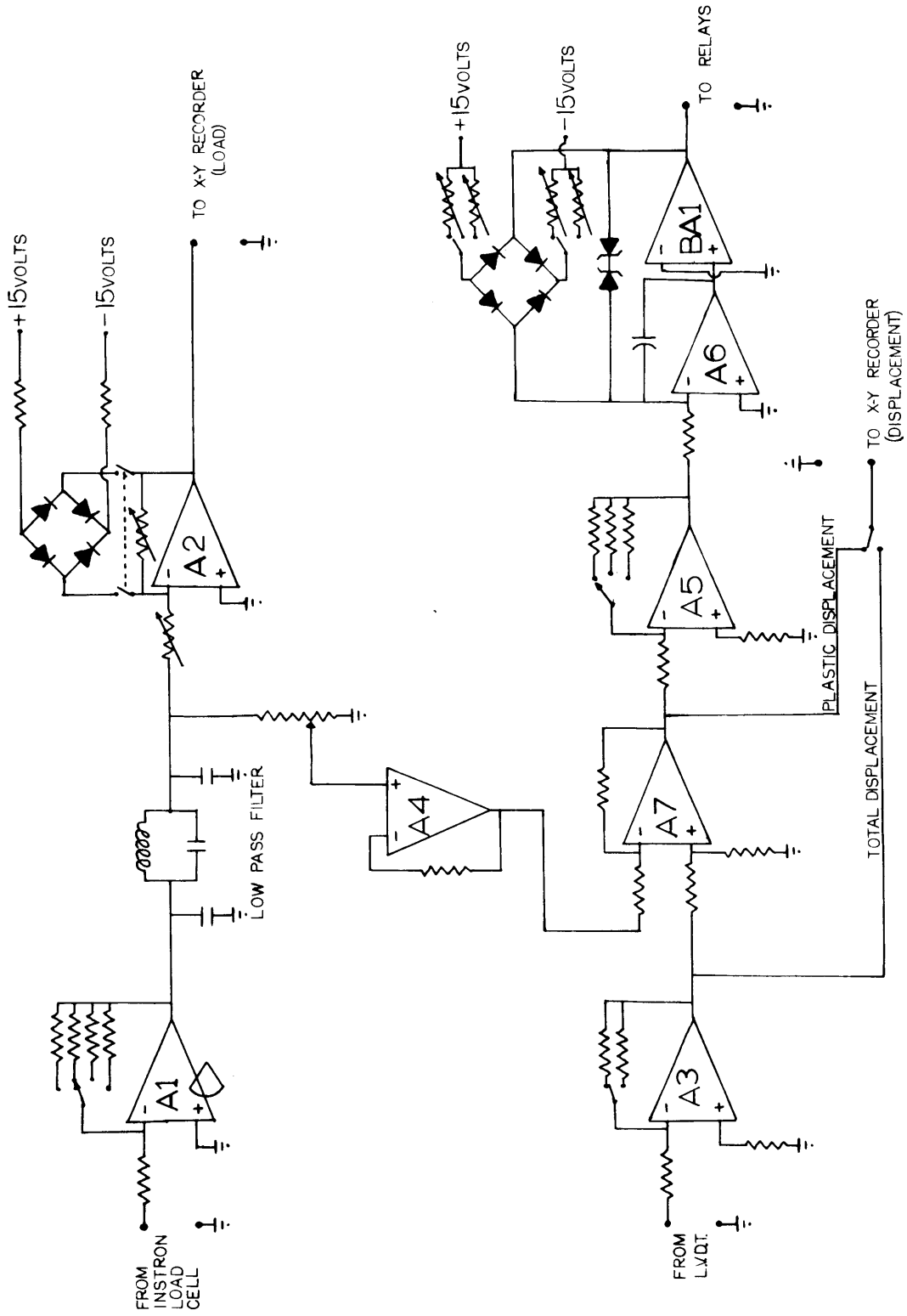Amplifier A2 is a low gain (x1 to x10) amplifier which

Figure A1. Schematic of Controller

has provision for suppressing an output signal until the input signal exceeds some preset value. This is accomplished by a diode bridge connected in parallel with the negative feedback loop. The diodes are forward biased by the applied voltages of +15v and -15v. For small input signals they provide a low resistance feedback path since the forward resistance of the diodes is low. As the input voltage is increased the diodes become back biased and will then exhibit a high resistance. The feedback resistance is then determined by only the resistor in parallel with the diode bridge. The input voltage necessary to cause this to occur may be altered by varying either the input resistance (as in amplifier A2) or the resistance between the applied voltage and the diode bridge (as in amplifiers A6/BA1).

The output from amplifier A2 is connected to the X-Y recorder.

8.2 Displacement Channel

The displacement signal is obtained from an L.V.D.T. attached to the shoulders of the specimen as shown in Figure 1. This signal is initially amplified by amplifier A3 (gain x10) and the resultant signal fed into one output of amplifier A7.

A portion of the filtered signal obtained from

amplifier A1 is tapped by means of a ten-turn potentiometer and fed into amplifier A4. Amplifier A4 is a voltage follower whose purpose is to lower the impedance of the signal derived from the potentiometer before it is fed into one input of amplifier A7.

Amplifier A7 is a unity gain differential amplifier which, as noted, accepts signals from amplifiers A3 and A4. The output from amplifier A7 is the difference between the signals obtained from amplifiers A3 and A4. When the correct signal is obtained from the ten-turn potentiometer, the output from amplifier A7 corresponds to the plastic displacement experienced by the sample.

The output from either amplifier A3 or amplifier A7 may be fed into the X-Y recorder. These correspond to total displacement and plastic displacement, respectively.

The output from amplifier A7 is further amplified by amplifier A5 (gain x5 to x20) before being fed into the power amplifier combination A6 and BA1.

Amplifier BA1 is a booster amplifier which forms part of the feedback loop around amplifier A6 permitting the combination (A6/BA1) to supply more power than amplifier A6 alone. This amplifier combination is designed to act as a switch. Like amplifier A2, the amplifier A6/BA1, produces no output signal until the input voltage exceeds some preset value, however, the gain is x1000. Thus when the input voltage exceed the threshold value the

amplifier saturates.   To preclude this, the output is
"clamped" by inserting two back-to-back Zener diodes in
the feedback loop, in parallel with the resistor and
the diode bridge.

The output from amplifier A6/BA1 is used to operate
two relays which in turn actuate the relays on the
Instron which control the motion of the crosshead.

A similar controller has been described by
Condit[73].

BIBLIOGRAPHY

1. J. C. Grosskrentz, Phys. Stat. Sol. (A), $\underline{47}$, No. 1,
    p. 11 (1971).

2. R. L. Segall, Adv. Mater. Res. $\underline{3}$, p. 109 (1968).

3. C. E. Feltner and C. Laird, Acta Met. $\underline{15}$ pp 1621-1653,
    (1967).

4. D. S. Kemsley and M. S. Paterson, Acta Met. $\underline{8}$, p. 453,
    (1960).

5. P. Charsley and N. Thomson, Phil. Mag. $\underline{3}$, p. 1098,
    (1958).

6. H. J. Gough and H. L. Cox, Proc. Roy. Soc. A, $\underline{123}$,
    p. 143, (1929).

7. M. Klesnil, M. Holzmann, P. Lukas and P. Rys, J.I.S.I.,
    $\underline{203}$, p. 47, (1965).

8. R. I. Stephens, J. Mater. $\underline{3}$, p. 386, (1968).

9. R. G. Dubensky and R. I. Stephens, Interamerican
    Conf. on Materials Technology, San Antonio, p. 510,
    (1968).

10. S. K. Agrawal and R. I. Stephens, J. Less Common
    Metals, $\underline{24}$, p. 93 (1971).

11. M. Klesnil and P. Lukas, J.I.S.I., $\underline{205}$ p. 746, (1967).

12. P. Beardmore and P. H. Thornton, Met. Trans. $\underline{1}$,
    p. 775, (1970).

13. M. R. Hempel, Fracture (M.I.T. Press) Averbach, et. al. eds., p. 376, (1959).

14. H. A. Lipsitt and G. T. Horne, International Conf. on Fatigue of Metals (Institute of Mech. Engineers/A.S.M.E.), (1956), p. 513.

15. F. V. Lawrence and R. C. Jones, Met. Trans. $\underline{1}$, p. 367 (1970).

16. A. Yoshikawa and M. Okamoto, Proc. Int. Conf. on the Strength of Metals and Alloys, Tokyo, 1967, p. 471.

17. D. S. Kemsley, Acta Met. $\underline{8}$, p. 740 (1960).

18. T. Broom and J. M. Summerton, Phil. Mag. $\underline{8}$, p. 1847 (1963).

19. E. Schmid and W. Fahrenhorst, Z. Metallk. $\underline{51}$ p. 323, (1931).

20. A. Lawley, J. F. Breedis and J. C. Meakin, Acta Met. $\underline{14}$, p. 1339, (1966).

21. P. Lukas, M. Klesnil and P. Rys, Z. Metallk, $\underline{56}$, p. 109, (1965).

22. J. C. Grosskrentz, W. H. Riemann and W. A. Wood, Acta Met. $\underline{14}$, p. 1549, (1966).

23. A. B. Mitchell and D. G. Teer, Met. Sci. Jrnl., $\underline{3}$, p. 183, (1969).

24. P. Beardmore and P. H. Thornton, Acta Met. $\underline{18}$, p. 109 (1970).

25. O. Vingsbo, G. Lagerberg, B. Hansson and Y. Bergstrom, Phil. Mag., 17, p. 441 (1968).

26. R. L. Segall and P. G. Patridge, Phil. Mag. 4, p. 912, (1959).

27. R. L. Segall, P. G. Partridge and P. B. Hirsch, Phil. Mag. 6, p. 1493, (1961).

28. T. H. Youssef, Phys. Stat. Sol. (B), 3, No. 3, p. 801 (1970).

29. P. Lukas and M. Klesnil, Czech. Jrnl. of Physics (B), 14, p. 600, (1964).

30. C. E. Feltner, Acta. Met. 11, p. 817, (1963).

31. E. E. Laufer and W. N. Roberts, Phil. Mag. 10, p. 883, (1964).

32. P. Lukas, M. Klesnil, J. Krejci and P. Rys, Phys. Stat. Sol. (A), 15, p. 71 (1966).

33. P. Lukas, M. Klesnil and J. Krejci, Phys. Stat. Sol. (A), 27, no. 2, p. 545, (1968).

34. R. P. Wei and A. J. Baker, Phil. Mag. 11, p. 1087, (1965).

35. R. P. Wei and A. J. Baker, Phil. Mag. 12, p. 1005 (1965).

36. R. L. Segall, Electron Microscopy and Strength of Crystals, eds. G. Thomas and J. Washburn (Interscience), p. 515, (1962).

37. D. L. Holt, J.A.P., 41, 3197 (1970).

38. D. L. Holt, Proc. Second Int. Conf. on the Strength
     of Metals and Alloys, Asilomar (1970), p. 477.

39. J. E. Pratt, Acta Met. 15, p. 319 (1967).

40. E. E. Laufer and W.N. Roberts, Phil. Mag. 14,
     p. 65 (1966).

41. E. A. Anderson, D. C. Jillson and S. R. Dunbar,
     Trans. A.I.M.E., 197, p. 1191, (1953).

42. F. D. Rosi, C. A. Dube and B. H. Alexander,
     Trans. A.I.M.E., p. 257 (1953).

43. A. T. Churchman, Proc. Roy. Soc. A. 226, p. 216,
     (1954).

44. H. Conrad and R. Jones, Trans. A.I.M.E. 245,
     p. 779 (1969).

45. N. E. Paton, PhD. Thesis, M.I.T. (1969).

46. J. C. Williams and M. J. Blackburn, Phys. Stat.
     Sol. (A), 25, p.k1, (1968).

47. T. R. Cass, The Science Technology and Applications
     of Titanium, eds. Jaffee and N. E. Promisel,
     (Pergamon), (1970), p. 459.

48. M. J. Blackburn and J. C. Williams, Boeing Scientific
     Research Laboratories Document D1-82-0812.

49. C. P. Biswas, Ph.D. Thesis, M.I.T. (1972).

50. A. W. Sommer and P.P. Tung, Technical Report no. 4 to the Office of Naval Research, NA-70-719.

51. P. R. Okamoto, E. Levine and G. Thomas, JAP, 38, p. 289, (1967).

52. P. B. Hirsch, et. al., Electron Microscopy of Thin Crystals, (Butterworths), p. 252, (1965).

53. P. B. Hirsch, et. al., Electron Microscopy of Thin Crystals (Butterworths), p. 178, (1965).

54. P. B. Hirsch, et. al., Electron Microscopy of Thin Crystals, (Butterworths), p. 202, (1965).

55. D.J.H. Cockayne, I. L. F. Ray and M. J. Whelan, Phil. Mag. 20, p. 1265, (1969).

56. W. M. Stobbs and C. H. Sworn, Phil. Mag. 24, p. 1365 (1971).

57. G. Thomas, Thin Films, published by American Society for Metals (1964), p. 227.

58. D. B. Snow, Sc.D. Thesis, M.I.T. (1971).

59. P. B. Hirsch, et. al., Electron Microscopy of Thin Crystals, (Butterworths), p. 271 (1965).

60. P. G. Patridge and C. J. Peel, The Science Technology and Application of Titanium, Jaffee and Promisel, eds., (Pergamon), p. 517, (1970.

61. P. J. Jones and J. W. Edington, Phil. Mag. 25, p. 729, (1972).

62. M. Klesnil, Conference on Microplastic Deformation and Fatigue of Metals, Brno, (November 1963), (reported in Ref. 29).

63. N. G. Turner and W. T. Roberts, Trans. A.I.M.E., 242, p. 1223 (1968).

64. J. J. Gilman, JAP, 33, p. 2703.

65. A. S. Tetelman, Acta. Met. 10, p. 813, (1962).

66. G. W. Groves and A. Kelly, Proc. Roy. Soc. A, 275 p. 223, (1963).

67. J. T. Fourie and H.G.F. Wilsdorf, JAP, 31, p. 2219, (1960).

68. J. T. Fourie and R.J. Murphy, Phil. Mag. 7, p. 1617, (1962).

69. P. D. Neumann, Acta. Met. 19, p. 1233 (1971).

70. T. Tanaka and H. Conrad, Acta. Met. 19, p. 1001, (1971).

71. C. F. Morrison, Jr., Generalized Instrumentation for Research and Teaching, published by Washington State University, (1964).

72. Applications Manual for Operational Amplifiers published by Philbrick/Mexus Research, Dedham, Mass. 02026.

73. R. E. Condit, Ford Technical Memorandum SLM-68-1, (1968).

BIOGRAPHICAL NOTE

Robin Stevenson was born in Falkirk, Scotland, on December 25, 1946. He attended high school in Motherwell, Scotland, before attending the University of Strathclyde in Glasgow.

In September 1967 he entered graduate school as a research assistant in the Department of Metallurgy and Materials Science at the Massachusetts Institute of Technology.